Master Thesis

Modelbased Control Design of High Temperature Fuel Cells

conducted at

Institut für Regelungs- und Automatisierungstechnik
University of Technology Graz, Austria

by
Marian Forster, BSc
1031275

Supervisor:
Univ.-Prof. Dipl.-Ing. Dr.techn. Martin Horn

Assessor:
DI Oswald Lackner

Graz, January 2017

Statutory Declaration

I declare that I have authored this thesis independently, that I have not used other than the declared sources/resources, and that I have explicitly marked all material which has been quoted either literally or by content from the used sources.

——————————————— ———————————————
date (signature)

Abstract

The fuel cell technology can offer many advantages over conventional energy conversion methods. High efficiency, zero to no emissions, low maintenance and noise are just a few of them. The high conversion efficiency is due to the direct conversion of chemical energy to electrical energy – without the need of lossy intermediate processes. If the waste heat is utilized in a combined heat and power (CHP) solution, the efficiency can be increased even further. Possible applications are therefore small power plants and even vehicles powered by fuel cells have been demonstrated already.

This thesis' focus lies on the modeling and controlling of *Solid Oxide Fuel Cells* (SOFC) – especially on the heat-up procedure of the cathode path. With an operating temperature of 800 to 900 °C, this technology belongs to the family of high temperature fuel cells. Reaching such high temperatures without damaging components due to overheating or too fast heat-up, illustrates a challenge to the control algorithm. Since practical tests are time consuming and expensive, a simulation model for an SOFC system is developed in this work. With the aid of this model, control strategies can be developed without the need of expensive tests.

The basis for this work is a prototype system with a power output of $\approx 10\,\mathrm{kW_{el}}$, developed by AVL List GmbH. The mathematical models for all the required components are fitted to measurement data from the prototype and connected to a complete system. After that, a controller structure is proposed to automatically heat up the system while keeping all temperatures within the given limits.

Zusammenfassung

Die Brennstoffzellen-Technologie bietet zahlreiche Vorteile gegenüber konventionellen Energiewandlungsmethoden. Dazu zählen eine hohe Effizienz, geringe bis keine Emissionen und ein wartungsarmer und leiser Betrieb. Der hohe Wirkungsgrad wird durch die direkte Konvertierung von chemischer zu elektrischer Energie erreicht und kann durch eine Kraft-Wärmekopplung noch weiter erhöht werden. Mögliche Anwendungen sind daher Kleinkraftwerke und auch der mobile Einsatz in Fahrzeugen ist denkbar.

Diese Arbeit beschäftigt sich mit der Modellierung und Regelung von Festoxid Brennstoffzellen für stationäre Anwendungen – im Speziellen mit dem Aufheizvorgang über den Kathodenpfad. Mit einer Betriebstemperatur von 800 bis 900 °C, zählt diese Art der Brennstoffzelle (engl. *Solid Oxide Fuel Cell*, SOFC) zu den Hochtemperatur Brennstoffzellen. Das Erreichen solch hoher Temperaturen, ohne dabei Komponenten durch zu schnelles Aufheizen oder Überhitzen zu beschädigen, stellt eine Herausforderung für den Regelalgorithmus dar. Praktische Test sind zeitaufwändig und teuer, daher wird in dieser Arbeit ein Simulationsmodell des Systems entwickelt. Mit dessen Hilfe ist es möglich, Regelstrategien zu entwickeln ohne teure Tests durchführen zu müssen.

Als Basis dient ein SOFC Prototyp ($\approx 10\,\mathrm{kW_{el}}$), welcher von der AVL List GmbH entwickelt wurde. Die mathematischen Modelle aller notwendigen Komponenten werden mit Messergebnissen des Prototypen abgeglichen um schließlich ein Gesamtsystem zu erstellen. Anschließend wird eine Reglerstruktur vorgestellt, welche den gesamten Aufheizvorgang automatisch durchführt und dabei sämtliche Grenzwerte einhält.

Contents

List of Figures

List of Tables

List of Symbols

Abbreviations

ACMP	Anode Compressor
AFC	Alkaline Fuel Cells
AHEX	Anode Heat Exchanger
AVL	Anstalt für Verbrennungskraftmaschinen List GmbH
BRNR	Burner
BTHR	Bypass Throttle Valve
CAT	Catalytic Converter
CCMP	Cathode Compressor
CHEX	Cathode Heat Exchanger
CTLR	Controller
EG	Exhaust Gas
FC	Fuel Cell
FCS	Fuel Cell Stack
FG	Forming Gas
JCTN	Pipe Junction
MCFC	Molten Carbonate Fuel Cells
MFLD	Manifold
NG	Natural Gas
PAFC	Phosphoric Acid Fuel Cells
PEMFC	Polymer Electrolyte Membrane Fuel Cell
PLNT	Plant Model
RTHR	Reformer Throttle Valve
SOFC	Solid Oxide Fuel Cell

Chemical Symbols

Ar	argon
$C_{12}H_{26}$	dodecane
C_2H_6O	ethanol
C_3H_8	propane
C_4H_{10}	butane

C_8H_{18}	octane		
CH_4O	methanol		
CH_4	methane		
CO_2	carbon dioxide		
CO	carbon monoxide		
H_2O	water		
H_2	hydrogen		
KOH	potassium hydroxide		
$LiAlO_2$	lithium aluminate		
N_2	nitrogen		
NOx	nitrogen oxide		
O_2	oxygen		
Y_2O_3	yttrium oxide		
ZrO_2	zirconium oxide		

Symbols

α	throttle plate angle		°
$\bar{R}$	universal gas constant		J/(mol K)
$\boldsymbol{\mu}$	mass concentration vector	14×1	kg/kg
ΔH_R	reaction heat		W
$\dot{m}$	mass flow		kg/s
$\dot{Q}$	heat flow		W
$\dot{W}$	heat capacity flow		W/K
η	efficiency		–
γ	ratio of specific heat capacities c_p/c_v		–
λ	air to fuel ratio		–
λ_f	friction coefficient		–
$\dot{\mathbf{m}}$	mass flow vector	14×1	kg/s
μ	dynamic viscosity		Pa s
ν	volume ratio		m³/m³
ω	angular velocity		red/s
ρ	density		kg/m³
ϑ	temperature		°C
A	area		m²
C_d	discharge coefficient		–
c_p	heat capacity		J/(kg K)
d, l, r	pipe dimensions: diameter, length and radius		m
f_{stoi}	stoichiometric constant		–
H_i	lower heating value		kWh/kg
I	electric current		A
k	thermal transmittance		W/(m² K)
M	molar mass		g/mol
m	mass		kg

n	number of mol	–
p	absolute pressure	Pa
R	heat capacity flow ratio	–
R	specific gas constant	J/(kg K)
Re	Reynolds number	–
T	temperature	K
T_s	sample time	s
u, U	voltage	V
V	volume	m^3
v	fluid velocity inside the pipe	m/s

1

Introduction

The fuel cell technology can offer many advantages over conventional energy conversion methods, for example high efficiency and little to no emissions. Although the principle is known for almost 180 years, there are not many applications yet. Due to very high temperatures, the operation involves complex control loops for thermal management and all (electro-) chemical reactions. In the past years, several fuel cell prototypes for both stationary and mobile applications have been developed by AVL List GmbH. This thesis focuses on the thermal behavior of high temperature fuel cells, and methods to reach operating temperature in every part of the system. To do so, mathematical models are developed to use computer simulation as a tool for control design. Measurements from the prototype are used to validate these models.

In this chapter, the basics of the fuel cell technology are introduced. It gives an overview over the working principle, different types of fuel cells and the challenges of controlling them. In chapter 2, the technology used in the prototype setup is explained in greater detail. The derivation and validation of every model, as well as the used software architecture is described in chapter 3. Finally a control structure to conduct a complete system heat-up is developed in chapter 4.

1.1 Overview Fuel Cell Technology

Conversion of energy to electricity and transportation in industrialized countries is a major source of air pollutants such as CO, CO_2, SO_2 and NO_x. As a result, the concentration of such greenhouse gases in the earth's atmosphere increased

significantly in the last century. With rising levels of greenhouse gases, the earth's surface temperature rises as well. Reduction of fossil fuel based energy sources and therefore reducing toxic emissions has become a very important topic in politics all over the world. A potential alternative to conventional energy conversion methods is the fuel cell technology. Fuel cells can convert chemical energy directly to electrical energy, they can work with a number of different types of fuels, have lower emissions and higher efficiency than internal combustion engines. [8]

The historical method of generating electricity using (fossil) fuels is:

- Combustion of the fuel to generate heat

- Boiling water to produce stream

- Run a turbine to produce mechanical energy

- Generate electrical energy from the mechanical energy using a dynamo.

All these steps go along with significant losses. A fuel cell bypasses all the intermediate steps and generates electricity without any moving parts. The only byproducts are heat and water – if pure hydrogen is used as fuel. The hydrogen does not need to be pure but can either be present in a mixture with other gases or as hydrocarbons such as natural gas or Diesel for example. [9, p. 16]

1.1.1 Working Principle

Although there are many different kinds of fuel cells, see section 1.1.3, the underlying principle is the same. A fuel cell consists of two porous electrodes (anode and cathode) separated by an electrolyte which is impermeable to gases but conductive for ions. At the interface between electrodes and electrolyte electrochemical reactions take place. In Proton Exchange Membrane (PEM) fuel cells hydrogen is split into protons and electrons, whereas the protons can travel through the electrolyte, the electrons are conducted by the electrodes and can travel though an electric network to perform work. [9, p. 10] In Solid Oxide Fuel Cells (SOFC) the electrolyte is a solid ceramic material, where oxygen atoms gather electrons at the cathode, form ions and then migrate through the oxide to the anode. At the anode side the oxygen ions react with H_2 or other fuels (e.g. CO or CH_4) and liberate electrons. The reaction products are H_2O (or CO_2) and heat. [10, p. 2][p2]. With different electrolytes the operating temperature and required peripheral components vary. SOFCs have a high operating temperature of around $850\,°C$ to $1000\,°C$ which poses many challenges in the thermal management. However a benefit is the flexibility in usable fuels due to the reforming process. The working principle of SOFCs is discussed in greater detail in chapter 2.

1.1.2 Historic Overview

The fuel cell principle was discovered by Sir William R. Grove[1] in 1839. For almost a century the idea remained untouched until the British scientist Francis T. Bacon[2] started working on a practical version in 1937. In 1959 he finished developing a working $6\,kW$ model. The U.S. Space Program was the first to use polymer electrolyte membrane fuel cells, developed by General Electric, in the Gemini Program. Also the Apollo Program used fuel cell technology to power different systems on the spacecraft. Until today the U.S. Space Program used fuel cells continuously, however little to no systems were developed for terrestrial applications until the 1990s. After a fuel cell powered submarine and bus, Perry Energy Systems built the first passenger car running on a polymer electrolyte membrane (PEM) fuel cell in 1993. Many car companies followed and had working prototypes by the end of the century. Even if the technology could not compete against the cheap oil then, the interest remained, as the number of filed patents on this topic shows. [9, p. 21]

1.1.3 Different Kinds of Fuel Cells

As mentioned earlier there are several different types of fuel cells with different properties, operating temperatures and therefore applications. They can be distinguished by the type of electrolyte they use and their operating temperatures. The following listing should give a brief overview over the technologies.

- **Polymer Electrolyte Membrane (PEMFC)**
  An ion exchange membrane is used as electrolyte. Since the membrane needs to be hydrated, the operation needs to be controlled in a range where the byproduct water does not evaporate faster than it is formed. Due to the critical water balance and a low operating temperature of the polymer (usually below $120\,°C$), pure or H_2-rich gas is used as fuel. [1, p. 17]

- **Alkaline Fuel Cells (AFC)**
  In AFCs concentrated potassium hydroxide (KOH) is used as electrolyte. The concentration depends on the operating temperature ($85\,\%$ by weight for $\approx 250\,°C$ and $35\,\%$ to $50\,\%$ by weight for temperatures below $120\,°C$). The carrier material is usually asbestos and a wide range of catalysts can be used. In AFCs the fuel needs to be very pure since CO is a poison and even the small amount of CO_2 in the air can react with the KOH. Typically pure H_2 is used as fuel. [1, p. 17]

- **Phosphoric Acid Fuel Cells (PAFC)**
  The electrolyte is phosphoric acid retained in silicon carbide. The operating

---

[1] William Robert Grove (1811 - 1896), British judge and physical scientist.
[2] Francis Thomas Bacon (1904 - 1992), British scientist.

temperature is between 150 °C to 220 °C. The ionic conductivity at lower temperatures is poor and CO poisoning of the electrocatalyst in the anode, typically made of platinum (Pt), takes place. The concentrated acid reduces the required water vapor pressure and therefore water management is simpler than in PEMFCs. [1, p. 18]

- **Molten Carbonate Fuel Cells (MCFC)**
  Usually a combination of alkali carbonates, retained in a ceramic matrix of lithium aluminium oxide ($LiAlO_2$) is used as electrolyte. The operating temperature is between 600 °C to 700 °C. At these high temperature the alkali carbonates form a highly conductive salt which provides also ionic conductivity. Noble metals as electorcatalysts are not required.

- **Solid Oxide Fuel Cells (SOFC)**
  A nonporous metal oxide is used as electrolyte, usually a zirconium oxide (ZrO_2) stabilized with yttrium oxide (Y_2O_3). The ceramic electrolyte conducts oxygen ions from the cathode to the anode. Operating temperatures are as high as 1000 °C where ionic conduction of oxygen ions takes place. The efficiency achievable by SOFC systems can be above 60 % and different fuels can be processed due to the high operating temperature. To reduce corrosion, often expensive materials are required. [11, p. 26]

Another key difference between the types of fuel cells, despite the composition of the electrolyte is the charge carrier. In low temperature fuel cells (PEMFC, AFC, PAFC) the charge carriers are protons and hydroxyl ions. In high temperature fuel cells (MCFC and SOFC) carbonate and oxygen ions carry the charge through the electrolyte. In Fig. 1.1 the path of the charge carriers for each kind of fuel cell is visualized.

1.1.4 Advantages and Disadvantages

This section should name and briefly introduce some of the most promising properties, as well as some potential downsides of the fuel cell technology.

Advantages

- **High efficiency** – The fuel cell efficiency exceeds the efficiency of internal combustion engines and traditional power plants. Dependent on the fuel process SOFCs can achieve an efficiency of 55 % to 65 %. [2]

- **Low to zero emissions** – Even if fossil fuels are used, in general the emissions are lower then those of conventional energy conversion methods. If pure hydrogen is used, the only waste products are heat and water. However hydrogen is not readily available and if hydrocarbons (like methanol, natural gas, Diesel...) are used, the greenhouse gas CO_2 is produced. [9, p. 12]

- **No moving parts** – Another big advantage over combustion engines is the
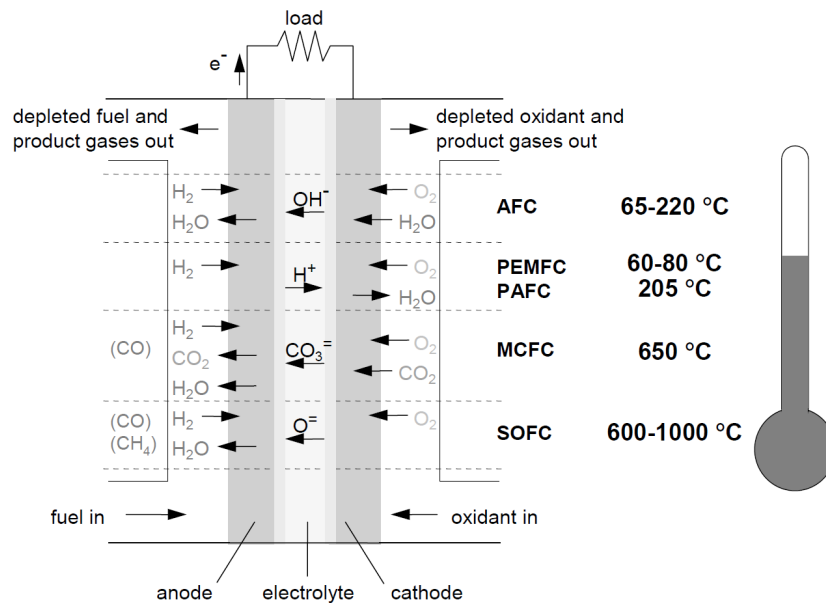
Figure 1.1: *Charge carriers in different fuel cells technologies. [9, p. 9]*

lack of moving parts. Besides the air blower, fuel pump and valves, there are no moving parts. Therefore no lubrication, oil change or rebores are necessary. The construction of a fuel cell stack is generally very simple and manufactured in large quantities, the cost could drop significantly.

- **Modularity** – If more power is required, more cells can be added. This makes up a very easily scalable system. It could be beneficial to the power grid to add more, smaller fuel cells since big power plants need extensive planing and the permitting process can be cumbersome.

- **Low noise** – The fuel cell itself is completely quiet, however some additional equipment may be required, for example an air blower. This qualifies the technology for application in houses or cars.

- **Residential application** – Fuel cell technology in residential applications can be benefitial as the waste heat can be used to heat water and the strain on the electricity grid is reduced. [11, p. 50]

Disadvantages

- **Availability of hydrogen** – Hydrogen is not a readily available fuel. It can be produced using electrolysis of water or by reforming hydrocarbon fuels. Water electrolysis has an efficiency of around 70 %, combined with a fuel cell efficiency of 65 % (in optimal conditions) half of the energy is wasted during the process. [9]

- **High cost** – Conventional combustion engines can be produced for as little as

$50\,\$/kW_{el}$ (not including a generator and other required components), whereas SOFCs are currently being manufactured for about $10\,000\,\$/kW_{el}$. Although mass production could decrease the price like it did for combustion engines. [10]

- **Expensive materials** – The high cost of a fuel cell is primarily because of the need of expensive materials (e.g. sulfonated fluoropolymers and noble metals). Cheaper materials and mass production techniques must be found.

- **Long start-up time (heat up)** – Depending on the type of fuel cell and the required operating temperature, the start-up time can be as long as several hours which poses a challenge in mobile application like cars.

- **Relatively slow response time** – Short current peaks, like they occur in automotive applications, can not be supplied by a fuel cell, since the reaction is comparatively slow. For such applications a battery, or some other form of energy storage, e.g. capacitor, is inevitable.

- **Storage of Hydrogen** – Pressurized hydrogen at $200\,bar$ results in relatively large tanks ($60\,liters/kg\ H_2$). Liquefaction uses about one-third of the energy stored in the liquid hydrogen and is therefore only suitable for aerospace applications, where achieving a high energy density is essential. Metal hydride storage is a safe storage form where the hydrogen atoms are embedded inside the lattice of the metal. However to form this bond, heat must be applied and more energy is lost.

Below $50\,kW_{el}$, combustion engines are not very economic. This may be a potential market for the fuel cell technology. Decades of development and mass use of the internal combustion engine technology decreased the price significantly. [10]

1.2 Motivation and Objective

As discussed in the section above, the fuel cell technology can offer many advantages over conventional energy conversion methods. However there are still many areas in which improvements are necessary, to make this technology competitive.

At AVL a stationary SOFC prototype system has been developed to be used in stationary applications like small power plants ($< 10\,kW_{el}$). Controlling this system illustrates a big challenge, since the components are very expensive and sensitive. Designing control strategies is time consuming and must be done very carefully.

The entire system involves physical, chemical and electrical domains, linked together. The task of developing a simulation model is therefore split into more segments. In this thesis the cathode air path is investigated in order to setup a computer simulation. The main objective is to model the thermal behavior as well as the dynamic gas flow throughout the system to use simulation as a tool for con-

trol design. Since the heat up procedure is currently done primarily by hand and takes several hours, computer simulation can drastically speed up the development process of control algorithms. In addition, expensive and sensitive components can be involved only if the system is tested well enough. Electrochemical procedures will be addressed in future research.

2

Solid Oxide Fuel Cells

In this chapter the operation of solid oxide fuel cells (SOFC) is investigated in more detail. Basic chemical processes, commonly used materials as well as the required peripheral components will be discussed. At the end of this chapter, the heat-up process and all involved actuators are explained to identify the required control loops.

2.1 Working Principle

SOFCs are galvanic elements which convert fuel without direct combustion or open flame. Because of the separation of fuel (at the anode, negative electrode) and oxygen (at the cathode, positive electrode) by the electrolyte, the reduction and oxidation reactions take place apart from one another. [1, p. 15] During these reactions, electrons are freed at the anode and collected at the cathode. This charge separation creates a potential difference between the electrodes which can be utilized by connecting an electric load. In Eq. 2.1 and 2.2 below, the chemical reactions at cathode and anode are stated.

Cathode Reaction:

$$\tfrac{1}{2}\,O_2(g) + 2\,e^- \longrightarrow O^{2e^-} \qquad (2.1)$$

Anode Reaction:

$$H_2(g) + O^{2e^-}(s) \longrightarrow H_2O(g) + 2\,e^- \tag{2.2}$$

$$H_2 + \tfrac{1}{2}O_2 \longrightarrow H_2O \tag{2.3}$$
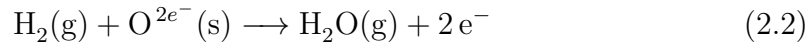
The porous electrodes are absorbing the gaseous oxygen and hydrogen molecules and dissociation takes place. This means that oxygen atoms gather two electrons each to form ions. The electrons are charging the conductive electrodes to different potentials, which depends on the equilibrium of adsorption and desorption. An electric connection (e.g. an ohmic load) disturbs the potential and the oxygen ions are attracted by the positively charged anode. They can travel through the electrolyte which is conducting ions but no gas or electrons. At the anode the oxygen ions react with hydrogen to water vapor, and the electrons are collected at the anode. In Fig. 2.1 the path of the molecules is illustrated. [2, p. 8]
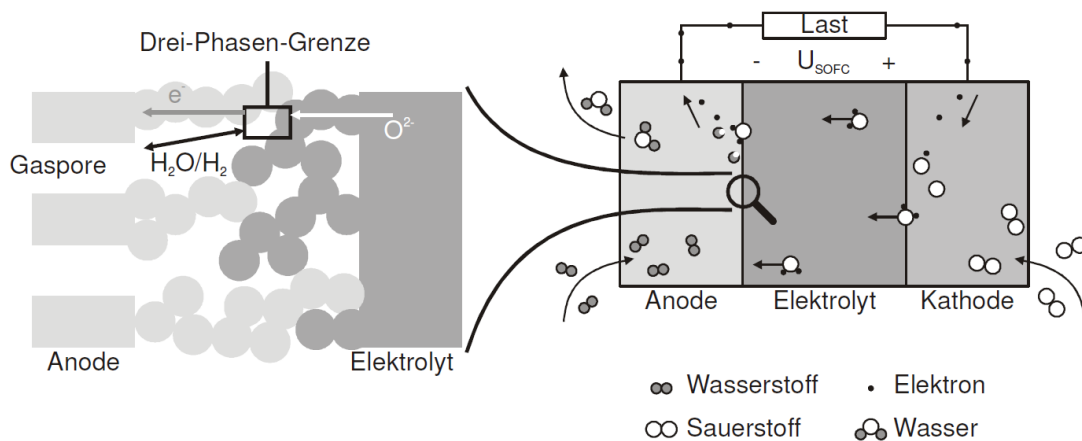
Figure 2.1: *Solid Oxide Fuel Cell (SOFC) principle. [2, p. 9]*

A different application of the fuel cell reaction is the oxygen (lambda) sensor in internal combustion engines. The same principle is used to measure the oxygen content in the exhaust gas. [10]

2.1.1 Materials

The electrolyte material needs to be gas tight, conductive to ions but not to electrons. It should also be mechanically durable and stable during oxidation and reduction reactions. The most commonly used material is zirconium oxide ZrO_2 with $8\,mol\%$ yttrium oxide Y_2O_3 doping. The doping with Y_2O_2 results in holes in the lattice, where O^{2-} ions can propagate. The charge transport is highly dependent on impurities caused by the manufacturing process and is only acceptable from $700\,°C$ and up. [2]

The cathode needs to withstand the oxidation reaction, act as a catalyst and conduct electrons. Also thermal properties need to be in the same range as the electrolyte to keep mechanical tension to a minimum. Presently the most commonly used material is strontium doped lanthanmanganat (LSM). This material is a p-type semiconductor and therefore conducts electrons well at high temperatures. The expansion coefficient is also a good match to the electrolyte. [2]

Similar to the cathode, the anode needs to be a good conductor, of porous structure to allow gas transport and it needs to have the same expansion coefficient as the electrolyte. The reduction reaction must be tolerated by the material as well. Typically Nickel-Zirkonium-Cermet is used. It is not only a catalyst for the cell reaction but also for the steam reformation of methane. A nickel content of 30 % or higher is required to get continuous conductive paths. [2, p. 35]

To increase the output voltage from $< 1\,\mathrm{V}$ per cell to usable values, cells are stacked and connected in series. To do so, a connective material is required between the cells. The material has to be gas tight, conductive to electrons and it needs to have similar thermal properties as the electrodes. Typically strontium or magnesium doped lanthanchromat ($\mathrm{La}_{1-x}\mathrm{Mg}_x\mathrm{CrO}_3$, $x = 0.02\dots0.1$) is used.

2.1.2 Steam Reforming

As mentioned before, one advantage of SOFCs is the flexibility in fuels. Many kinds of hydrocarbons can be used, however in the end the energy carrier is hydrogen. It is possible to convert CO or CH_4 and also generate electricity but this requires different materials and is not a topic of this thesis. Since water electrolysis is not economical to produce hydrogen at this time, usually hydrogen rich fossil fuels like natural gas, Diesel but also bio-fuels are used. A high H/C ratio is preferred due to smaller CO_2 emissions. Most important in stationary applications is therefore natural gas. To provide an H_2-rich gas to the fuel cell, steam reformation is needed. It is an endothermic, catalytic process to break up hydrocarbons using water vapor, hence the name.

The following equation shows the endothermic chemical reaction of the steam reforming process for general hydrocarbons and especially methane. Note that the reaction is endothermic, so the reaction enthalpies ΔH^0 are negative. [12, p. 14] [2, p. 21]

$$\mathrm{C}_x\mathrm{H}_y + x\mathrm{H}_2\mathrm{O} \longrightarrow x\mathrm{CO} + (x + y/2)\mathrm{H}_2 - \Delta H^0 \qquad (2.4)$$

$$\mathrm{C}_x\mathrm{H}_y\mathrm{O}_z + (x - z)\mathrm{H}_2\mathrm{O} \longrightarrow x\mathrm{CO} + (x - z + y/2)\mathrm{H}_2 - \Delta H^0 \qquad (2.5)$$

$$\mathrm{CH}_4 + \mathrm{H}_2\mathrm{O} \longrightarrow \mathrm{CO} + 3\,\mathrm{H}_2 - \Delta H^0 \qquad (2.6)$$
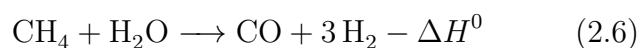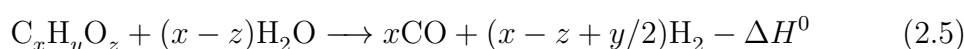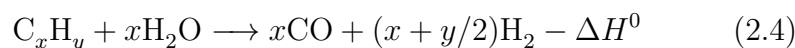
The enthalpy change for methane reformation with gaseous H_2O is for example $\Delta H^0 = 206\,\text{kJ/mol}$ at ambient pressure $0.1\,\text{MPa}$ and $298\,\text{K}$. [12, p. 10] The production of the synthesis gas (right hand side of the equation) requires a catalyst, typically metals of the VIII group (e.g. nickel). The highest hydrogen ratios ($72\,\%$) can be achieved at low pressures and a temperature of $680\,°\text{C}$. Steam reforming typically takes place in a separate component (so in the prototype) but could potentially be done at the anode of the fuel cell. The heat and water of the fuel cell reaction is then used for the reforming and external heat/vapor supply is not required. [2, p. 21]

To avoid carbon deposits which can cover the catalytic area and slow down the reformation, usually more water vapor is supplied than the stoichiometric required amount. A steam-to-carbon ratio (S/C) greater than 1 means that also water vapor is present in the reformat.

2.2   Prototype System

The fuel cell and the steam reformer (explained above) are the central processes in an SOFC system. However there are a number of other components required to run such a system. In this section the working prototype developed at AVL is explained with all its components. In chapter 3 mathematical models for each component are developed. A flow-sheet of the complete system is shown in Fig. 2.2.
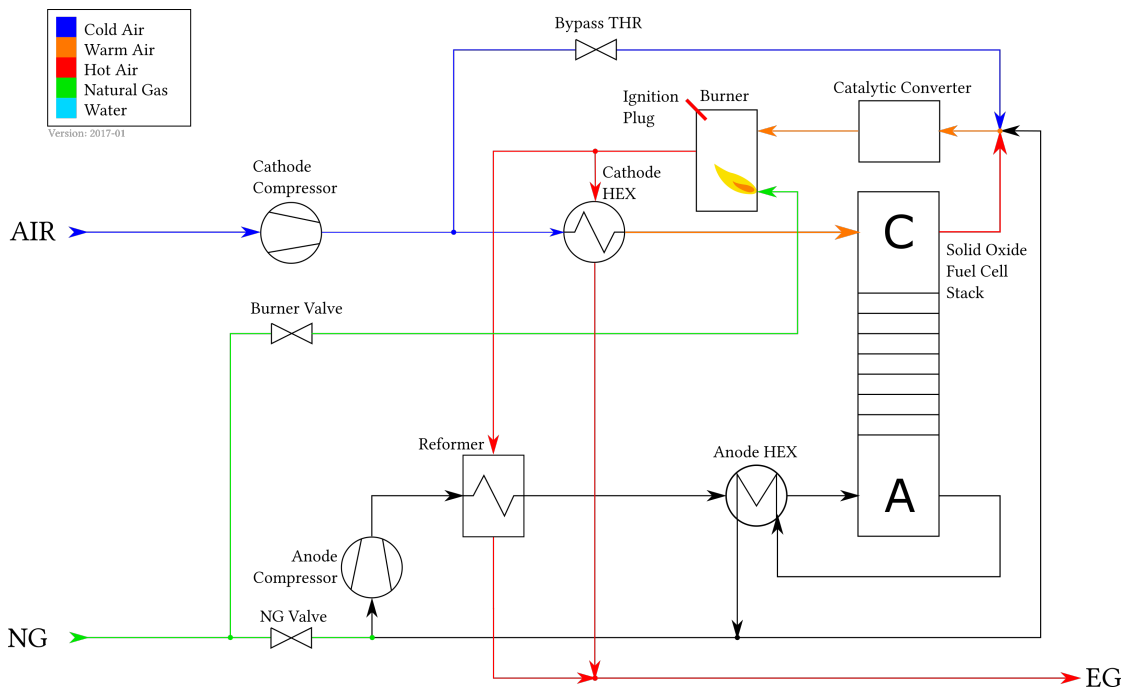
Figure 2.2: *SOFC prototype flow-sheet.*

Fuel Cell Stack:
The fuel cell stack is the central component of the system where. Typically 30 to 80 fuel cells are stacked to achieve higher operating voltages. Besides the conversion of H_2, also CH_4 and CO can be converted to electric energy. It is common to consider only the H_2 reactions, since the others are comparatively small. [1]

Reformer:
The reformer is situated in the anode path and contains nickel based catalyst pallets. It is responsible to convert hydrocarbons to a hydrogen rich gas. A secondary gas stream, controlled by a throttle valve, heats up the unit to its operating temperature.

Cathode Compressor:
The cathode compressor drives the air supply to the cathode, as well as the hot air flow to the cathode heat exchanger and reformer.

Catalytic Converter:
The anode and cathode exhaust gas is mixed after the fuel cell stack and then piped into a catalytic converter. It is capable of converting residual H_2 and CO at lower temperatures and is needed to lower the emissions.

Burner:
To heat up the entire system to operating temperature, a start-up burner is used. The hot air leaving the burner is used to heat up the fuel cell stack and the reformer. To ignite the air/fuel mixture, two ignition plugs are mounted inside.

Heat Exchangers:
The gas entering both anode and cathode is preheated by heat exchangers. For the cathode heat exchanger, during start up the hot gas is heated by the burner. During operation the cathode exhaust gas is hot enough to supply the energy. The heat exchangers can operate at temperatures up to $900\,°C$.

Throttle Valves:
There are valves which are primarily used for thermal management of the system. The bypass throttle is used to control the air flow through the cathode heat exchanger and therefore the energy transferred to the fuel cell stack.

Anode Compressor:
The compressor in the anode path is used to recirculate the anode exhaust gas. This increases the fuel utilization.

During operation the complete system is submerged in insulation material to reduce thermal losses to the environment. In Fig. 2.3 the prototype is visualized where the fuel cell stack is replaced by bypass pipes for testing purposes.

Figure 2.3: *Prototype without stack. (AVL)*

2.2.1 System Operation

Although the system is being developed to run on various types of fuels, during this work all tests were performed with Diesel. In this section the operation procedure is described.

The upper part of the schematic in Fig. 2.2 represents the cathode supply path. The cathode compressor forces fresh air through the cathode heat exchanger to heat it up. The hot air then enters the cathode of the fuel cell stack, where the main fuel cell reaction takes place. This reaction is exothermic, so the air gets heated up to the stack operating temperature. Downstream of the stack, the cathode and anode exhaust gas gets mixed with cold air, which can be controlled via the bypass throttle valve. Then this mixture enters the catalytic converter to burn the residual H_2 (to H_2O) and CO (to CO_2).

After this stage, the air enters a start-up burner which is only needed during start up of the system. The amount of burnt fuel can be controlled to achieve an outlet temperature of 850 °C. The air leaving the burner is heating the cathode heat exchanger as well as the reformer. After the system is heated to its operating temperature, the burner can be turned off since the energy released in the fuel cell and catalyst is enough to hold the temperatures. Forming gas[1] (FG) is used to protect the anode during different operating modes in which no fuel is supplied (e.g. during heat up).

---

[1] Forming gas consists of 5 % H_2 and 95 % N_2 and has to be stored in a tank.

If current wants to be drawn from the stack, hydrogen needs to be supplied to the anode. In the anode path there is a recirculation compressor to control the amount of reused anode exhaust gas. This way the hydrogen utilization can be increased.

2.3 Actuators and Control Loops

The prototype features many sensors spread throughout the system. All sensor values are currently logged by a National Instruments CompactRIO (cRIO) system. The logged signals are important for the modeling of each component, described in chapter 3.

The controlled variables in the system are listed below:

- Cathode air mass flow,

- Anode fuel mass flow,

- Bypass air mass flow,

- Burner ignition plugs,

- Burner fuel mass flow,

- Reformer hot air mass flow and

- Recirculation mass flow.

As mentioned earlier, this thesis' objective is to find a suitable strategy to heat up the fuel cell stack as fast as possible and as slow as necessary. The ceramic electrolyte is very brittle and could break if the temperature gradient is too high. The dependencies of all manipulated variables (actuators) and system variables (primarily temperatures) are very complex, so at first the required control loops are identified. Since there are no temperature sensors inside the FCS, the main control variable is the temperature of the gas leaving the cathode.

Loop1: Cathode Air Mass-flow
The air mass flow provided by the cathode compressor determines how much energy is transmitted into the fuel cell stack. The cathode air compressor has an on-board speed controller and a mass-flow sensor at the air inlet is also available.

Loop2: Burner Downstream Temperature
The gas leaving the burner is fed into the cathode heat exchanger and the reformer. To achieve reasonable emission levels, the temperature must be between $800\,°C$ to $1000\,°C$. However the maximum inlet temperature of the cathode heat exchanger is $900\,°C$, which also needs consideration. The manipulated variable in this control loop is the injected fuel quantity.

Loop3: Cathode Heat Exchanger Mass-flow
The cathode heat exchanger preheats the gas entering the stack. The ratio between hot and cold gas streaming through the unit has an influence on the transmitted energy. More cold than hot gas leads to a lower outlet temperature and vice versa. The flow ratio can be controlled by the bypass throttle valve. To reach the operating temperature of the stack, the cold air flow needs to be smaller towards the end of the heat-up process to achieve higher temperatures.

Additional Loops
Outside of the scope of this thesis are the amount of fuel at the anode, the water supply and evaporator for the reforming process and the recirculation of the anode exhaust gas.

To implement the proposed control loops above, it is important to have good mathematical models, especially for the mass flow and temperatures through each component. Big temperature gradients of several hundred degrees throughout the system pose a challenge. In addition the models should be parameterizable and modular to allow architectural changes or reuse in different projects.

3

Modeling of the Cathode Airpath

In this chapter the different components are modeled individually with the objective to connect them together to a full system (see section 3.11). The key components are the cathode compressor (CCMP), the cathode heat exchanger (CHEX), bypass throttle valve (BTHR), fuel cell stack (FCS), catalytic converter (CAT) and start up burner (BNR). For thermal simulation of the system it is important to know the fluid mass flow in each section. Due to chemical reactions inside the catalytic converter as well as in the fuel cell stack and reformer (REF), heat is generated or consumed in certain components.

In Fig 3.1 the cathode path is drawn to see all relevant components in this part of the system. The diagram also shows all sensors which are available (T for temperature, and P for pressure). In addition to these sensors, there is also an air mass flow sensor ($\dot{m}_{air}$) in the intake manifold. All other mass flows are not measured. Test runs on the real system have been performed by AVL and the resulting data was used during modeling.
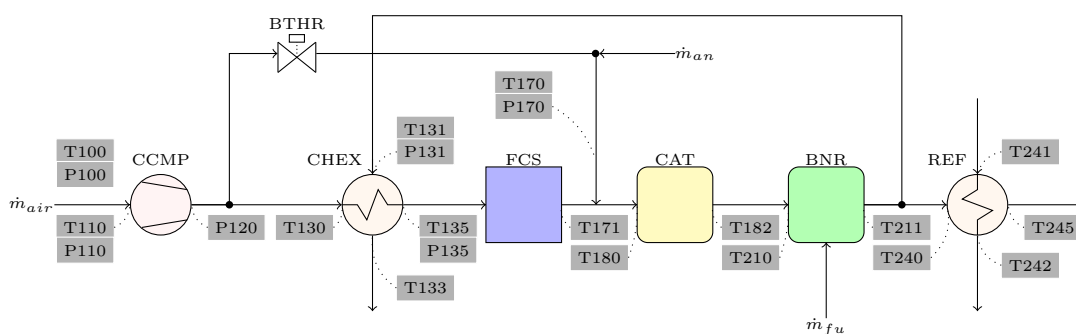
Figure 3.1: *Schematic of the cathode path with sensor positions.*

3.1 Cathode Compressor Model

The first component in the cathode path is a compressor. It supplies the cathode with oxygen but also plays an important role during the heat-up of the system, since air is the medium used to transmit energy and manage the temperatures. In Fig. 3.2 a block diagram shows all inputs and outputs, as well as the states of this component. [13]
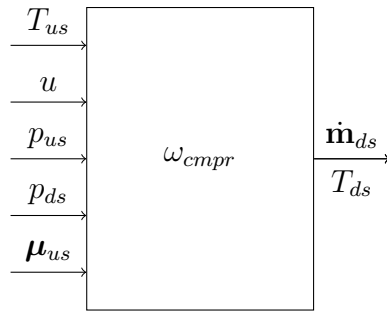
Figure 3.2: *Schematic of the cathode compressor.*

T_{us} is the temperature of the upstream gas [K],
u is the operating voltage [V],
p_{us} is the pressure at the inlet [Pa],
p_{ds} is the pressure at the outlet [Pa],
$\boldsymbol{\mu}_{us}$ is the mass concentration vector of the upstream gas [kg/kg],
ω_{cmpr} is the angular velocity [rad/s],
$\dot{\mathbf{m}}_{ds}$ is the downstream mass flow vector [kg/s] and
T_{ds} is the temperature of the downstream gas [K].

The mass flow leaving the compressor $\dot{\mathbf{m}}_{ds}$ is handled as a vector of 14 gas species. In the model, this vector is passed between all components because the composition of gases is important to know for chemical reactions (e.g. in the catalyst, burner, reformer or fuel cell). Some gas properties like heat capacity and enthalpy are also temperature dependent. The gases contained in the vector are listed in Tab. 3.1. Since the compressor is a mass flow source, one input is the composition of gases at the inlet as a mass concentration vector $\boldsymbol{\mu}_{us}$. The composition of air in mass concentration μ and volume concentration ν is given in Tab. 3.1.

The compressor is equipped with an industrial controller which is well tuned for the given system. The rotor speed is controlled according to the measured mass flow at the inlet. A compressor is usually characterized by a 2D look-up table with inputs rotor speed and pressure difference.

Since the compressor map is not available and the controller is performing very well, the cathode compressor was considered to be a constant mass flow source. To model the step response of the system, the demand value is filtered by a cascade of four PT_1 elements (see Fig. 3.3).

Table 3.1: *Gas vector species and air composition [6]*

Nr.	Gas	Name	Molar Mass [g/mol]	μ_{air} [kg/kg]	ν_{air} [m^3/m^3]
1	CO	carbon monoxide	28.01	0	0
2	CO_2	carbon dioxide	44.0095	0.000 58	0.000 40
3	H_2O	water	18.015	0	0
4	H_2	hydrogen	2.0159	0	0
5	CH_4	methane	16.043	0	0
6	O_2	oxygen	31.9988	0.231 35	0.209 46
7	N_2	nitrogen	28.0134	0.755 18	0.780 84
8	Ar	argon	39.948	0.012 88	0.009 34
9	C_3H_8	propane	44.097	0	0
10	C_4H_{10}	butane	58.123	0	0
11	C_2H_6O	ethanol	46.069	0	0
12	CH_4O	methanol	32.042	0	0
13	$C_{12}H_{26}$	dodecane	170.337	0	0
14	C_8H_{18}	octane	114.231	0	0

The first order low-pass filter (PT_1) is an element that is used several times in the system. We therefore give a short explanation at this point. The continuous time transfer function is given by:

$$H(s) = \frac{K}{1 + \tau \cdot s}, \tag{3.1}$$

where K is the system gain and τ is a time constant. Since the algorithms are implemented in discrete time, the derivation of the difference equation is now stated. The discrete transfer function and difference equation of a first order low-pass filter is given by:

$$H(z) = \frac{1 - \alpha}{1 - \alpha z^{-1}} \tag{3.2}$$

$$y[n] = \alpha \cdot y[n-1] + (1 - \alpha) \cdot x[n]. \tag{3.3}$$

This filter has a single, real pole at α and is therefore stable for $0 \leq \alpha < 1$ (the pole needs to be inside the unit circle). Let T_s be the sample period and τ the desired decay time to reach e^{-1}. Then α is given by

$$\alpha = e^{-\frac{T_s}{\tau}}. \tag{3.4}$$

Typically the decay time constant τ is much bigger than the sample period T_s, so α can be approximated by:

$$\alpha \approx 1 - \frac{T_s}{\tau}. \tag{3.5}$$

If this relation is substituted for α in Eq. 3.2, the final equations are obtained.

$$H(z) = \frac{\frac{T_s}{\tau}}{1 - \left(\frac{\tau - T_s}{\tau}\right) z^{-1}} \tag{3.6}$$

$$y[n] = \frac{T_s}{\tau}(x[n] - y[n-1]) + y[n-1] \tag{3.7}$$

The Simulink implementation of the filter can be found in the appendix (Fig. A.1).
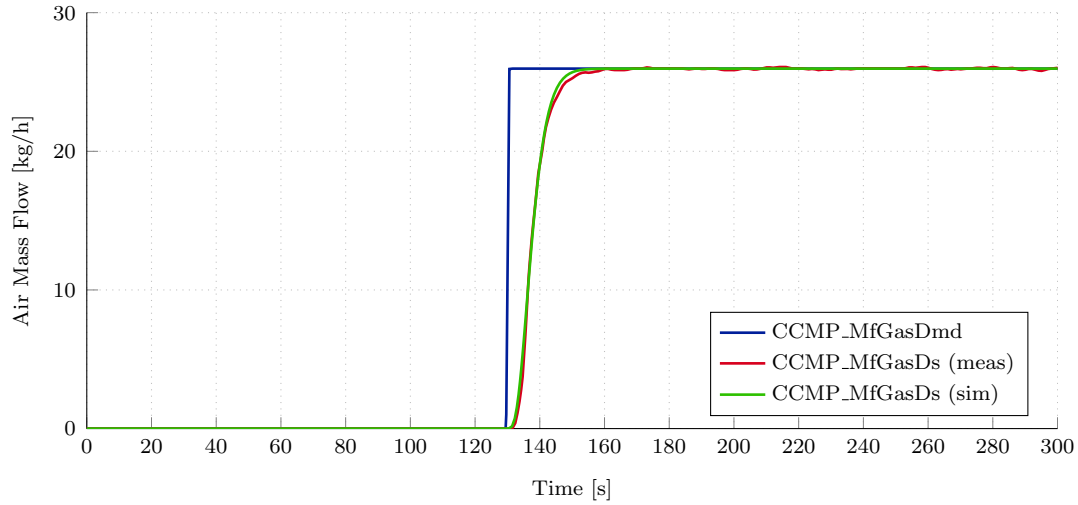
Figure 3.3: *CCMP downstream mass flow demand, measured and modeled.*

At this time there is no need for a detailed model, although a more advanced calculation can be easily inserted in the future. The outlet temperature of the compressor is assumed to be the same as the ambient temperature. This is a simplification because measurement data shows that the temperature does rise to about $40\,°C$. Given the high temperature of the heat exchanger following the compressor, this error can be tolerated. If more data on the compressor turns up in the future (e.g. compressor efficiency), the outlet temperature can be calculated using Eq. 3.8 below. [13, p. 17]

$$T_{ds} = T_{us} + \frac{T_{us}}{\eta_{cmp}}\left[\left(\frac{p_{ds}}{p_{us}}\right)^{\frac{\gamma-1}{\gamma}} - 1\right], \tag{3.8}$$

where T_{ds} is the temperature of the downstream gas [K],
$\quad$ T_{us} is the temperature of the upstream gas [K],
$\quad$ p_{us} is the pressure at the inlet [Pa],
$\quad$ p_{ds} is the pressure at the outlet [Pa],
$\quad$ η_{cmp} is the compressor efficiency [-] and
$\quad$ γ is the ratio of specific heats [-].

The compressor efficiency η_{cmp} can be stored in a lookup table with compressor speed and mass flow as inputs.

3.2 Cathode Heat Exchanger Model

If heat needs to be transfered from one fluid stream to another, both streams are fed into a heat exchanger. The streams are separated by a wall through which the heat transfer from the hot to the cold medium takes place. [14, p. 69]

The prototype features three heat exchangers: one in the cathode air path (CHEX), one in the anode fuel path (AHEX) and the third one is the reformer unit (REF) which is also heated by a secondary gas stream. These heat exchangers play a key role in the system since they are important, not only to heat up the stack, but also to remain its temperature during operation.

Although the overall model described below applies for all three devices, the parameters like size and thermal mass can differ. This section is dedicated to the cathode heat exchanger (CHEX) which is pictured in Fig. 3.4. Cold air is coming from the cathode compressor, entering at the bottom and leaving the CHEX through the center outlet at the top. The hot gas is supplied by the start-up burner and is entering the CHEX at the bottom left. The hot gas is streaming perpendicular to the cold gas (from left to right) as pictured in Fig. 3.4.
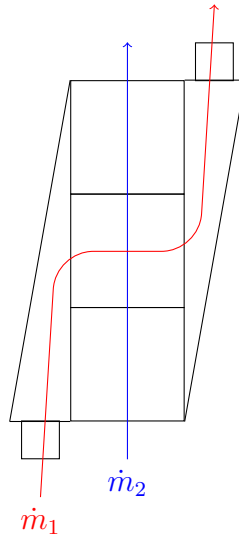
Figure 3.4: *Air flow paths inside of the cathode heat exchanger CHEX.*

At first a basic heat exchanger is explained to understand the principle. In the course of this section, a more complex model is developed which offers a good fit to the measurement data as well as a fast simulation speed.

A heat exchanger seen as a single system is drawn in Fig. 3.5. There are two gas streams with different temperatures, which are separated by a wall but thermally coupled. The unit itself has a mass m_{hex} with a material dependent heat capacity $c_{p,hex}$. This is important for dynamic simulation, because energy is needed to heat up this mass. Although the CHEX is insulated, there is a heat flow to the

environment $\dot{Q}_{env}$. The goal of this subsection is to find a mathematical description of both outlet temperatures.
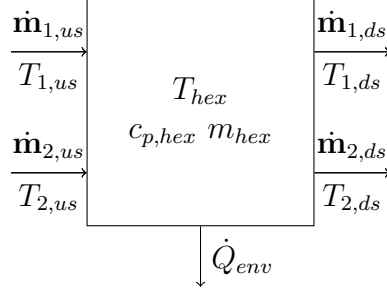
Figure 3.5: *Schematic of the cathode heat exchanger.*

Where $\dot{\mathbf{m}}_1$ is the hot gas mass flow vector [kg/s],
 $\dot{\mathbf{m}}_2$ is the cold gas mass flow vector [kg/s],
 $T_{1,us}$ is the upstream temperature of the hot gas [K],
 $T_{2,us}$ is the upstream temperature of the hot fluid [K],
 $T_{1,ds}$ is the downstream temperature of the hot gas [K],
 $T_{2,ds}$ is the downstream temperature of the cold gas [K],
 $c_{p,hex}$ is the heat capacity of the heat exchanger [J/(kg K)],
 m_{hex} is the mass of the heat exchanger [kg] and
 $\dot{Q}_{env}$ is the heat flow to the environment [W].

There are different types of heat exchangers, primarily distinguished by the direction of the gas flow. In a *parallel-flow* unit both, the hot and cold fluids are streaming in the same direction. The temperature difference between the two gases is decreasing with the length of the heat exchanger, but in practice will never be zero. A different arrangement is to invert one flow direction and thus get a *counter-flow* heat exchanger.

In Fig. 3.6 the temperature curves inside *parallel-* and *counter-flow* heat exchangers are illustrated, where x is the length of the device. One advantage of the counter-flow model is that the outlet temperature of the cold side can be higher than the outlet temperature of the hot side. At first the simpler *parallel-flow* heat exchanger is considered and compared against the measurement data.

The heat flow from one medium to the other, assumed that no heat is lost to the environment, is given in by the following equation. [15, p. 6].

$$\dot{Q} = \dot{m}_1 \cdot c_{p1} \cdot (\vartheta_1' - \vartheta_1''), \tag{3.9}$$

where $\dot{Q}$ is the heat flow [W],
 $\dot{m}_1$ is the mass flow [kg/s] at the hot side,
 c_{p1} is the heat capacity of the hot fluid [J/(kg K)] and
 $(\vartheta_1' - \vartheta_1'')$ is the temperature difference between inlet and outlet [°C].

Note that the hot medium is always denoted with index 1 and the outlet temperature with two dashes: ϑ''. To calculate the output temperature of the cold
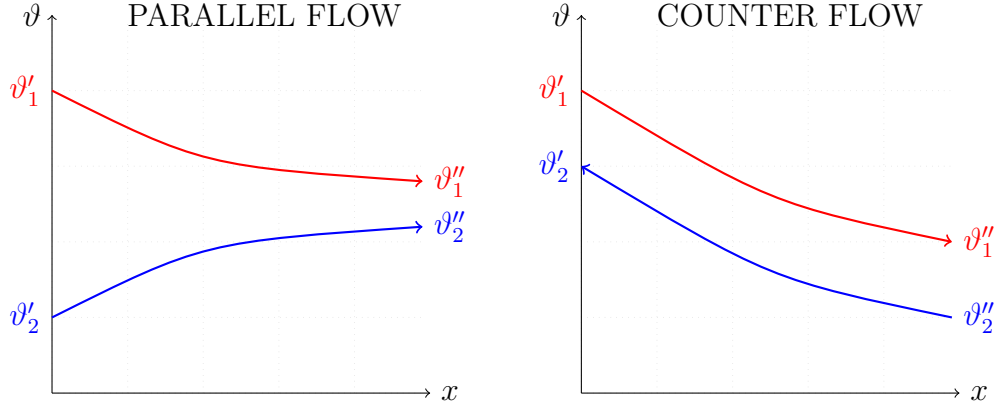
Figure 3.6: *Temperature curves inside a parallel- and counter flow heat exchanger.*

medium, Eq. 3.10 below can be used. This equation does not consider the thermal mass of the heat exchanger and is only valid for stationary conditions.

$$\vartheta_2'' = \vartheta_2' + \frac{\dot{Q}}{\dot{m}_2 \cdot c_{p2}}. \tag{3.10}$$

To model the heat up of the heat exchanger mass, the heat flow difference between hot and cold stream is calculated and the output temperatures ϑ_1'' and ϑ_2'' are assumed to be the same as the heat exchanger temperature.

$$\dot{Q}_1 = \dot{m}_1 \cdot c_{p1} \cdot (\vartheta_1' - \vartheta_{hex}) \tag{3.11}$$

$$\dot{Q}_2 = \dot{m}_2 \cdot c_{p2} \cdot (\vartheta_2' - \vartheta_{hex}) \tag{3.12}$$

$$\dot{Q}_{hex} = \dot{Q}_1 - \dot{Q}_2 \tag{3.13}$$

$$\vartheta_{hex} = \int \frac{\dot{Q}_{hex}}{c_{p,hex} \cdot m_{hex}} \, dt \tag{3.14}$$

The index *hex* denotes the properties of the heat exchanger. Mass and thermal capacity can be derived from the measurements. In practice however, the output temperature of a parallel flow HEX will never reach ϑ_{hex}. This behavior depends on the mass flow of the medium. Very small flow rates result in a smaller error between ϑ_{hex} and the actual outlet temperature ϑ''.

Although the gas properties like heat capacity of exhaust gas and fresh air are very similar, the model passes a gas vector of 14 gas species (see Tab. 3.1) to calculate properties of the gas with greater accuracy. Knowing the composition of gases, Eq. 3.15 is used to calculate the resulting heat capacity.

$$c_{p1,2} = \frac{\dot{m}_1 \cdot c_{p1} + \dot{m}_2 \cdot c_{p2}}{\dot{m}_1 + \dot{m}_2}, \tag{3.15}$$

where the index denotes a certain gas.

The method above is simple, fast and includes dynamic behavior, however it does not model the measurements very well, since the CHEX is of *cross-flow* type.

3.2.1 Cell Approach

In [15, p. 232] a cell based calculation for heat exchangers in stationary conditions is proposed. With this method quite complicated structures can be calculated. In the following we set up a system of equations, two for each cell (hot and cold outlet temperature). The equations are coupled through the outlet temperatures which are used as inputs for following cells. To set up the equations, a number of dimensionless values is used:

The heat capacity flow $\dot{W}$ and the heat capacity flow ratio R:

$$\dot{W}_1 = \dot{m}_1 \cdot c_{p1} \qquad\qquad \dot{W}_2 = \dot{m}_2 \cdot c_{p2} \qquad (3.16)$$

$$R_1 = \dot{W}_1/\dot{W}_2 \qquad\qquad R_2 = \dot{W}_2/\dot{W}_1 \qquad (3.17)$$

NTU denotes the number of transfer units (calculated cells):

$$NTU_{1ges} = \frac{k \cdot A}{\dot{W}_1} \qquad\qquad NTU_{2ges} = \frac{k \cdot A}{\dot{W}_2} \qquad (3.18)$$

$$NTU_1 = NTU_{1ges}/N_{cells} \qquad\qquad NTU_2 = NTU_{2ges}/N_{cells} \qquad (3.19)$$

where k is the thermal transmittance [W/(m^2 K)],
$\quad$ A is the wall area [m^2] and
$\quad$ N_{cells} is the number of cells [-].

The dimensionless temperature change P_1 and P_2 depends on the type of heat exchanger (*parallel-*, *counter-* or *cross-flow*). This is the equation for a cross-flow assembly:

$$P_1 = 1 - \exp((\exp(-R_1 \cdot NTU_1) - 1)/R_1) \qquad (3.20)$$

$$P_2 = 1 - \exp((\exp(-R_2 \cdot NTU_2) - 1)/R_2) \qquad (3.21)$$

General equation for a cell j between two other cells p (previous) and q (following):

$$T_{1j} = (1 - P_1) \cdot T_{1p} + P_1 \cdot T_{2q} \qquad (3.22)$$

$$T_{2j} = (1 - P_2) \cdot T_{2q} + P_2 \cdot T_{1p} \qquad (3.23)$$

The following equations are required if cell j is the first cell for stream 1 or 2:

$$T_{1p} = 1 \tag{3.24}$$

$$T_{2q} = 0 \tag{3.25}$$

If the cell j is the last cell for stream 1 or 2:

$$T_{1j} = (1 - P_1) \cdot T_{1p} + P_1 \cdot T_{2q} = 1 - P_{1,ges} \tag{3.26}$$

$$T_{2j} = (1 - P_2) \cdot T_{2q} + P_2 \cdot T_{1p} = P_{2,ges} \tag{3.27}$$

To calculate the real temperatures from the dimensionless results, the following equation is used:

$$T_{1j} = \frac{\vartheta_{1j} - \vartheta_2'}{\vartheta_1' - \vartheta_2'} \tag{3.28}$$

$$\vartheta_1'' = T_{1j} \cdot (\vartheta_1' - \vartheta_2') + \vartheta_2' \tag{3.29}$$

$$\vartheta_2'' = T_{2j} \cdot (\vartheta_1' - \vartheta_2') + \vartheta_2' \tag{3.30}$$

The index q denotes the previous cold cell outlet temperature and p the hot cell upstream. T_{1j} is the hot outlet temperature of the current cell and T_{2j} denotes the cold outlet temperature. If a cell system of n cells is set up, a system of $2n$ unknowns and $2n$ equations is given. This system can be solved using standard algebraic methods. Detailed description of this method can be found in [15].
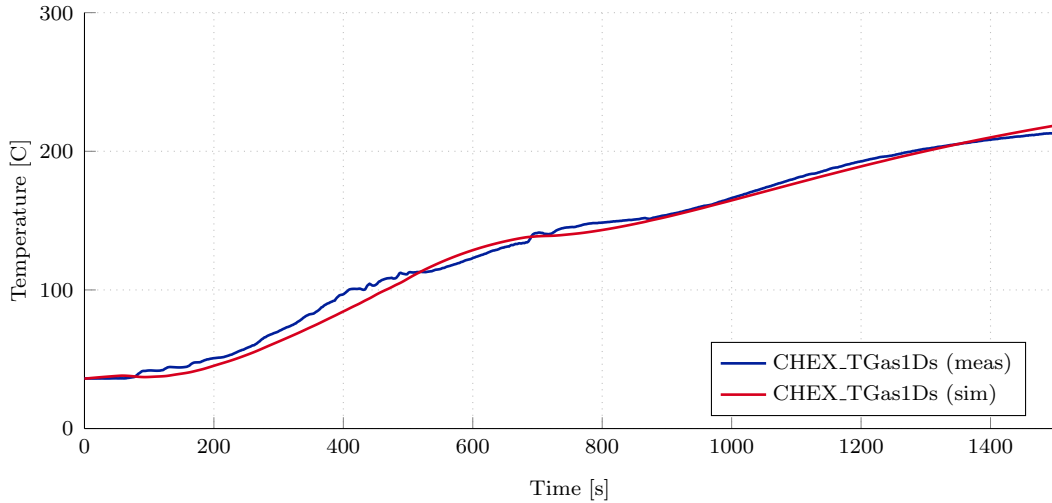
Figure 3.7: *CHEX downstream temperature gas1, measured and modeled.*

Since a single cross-flow cell does not model the HEX very well, a 3 cell implementation was used. The cold stream passes through all cells in a row, while 1/3 of

the hot stream passes only through one cell and gets mixed together at the output. This is due to the geometry of the CHEX (see Fig. 3.4). To model the dynamic behavior, a first order low-pass filter is used at the output. One downside of this method is that no heat flow to the environment is modeled, but it is hidden inside of some parameters.

There was only one usable heat up measurement on which the parameters where fitted by hand. In Fig. 3.7 and 3.8 the outlet temperatures of the models are plotted against the measurements. Although there where big fluctuations in the air mass flow, the results are within a few percent.
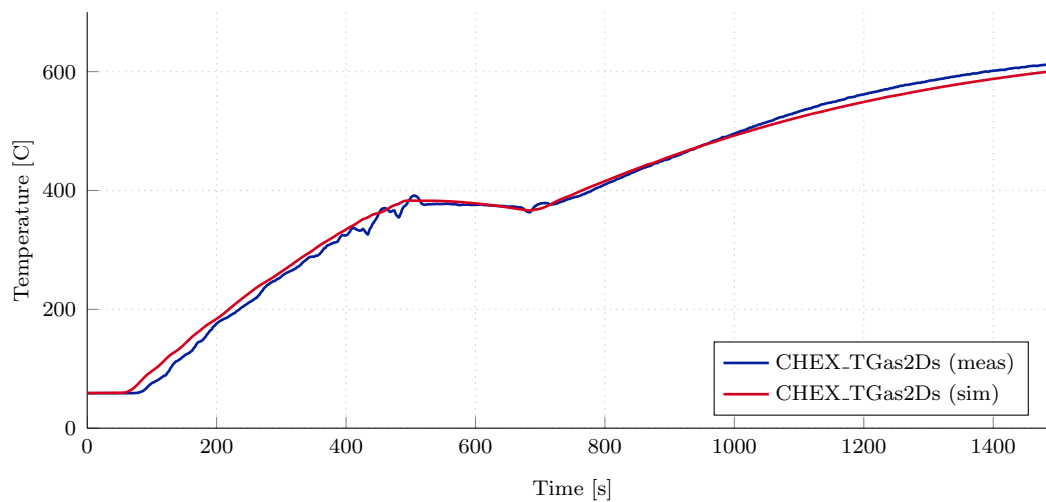
Figure 3.8: *CHEX downstream temperature gas2, measured and modeled.*

3.3 Throttle Valve Model

The prototype features two throttle valves: one to control the air bypass of the CHEX and the other one to control the reformer heating. Both valves are important for the thermal management and have a big influence on the mass flow ratios in the system. Fig. 3.9 shows all inputs and outputs of the component.
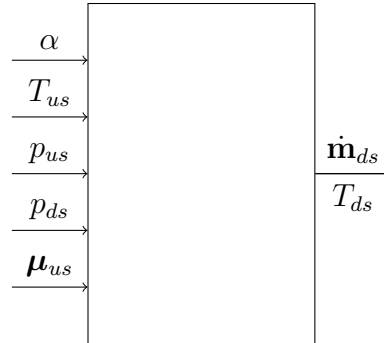
Figure 3.9: *Schematic of a throttle valve.*

Where α is the throttle plate angle [°],
T_{us} is the upstream gas temperature [K],
p_{us} is the pressure before the valve [Pa],
p_{ds} is the pressure after the valve [Pa],
$\boldsymbol{\mu}_{us}$ is the mass concentration vector of the upstream gas [kg/kg],
$\dot{m}_{ds}$ is the mass flow leaving the valve [kg/s] and
T_{ds} is the gas temperature after the valve [K].

Both valves are equipped with a control unit which takes care of the following tasks:

- capturing the set value from the ECU

- throttle position sensing

- throttle position controlling

- driving of the DC-motor

- actuator diagnostics

- report the status to the respective ECU

In Fig. 3.10 a butterfly throttle valve is shown, where α denotes the plate angle. The resting angle α_0 is typically larger than zero to prevent binding to the walls. A plate angle of $90°$ means a fully open valve. It is common to use % instead of degrees inside control algorithms. In automotive software usually the application of the valve decides if 100% means opened or closed. For example a throttle valve situated in the intake manifold of a Diesel engine is fully closed at 100% since it

is *throttling* the air flow. In case of the bypass valve, $100\,\%$ means fully opened since it is used to *bypass* fresh air.
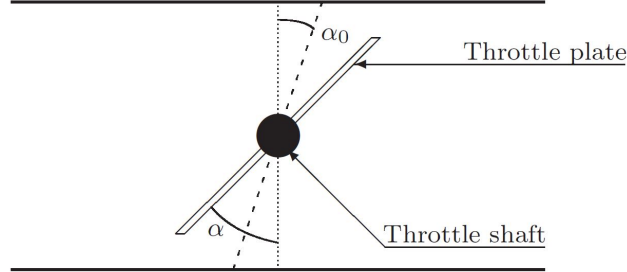
Figure 3.10: *Cross section of a throttle valve with plate, shaft and angles. [3]*

The air flow through the geometry depends on three physical rules: conservation of mass, Newtons second law ($\mathbf{F} = m \cdot \mathbf{a}$) and the conservation of energy. The set of partial differential equations is known as the Navier-Stokes[1] equations. For a Newtonian fluid they are given by: [3, p. 20]

In x direction:

$$\frac{\partial(\rho u)}{\partial t} + \frac{\partial(\rho u^2)}{\partial x} + \frac{\partial(\rho uv)}{\partial y} + \frac{\partial(\rho uw)}{\partial z} = -\frac{\partial p}{\partial x} + \frac{\partial}{\partial x}\left[\lambda \nabla \cdot V + 2\mu \frac{\partial u}{\partial x}\right]$$

$$+ \frac{\partial}{\partial y}\left[\mu \left(\frac{\partial v}{\partial x} + \frac{\partial u}{\partial y}\right)\right] + \frac{\partial}{\partial z}\left[\mu \left(\frac{\partial u}{\partial z} + \frac{\partial w}{\partial x}\right)\right] + \rho f_x \quad (3.31)$$

In y direction:

$$\frac{\partial(\rho v)}{\partial t} + \frac{\partial(\rho uv)}{\partial x} + \frac{\partial(\rho v^2)}{\partial y} + \frac{\partial(\rho vw)}{\partial z} = -\frac{\partial p}{\partial y} + \frac{\partial}{\partial x}\left[\mu \left(\frac{\partial v}{\partial x} + \frac{\partial u}{\partial y}\right)\right]$$

$$+ \frac{\partial}{\partial y}\left[\lambda \nabla \cdot V + 2\mu \frac{\partial v}{\partial y}\right] + \frac{\partial}{\partial z}\left[\mu \left(\frac{\partial w}{\partial y} + \frac{\partial v}{\partial z}\right)\right] + \rho f_y \quad (3.32)$$

In z direction:

$$\frac{\partial(\rho w)}{\partial t} + \frac{\partial(\rho uw)}{\partial x} + \frac{\partial(\rho vw)}{\partial y} + \frac{\partial(\rho w^2)}{\partial z} = -\frac{\partial p}{\partial z} + \frac{\partial}{\partial x}\left[\mu \left(\frac{\partial u}{\partial z} + \frac{\partial w}{\partial x}\right)\right]$$

$$+ \frac{\partial}{\partial y}\left[\mu \left(\frac{\partial w}{\partial y} + \frac{\partial v}{\partial z}\right)\right] + \frac{\partial}{\partial z}\left[\lambda \nabla \cdot V + 2\mu \frac{\partial w}{\partial z}\right] + \rho f_z \quad (3.33)$$

For an analytical solution of this set of equations, the following simplifying assumptions are used: [3]

---

[1] Claude Louis Marie Henri Navier (1785 to 1836), French mathematician and physicist and George Gabriel Stokes (1819 to 1903), Irish mathematician and physicist

- The flow is only in one direction (X)

- The gas is assumed to be ideal, $p = \rho R T$

- The flow is assumed to be at steady state, $\frac{\partial}{\partial t} = 0$

- The gas is assumed to have constant specific heat, $e = c_v T$

- Body forces are neglected, $f_x = f_y = f_z = 0$

- Viscosity is neglected, $\mu = \lambda = 0$

- thermal conductivity is neglected, $k = 0$

- No heat-flow is present, $\dot{q} = 0$

After these simplifications (a detailed explanation can be found in [3]) the following equations are obtained:

$$\Pi = \max \left(\frac{p_{ds}}{p_{us}}, \; \frac{2}{\gamma + 1}^{\frac{\gamma}{\gamma - 1}} \right) \tag{3.34}$$

$$\Psi(\Pi) = \sqrt{\frac{2\gamma}{\gamma - 1} \cdot \left(\Pi^{\frac{2}{\gamma}} - \Pi^{\frac{\gamma + 1}{\gamma}} \right)} \tag{3.35}$$

$$\dot{m}_{thr} = \frac{p_{us}}{\sqrt{R \cdot T_1}} \cdot A_{thr}(\alpha) \cdot C_d \cdot \Psi(\Pi), \tag{3.36}$$

where p_{us} is the pressure before the valve [Pa],
$\quad$ p_{ds} is the pressure after the valve [Pa],
$\quad$ γ is the specific heat ratio [-],
$\quad$ A_{thr} is the opening area [m^2] and
$\quad$ C_d is the discharge coefficient [-].

The discharge coefficient C_d characterizes the given throttle valve. It ranges from 0 to 1 and describes the flow difference to an orifice of the same dimensions. [3, p. 15] Tests showed that the discharge coefficient also depends on the throttle angle. The exact calibration was not yet possible, since at the time there was no pressure sensor after the throttle valve and therefore the exact conditions were unknown.

To determine the throttle area, Eq. 3.37 below was used. This equation neglects the thickness of the throttle shaft and plate. These two factors limit the maximum area from about $75\,^\circ$ plate angle to $80\,\%$ of the pipe cross section area as shown in Fig. 3.11. Since the area is implemented as a lookup table in the Simulink model, the curve can easily be updated in the future.

$$A(\alpha) = \frac{\pi d^2}{4} \left(1 - \frac{\cos(\alpha)}{\cos(\alpha_0)} \right) \tag{3.37}$$
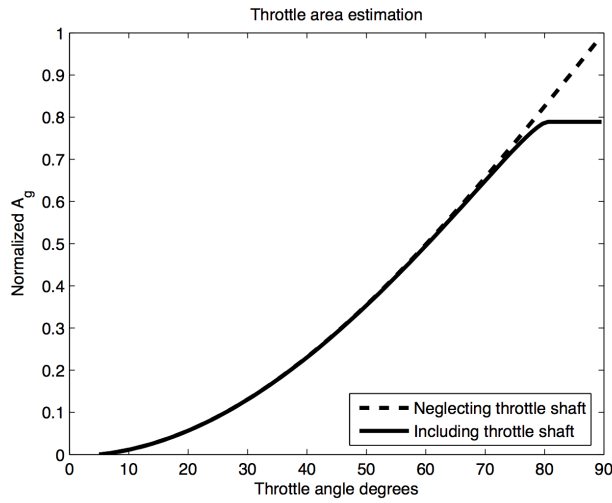
Figure 3.11: *Normalized throttle area over plate angle. [3]*

3.3.1   Throttle Model Validation

Since there is no pressure sensor after the throttle valve, it is assumed that a fully opened valve has the same flow resistance as the heat exchanger. This assumption is based on pressure drop measurements performed in cold conditions (shown in Fig. 3.12). A mass flow over pressure drop map was generated which shows a 50 % flow for a fully opened valve. Since the counter pressure increases with the CHEX temperature, hot conditions could not be validated. As a result, the mass flow ratio is 1:1. This assumption is used to find a base calibration for the discharge coefficient. In Fig. 3.12 a test run is shown where the compressor mass flow is constant and the throttle valve is stepped from 0 % to 100 % in 10 % increments. It can be seen that the mass flow through the throttle valve decreases towards 100 %.
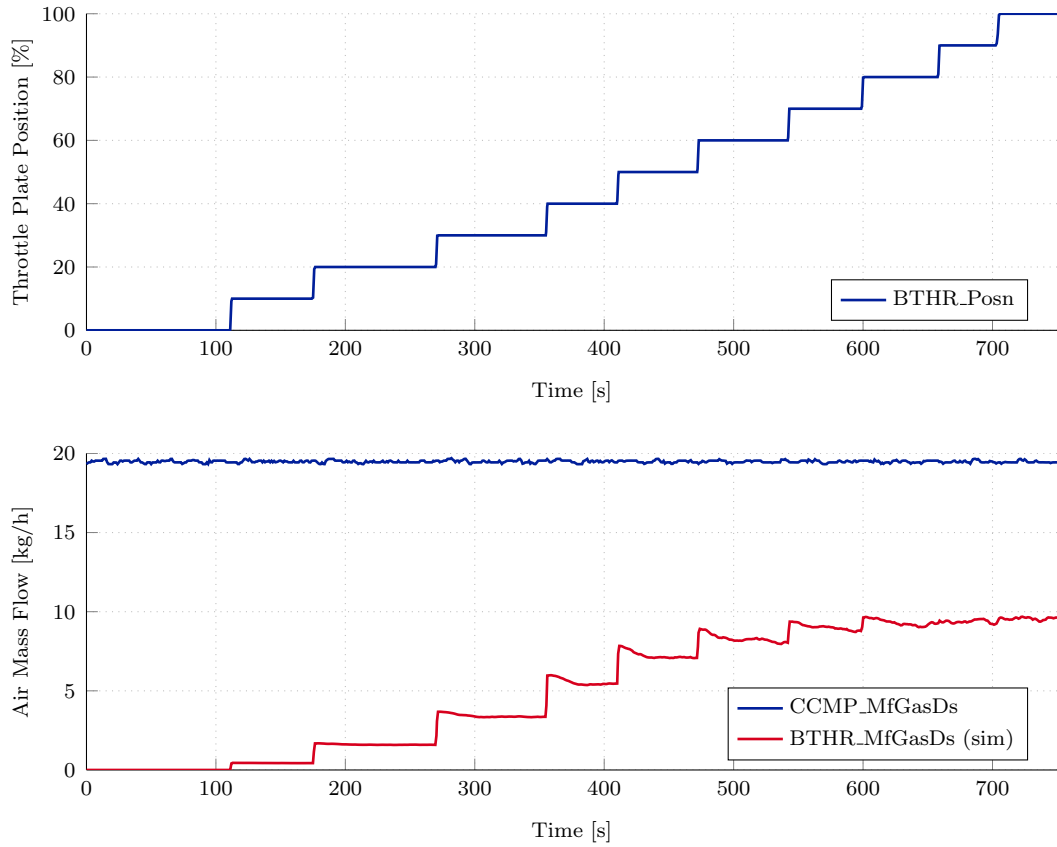
Figure 3.12: *BTHR mass flow for different plate positions, modeled.*

3.4 Pipe Model

Since all components are interconnected with pipes, there should be a reusable block which calculates the gas flow based on the pressure difference and the geometry of the pipe. The key parameters are pipe length, diameter and a friction coefficient. Since there can be a significant temperature difference between inlet and outlet of a pipe section, the temperature should also be considered. In Fig. 3.13 the pipe block is shown.
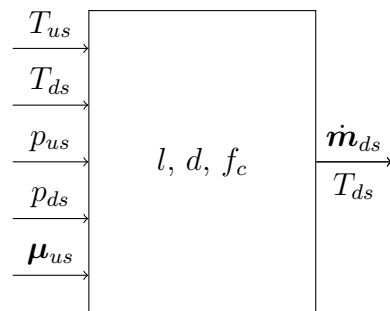
Figure 3.13: *Schematic of a pipe.*

Where T_{us} is the temperature of the upstream gas [K],

$\quad T_{ds}$ is the temperature of the downstream gas [K],

$\quad p_{us}$ is the pressure at the inlet [Pa],

$\quad p_{ds}$ is the pressure at the outlet [Pa],

$\quad \boldsymbol{\mu}_{us}$ is the mass concentration vector of the upstream gas [kg/kg],

$\quad l$ is the length of the pipe [m],

$\quad d$ is the diameter of the pipe [m],

$\quad f_c$ is friction coefficient [-],

$\quad \dot{\mathbf{m}}_{ds}$ is the downstream mass flow vector [kg/s] and

$\quad T_{ds}$ is the temperature of the downstream gas in [K].

The pressure along a pipe, flown through by a compressible fluid is decreasing along the pipe due to friction. A result of this pressure drop is the expansion of the fluid accompanied by a temperature and volume change according to the gas law. Due to this expansion currents, the fluid velocity increases even in pipes with a constant cross section area. A higher fluid velocity causes an even higher pressure drop, according to Darcy[2]. The pressure is therefore decreasing disproportionally along the flow direction. [4, p. 384]. The dependency between pipe geometry and pressure difference is given by:

$$\frac{p_{us}^2 - p_{ds}^2}{2 \cdot p_{us}} \approx \rho_{us} \cdot \lambda_f \cdot \frac{l}{d} \cdot \frac{v^2}{2} \cdot \frac{\bar{T}}{T_{us}}, \tag{3.38}$$

where p_{us} and p_{ds} are the pressures up- and downstream [Pa],

$\quad \lambda_f$ is the pipe friction coefficient [-],

$\quad l$ is pipe length [m],

$\quad d$ is pipe diameter [m],

$\quad \rho_{us}$ is fluid density at the pipe inlet [kg/m^3],

$\quad v$ is fluid velocity inside the pipe [m/s],

$\quad \bar{T}$ is the mean temperature along the pipe [K],

$\quad T_{us}$ is the temperature at the pipe inlet [K],

$\quad \dot{m}$ is mass flow through the pipe [kg/s] and

$\quad A$ is pipes cross section area [m^2].

The friction coefficient λ_f is not constant but depends on the Reynolds[3] number which is explained in section 3.4.1. The approximate equation for the pressure drop is only valid for fluid velocities below $0.7\,\text{Ma}$ (Mach) which are not reached in this system.

---

[2] Henry DARCY (1803 to 1855), French engineer.

[3] Osborne REYNOLDS (1842 to 1912), British physicist.

After further simplifications (details can be found in [4] and [17]) the pressure drop equation can be written and transformed as shown below:

$$\Delta p \approx \rho_1 \cdot \lambda_f \cdot \frac{l}{d} \cdot \frac{v^2}{2} \cdot \frac{\bar{T}}{T_{us}} \tag{3.39}$$

$$v = \sqrt{\frac{(p_{us} - p_{ds}) \cdot 2 \cdot d \cdot T_{us}}{\lambda_f \cdot l \cdot \rho_{us} \cdot \bar{T}}} \tag{3.40}$$

$$\dot{m} = v \cdot A \cdot \rho_{ds} \tag{3.41}$$

3.4.1 Reynolds number

The flow conditions inside a pipe drastically change between laminar and turbulent flow. During laminar flow the particles are moving on parallel lines whereas during turbulent flow, the main flow direction is superimposed with vortexes. To determine the type of flow in a certain component, the Reynolds number is used. It is a dimensionless number which relates inertia to viscosity of the fluid [18] [4]. For $Re < 2300$ the flow is considered laminar. Between 2300 and around 4000, a mixed flow is present (critical area). Above 4000 the flow is turbulent except for a laminar boundary layer at the surface of the pipe. In Eq. 3.42 the calculation of Re is shown:

$$Re = \frac{\rho \cdot v \cdot d_h}{\mu} = \frac{v \cdot d_h}{\nu}, \tag{3.42}$$

where ρ is the density of the fluid [kg/m^3],
$\quad v$ is the flow velocity [m/s],
$\quad d_h$ is the hydraulic diameter of the pipe [m],
$\quad \mu$ is the dynamic viscosity of the fluid [Pa s] and
$\quad \nu$ is the kinematic viscosity [m^2/s].

It is important to know the Reynolds number and with it the flow conditions in each component and for the entire range of air flow rates. To do so, the mass flow $\dot{m}$ and component cross section area A are substituted into the equation:

$$Re = \frac{\rho \cdot \dot{V} \cdot d_h}{\mu \cdot A} = \frac{\cancel{\rho} \cdot \dot{m} \cdot d_h}{\mu \cdot A \cdot \cancel{\rho}} = \frac{\dot{m} \cdot d_h}{\mu \cdot A} \tag{3.43}$$

The diameter of the pipes connecting the components is $4.0\,\text{cm}$ and the maximum mass flow is about $100\,\text{kg/h}$. The dynamic viscosity of air is $1.725 \times 10^{-5}\,\text{Pa s}$, so the maximum Re for the pipes is given by:

$$Re = \frac{\dot{m} \cdot d}{\mu \cdot A} = \frac{90/3600 \cdot 0.04}{1.725 \times 10^{-5} \cdot (0.02^2 \cdot \pi)} = 51\,257 \tag{3.44}$$

A typical operating point of the cathode compressor is at $40\,\text{kg/h}$ which results in a Reynolds number of $20\,503$. The roughness of the pipe surface, which normally increases over time (corrosion, dirt,...), affects the friction at the pipe walls. The friction coefficient λ_f for pipes with different surfaces can be found in a *Moody* diagram (Fig. 3.14). For hydraulically smooth pipes, where the roughness is below the laminar boundary layer, the Blasius[4] equation (3.45) can be used to determine the friction factor λ_f. [18, B48]

$$\lambda_f = 0.3164/\sqrt[4]{Re} \quad \text{for} \quad 2320 < Re < 10^5 \tag{3.45}$$
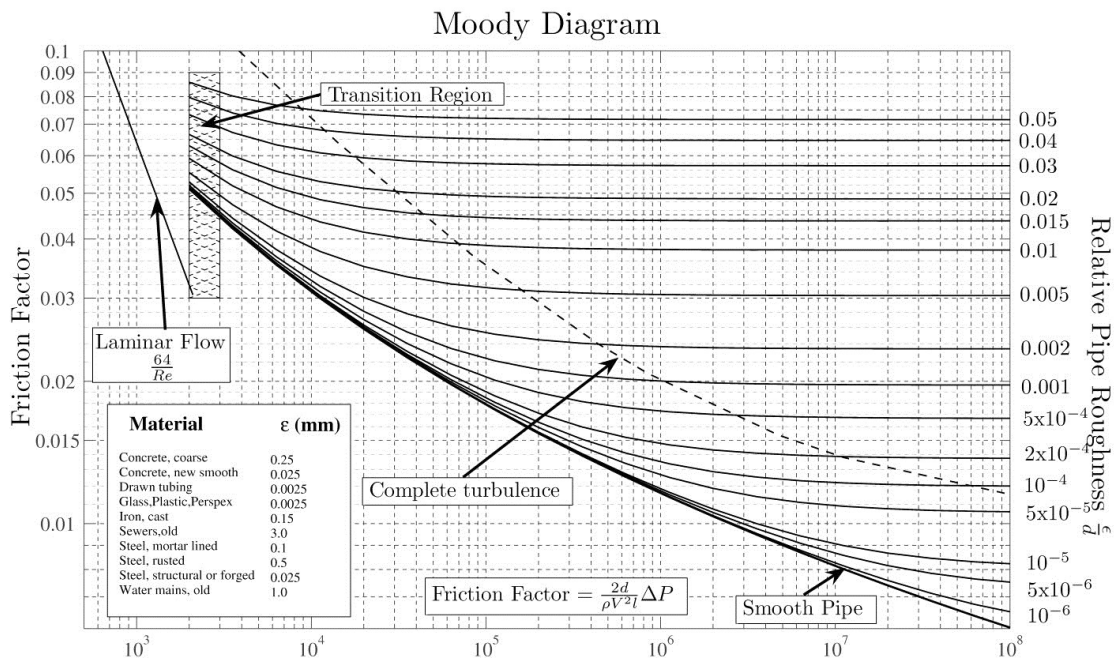
Figure 3.14: *Moody diagram. [4]*

3.4.2   Flow Through the Cathode Heat Exchanger

For thermal simulation it is especially important to know the flow through the cathode heat exchanger. This is also the component with the largest temperature difference between in- and outlet (several hundred °C). Furthermore the exact geometry of the device is unknown.

To characterize the CHEX regarding flow and pressure drop, different measurements have been performed by AVL, first in cold conditions. The bypass throttle valve was stepped in $10\,\%$ increments while the flow-rate was held constant. The result is a map of pressure drop over mass-flow for each throttle position (see Fig. 3.15).

---

[4]   Paul Richard Heinrich BLASIUS (1883 – 1970), German fluid dynamics physicist.

Since there is no flow or pressure sensor in the bypass path, this is the only data available to characterize the CHEX. Note that 100 % means a fully opened bypass valve. Similar to an electric circuit, the network can be seen as a parallel connection of two resistors. The CHEX represents a constant resistance whereas the throttle valve can be varied from infinite (fully closed) to a certain value (depending on opening area, surface roughness,...). Since the compressor is controlled to hold a certain flow rate, it can be seen as a constant current (flow) source. If the throttle valve is closed, the entire flow passes through the CHEX, and therefore the pressure drop is at a maximum.

Using the pressure drop at a fully closed bypass throttle, a lookup table can be generated to model the mass flow in cold conditions, where no energy is transfered inside the CHEX. This empirical model is used to validate the physical model. However the temperature dependent counter pressure, induced by the heat up of the gas (in operating conditions from 40 °C to 750 °C) has a big influence on the mass flow.
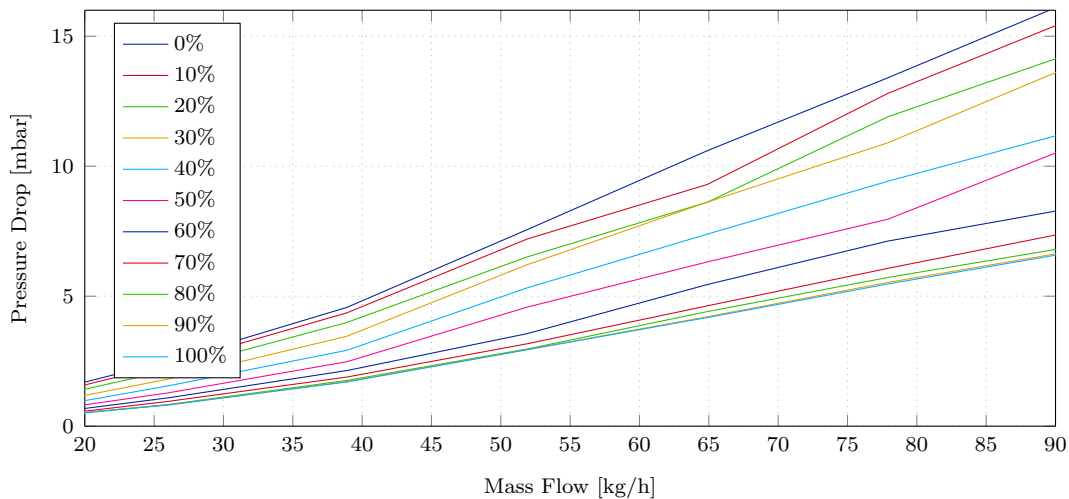
Figure 3.15: *Pressure drop over CHEX for different BTHR positions (cold).*

In Fig. 3.18 the map based mass flow is plotted against the measurement and the physical model explained above. Note that the lines should match in the periods where the throttle valve is fully closed. Only then the cathode path mass flow provided by the cathode compressor is the same as the CHEX mass flow. It can be seen that the map based mass flow (green) matches the measurement (blue) perfectly in this operating point (cold air and components). However the physical model is also very close even if pipe friction coefficient λ_f was held constant during this simulation. As mentioned earlier, the friction coefficient depends on the Reynolds number Re. Since the Reynolds number is derived from the flow velocity, the friction coefficient map depends on the pressure drop over the CHEX. This map was calibrated to fit the measurements. In Fig. 3.17, λ_f over Δp as well as the three flow regions are plotted.
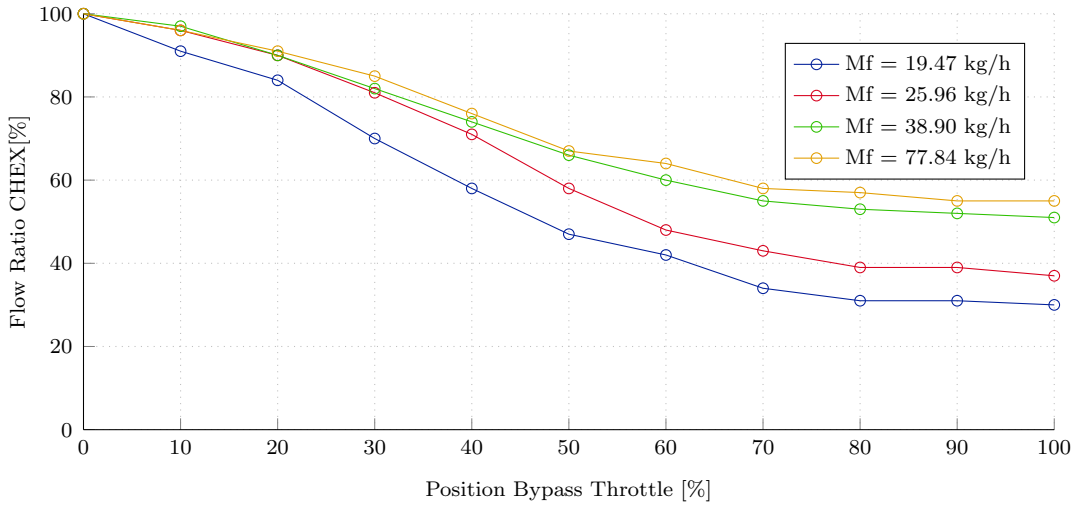
Figure 3.16: *Flow rate ratio through CHEX over BTHR position (cold).*
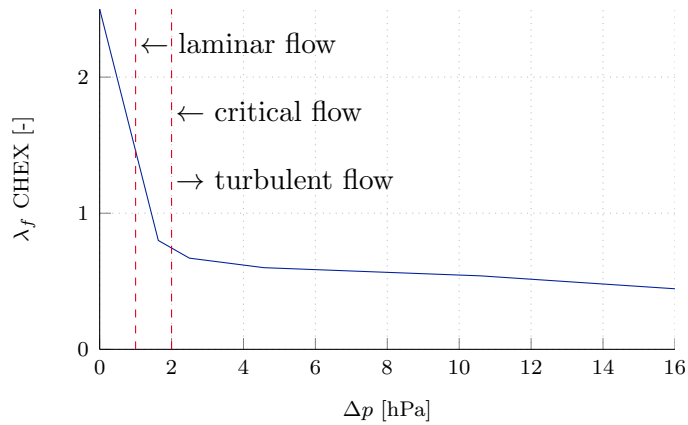
Figure 3.17: *Friction coefficient of the CHEX over pressure drop.*

The results can be seen in Fig. 3.19, where the friction coefficient λ_f comes from a calibrated map. The match of the physical flow model and the map based calculation are very good, at least in cold conditions.

From new measurements, also a greater temperature difference between inlet and outlet was derived. It seems that the approach using a map based on pressure difference is not enough to model λ_f. A possible explanation is that λ_f in theory depends on Re which is a function of inertia and viscosity of the fluid. While inertia is probably sufficiently modeled by the pressure difference, the viscosity is also temperature dependent. For this reason we introduce a temperature dependent correction map for λ_f with calibrated values. The flow equation with the explained updates is now given by:
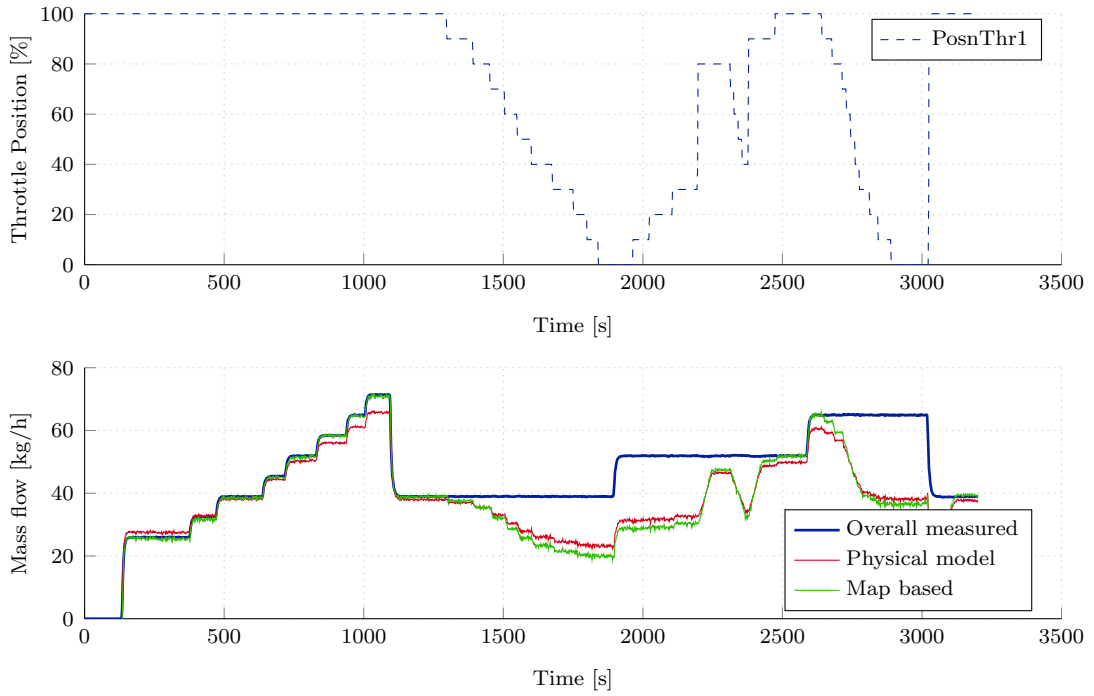
Figure 3.18: *Mass flow measured against physical model (Eq. 3.38) and map .*
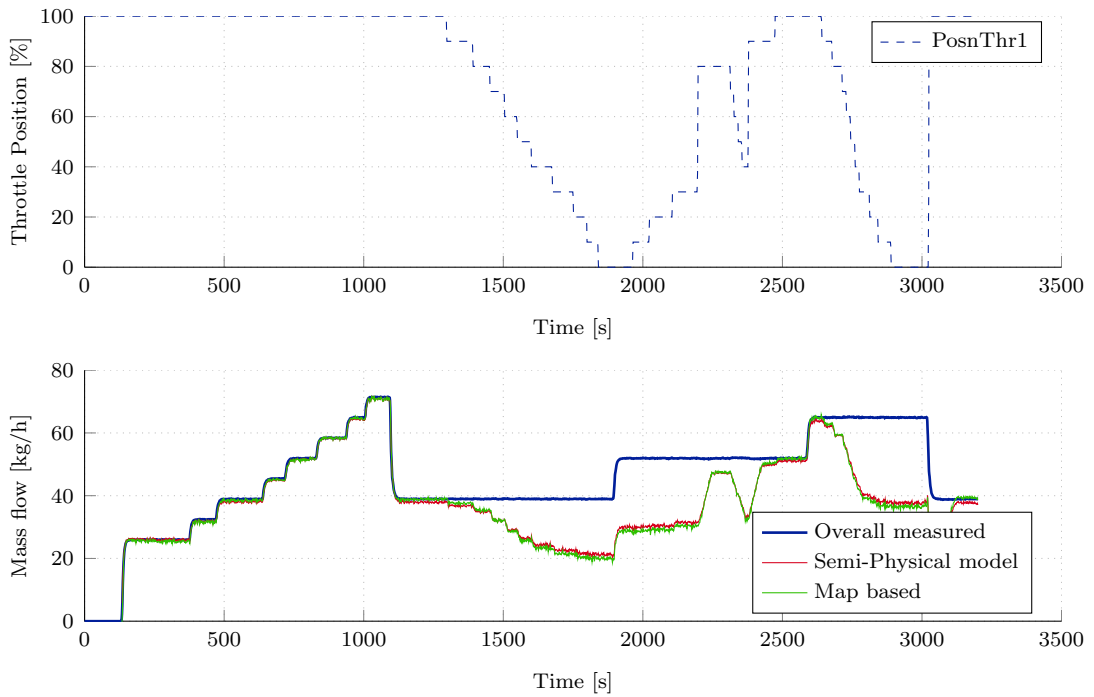
Figure 3.19: *Mass flow measured against physical model (Eq. 3.46) and map.*

$$v_{ds} = \sqrt{\frac{(p_{us} - p_{ds}) \cdot 2 \cdot d \cdot T_{us}}{p_{us} \cdot \lambda_f(\Delta p) \cdot \lambda_{f,corr}(\bar{T}) \cdot l \cdot \rho_{us} \cdot \bar{\bar{T}}}} \qquad (3.46)$$

$$\dot{m} = v_{ds} \cdot A \cdot \rho_{ds}, \tag{3.47}$$

where $\lambda_f(\Delta p)$ is the pressure dependent friction coefficient and
$\lambda_{f,corr}(\bar{T})$ is the temperature dependent correction term.

3.5 Junction Model

The junction component models the joining of two pipes to mix two gases. The mass flow vectors are added and the resulting temperature is calculated. In addition the junction has a thermal mass to model the dynamics if the mass flow is turned off. In that case the thermal mass will not immediately drop the outlet temperature but cool down gradually due to losses to the environment. In Fig. 3.20 the system is visualized.
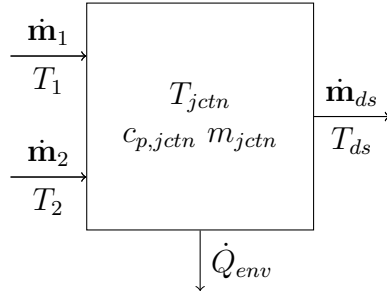
Figure 3.20: *Schematic of a two-to-one pipe junction.*

Where $\dot{\mathbf{m}}_1$ is the first mass flow vector [kg/s],
$\dot{\mathbf{m}}_2$ is the second mass flow vector [kg/s],
T_1 is the first gas temperature [K],
T_2 is the second gas temperature [K],
T_{jctn} is the temperature of the junction body [K],
$c_{p,jctn}$ is the heat capacity of the body [J/(kg K)],
m_{jctn} is the mass of the body [kg],
$\dot{Q}_{env}$ is the heat flow to the environment [W],
$\dot{\mathbf{m}}_{ds}$ is the downstream mass flow vector [kg/s] and
T_{ds} is the downstream gas temperature [K].

To calculate the resulting gas concentration and temperature, the following equations are used. Note that the mass flow $\dot{m}_{sum}$ in Eq. 3.49 is the sum off all 14 gas mass flows while $\dot{\mathbf{m}}$ represents the vector of 14 individual mass flows, one for each

gas. The thermal mass block used in this model is documented in section 3.7.

$$\dot{\mathbf{m}}_{ds} = \dot{\mathbf{m}}_1 + \dot{\mathbf{m}}_2 \tag{3.48}$$

$$T_{ds} = \frac{\dot{m}_{sum,1}}{\dot{m}_{sum,1} + \dot{m}_{sum,2}} \cdot T_1 + \frac{\dot{m}_{sum,2}}{\dot{m}_{sum,1} + \dot{m}_{sum,2}} \cdot T_2 \tag{3.49}$$

3.6 Manifold Filling Model

To connect flow elements like pipes or throttle valves together, pressure nodes are required. These components resemble the lumped volume of the manifold and pipes and buffer the gas. In Fig. 3.21 the simplified counter pressure model is shown. The network of components can be seen as a combination of pressure nodes and flow elements. Pressure is the cause of any flow, and the boundary condition is atmospheric pressure at both ends of the system. To achieve an air flow, the compressor (situated between p_0 and p_1) needs to create a pressure difference. The pressure in the manifold p_1 is given by Eq. 3.53 below. This equation is derived from the ideal gas law and the conservation of mass. The mass flow out of the node is calculated by the next flow elements ($\dot{m}_2 + \dot{m}_3$) which themselves determine the flow from the pressure difference between p_1 and p_2 and so on. This method can be used to model arbitrary complex networks. [19]

It is important to note that the two kinds of basic components (pressure node and flow element) combine the volume of pipes and manifolds into the pressure node, where the dynamics are modeled. Flow elements do not have a volume and therefore they cannot accumulate gas.
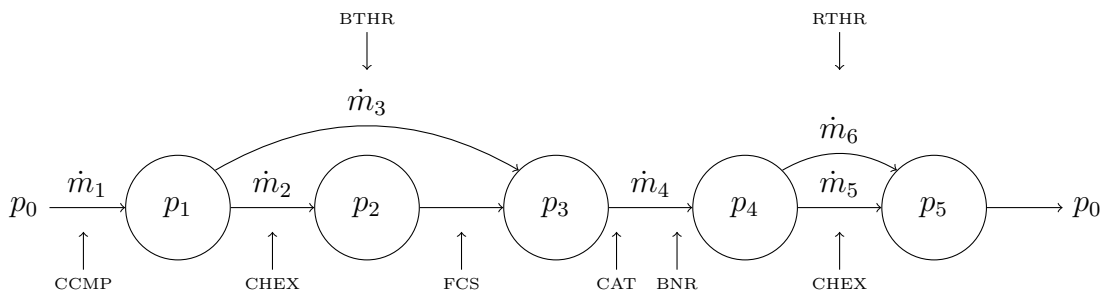
Figure 3.21: *Pressure network.*

The principle of mass conservation and the ideal gas law are applied to model the pressure node element, all the required equations are listed below. [13, p. 20]

$$pV = n\bar{R}T = mRT \tag{3.50}$$

$$\frac{dm}{dt} = \dot{m}_{in} - \dot{m}_{out} \tag{3.51}$$

$$\frac{dp}{dt} = \frac{T \cdot R_{air}}{V} \cdot (\dot{m}_{in} - \dot{m}_{out}) \tag{3.52}$$

$$\frac{dp}{dt} = \frac{\gamma \cdot R}{V} \cdot (\dot{m}_{in} \cdot T_{in} - \dot{m}_{out} \cdot T_{out}) \tag{3.53}$$

$$T_{out} = \frac{p \cdot V}{m \cdot R} \tag{3.54}$$

Where p is the manifold pressure [Pa],
V is volume of the manifold [m^3],
$\bar{R}$ is the universal gas constant [J/mol K],
R is the special gas constant [J/kg K],
T is the gas temperature [K],
n is the number of mol inside the manifold [-],
m is the mass inside the manifold [kg],
$\dot{m}$ is the mass flow into the manifold [kg/s] and
γ is the ratio of the specific heat capacities C_p/C_v [-].

If the temperature difference between inlet and outlet can be neglected, the isothermal relation (Eq. 3.52) should be used. If not, also the ideal gas law is applied (Eq. 3.53) which is called pressure dynamic equation. [13]

3.7 Thermal Mass

One component which is used several times in the full system is the thermal mass. Basically it models the thermal behavior of a body and a hot gas streaming through it. Two heat flows were considered: the reaction heat $\dot{Q}_{rctn}$ and the environmental losses $\dot{Q}_{env}$. The reaction heat is especially important for the catalytic converter, the burner and the fuel cell stack in which exothermic reactions take place. The heat transfer between gas and mass is split into three parts. First the adiabatic reaction is calculated, which heats up only the gas. In the burner the heat flow is calculated using the heating value of Diesel and in the catalyst the heat of reaction is determined. Knowing the heat capacity of the gas mixture, the resulting gas temperature can be calculated. The next step is the heat flow between gas and the walls through convection and radiation. This depends on the heat transfer properties of the wall, as well as the temperature difference. The energy of the thermal mass rises and the gas temperature decreases accordingly. Important

values are the gas and body temperature. The body temperature is required for devices in which chemical reactions take place (catalytic converter, burner,. . .).
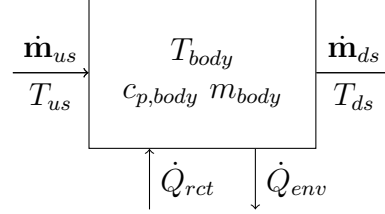
Figure 3.22: *Schematic of a thermal mass.*

Where $\dot{\mathbf{m}}_{us}$ is the upstream gas mass flow vector [kg/s],
$\quad$ T_{us} is the upstream temperature of the gas [K],
$\quad$ T_{body} is the temperature of the body [K],
$\quad$ $c_{p,body}$ is the heat capacity of the body [J/(kg K)],
$\quad$ m_{body} is the mass of body [kg],
$\quad$ $\dot{Q}_{rct}$ is the heat of reaction [W],
$\quad$ $\dot{Q}_{env}$ is the heat flow to the environment [W],
$\quad$ $\dot{\mathbf{m}}_{ds}$ is the downstream gas mass flow vector [kg/s] and
$\quad$ T_{ds} is the downstream temperature of the gas [K].

Adiabatic Combustion
The combustion heat is determined by either the heating value of the used fuel (Diesel in case of the burner) or by the change in enthalpy of the gas. The outlet temperature is then calculated by:

$$T_{ds} = T_{us} + \frac{\dot{Q}_{rctn}}{\dot{m} \cdot c_{p,gas}}. \tag{3.55}$$

Gas-Wall Heat Transfer
The heat flow from the heated up gas to the walls of the body can be determined by the following equation:

$$\dot{Q}_{g2w} = (T_{gas} - T_{body}) \cdot A \cdot k. \tag{3.56}$$

Thermal Mass
The thermal mass' temperature depends on the net heat flow, the mass and heat capacity of the body. An integrator is used in the Simulink model to determine the temperature.

$$T_{body} = \int \frac{\dot{Q}_{g2w} + \dot{Q}_{env}}{m_{body} \cdot c_{p,body}} \, dt \tag{3.57}$$

To keep the energy balance, the heat flow from the gas to the body now cools down the gas. To calculate the outlet temperature we use 3.55 in the following

form:

$$T_{ds} = T_{us} + \frac{-\dot{Q}_{g2w}}{\dot{m} \cdot c_{p,gas}}. \tag{3.58}$$

Heatflow to the Environment

There is also a heat-flow from the component to the environment. This can be modeled by:

$$\dot{Q}_{env} = \alpha \cdot A \cdot (\vartheta_{env} - \vartheta_{hex}). \tag{3.59}$$

In the given setup, the heat exchanger is embedded in an insulation material. The heat flow through a wall, in one dimension can be calculated by the equation below. [15, p. 21]

$$\dot{Q} = \frac{\lambda}{s} \cdot A \cdot (\vartheta_1 - \vartheta_2), \tag{3.60}$$

where $\dot{Q}$ is the heat flow through the wall [W],
λ is the heat conductivity coefficient [W/(m K)],
k is the thermal transmittance [W/(m^2 K)],
α is the heat transfer coefficient [W/(m^2 K)],
s is the wall thickness [m],
A is the wall area [m^2],
ϑ_1 is the higher temperature [°C] and
ϑ_2 is the lower temperature [°C].

The heat transfer coefficient α characterizes the ability of a fluid to transfer heat to or from a surface. For plane walls it can be calculated by $\alpha = \lambda/s$. For walls with different layers the thermal transmittance k is introduced. The inverse of k is the heat transfer resistance R_T.

$$k = \left(\frac{1}{\alpha_{hex}} + \frac{1}{\alpha_{ins}} + \frac{1}{\alpha_{air}} \right)^{-1} \tag{3.61}$$

$$\dot{Q} = k \cdot A \cdot (\vartheta_1 - \vartheta_2) \tag{3.62}$$

It should also be considered that the insulation material has different properties in different temperatures. The heat conductivity almost doubles from 30 °C to 800 °C.

3.8 Fuel Cell Stack Model

The fuel cell stacks electro chemistry and reaction kinetics will be addressed in a future thesis. For this work only the thermal behavior is considered. To do so the

thermal mass model documented in section 3.7 is used as well as the pipe model (see section 3.4). The pipe model determines the flow through the stack based on the pressure difference and the flow is used for the heat transfer calculation. In Fig. 3.23 the system is shown.
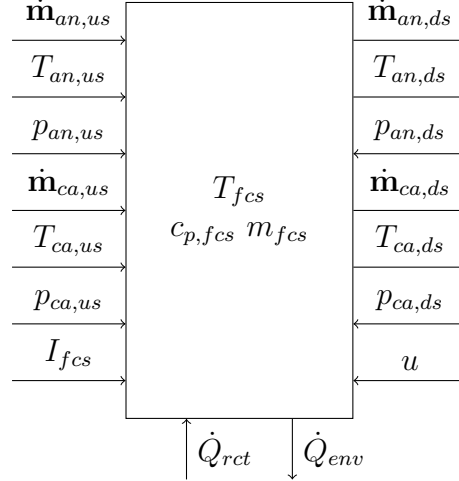
Figure 3.23: *Schematic of the fuel cell stack.*

Where $\dot{\mathbf{m}}_{an}$ is the anode gas mass flow vector [kg/s],
T_{an} is the temperature of the gas at the anode [K],
p_{an} is the gas pressure at the anode [Pa],
$\dot{\mathbf{m}}_{ca}$ is the cathode gas mass flow vector [kg/s],
T_{ca} is the temperature of the gas at the cathode [K],
p_{ca} is the gas pressure at the cathode [Pa],
I_{fcs} is the drawn current from the fuel cell stack [A],
T_{fcs} is the temperature of the fuel cell stack [K],
$c_{p,fcs}$ is the heat capacity of the fuel cell stack [J/(kg K)],
m_{fcs} is the mass of fuel cell stack [kg],
$\dot{Q}_{rct}$ is the heat of reaction [W],
$\dot{Q}_{env}$ is the heat flow to the environment [W] and
u is the stack voltage [V].

Even if the model will be extended in the future, the interface to the rest of the system has been defined already. For the electro chemistry the following signals are required: gas composition at the anode and cathode ($\dot{\mathbf{m}}_{an}$ and $\dot{\mathbf{m}}_{ca}$, respectively), gas temperature at anode and cathode ($T_{an,us}$ and $T_{ca,us}$, respectively), stack temperature (T_{fcs}), upstream and downstream pressure for both anode and cathode ($p_{us,an}$, $p_{ds,an}$, $p_{us,ca}$ and $p_{ds,ca}$, respectively) and the current drawn from the stack (I_{fsc}).

During heat up, the cathode gas is the main energy source. Since the fuel cell reaction is exothermic, another heat flow depending on the drawn current is present ($\dot{Q}_{rctn}$) during operation. The gas composition of the cathode gas also changes

inside the stack, because O_2 is diffusing through the electrolyte to the anode, where it recombines with hydrogen. This is important for the following stages (catalyst and burner). Under full load, the O_2 concentration at the cathode outlet drops to about 16% by volume.

3.9 Catalytic Converter Model

The catalytic converter, situated after the fuel cell stack, has the purpose to burn residual H_2, CO and CH_4. Due to the high temperatures during the fuel cell operation, it is assumed that 100% of the gases are oxidized. In the future more detailed models for the reaction kinetics will be introduced. The important results of the model are the mass ratio of the 14 gases (needed for the reaction in the burner) and the heat of reaction to determine the gas and catalyst temperature. In Fig. 3.24 the system is shown.
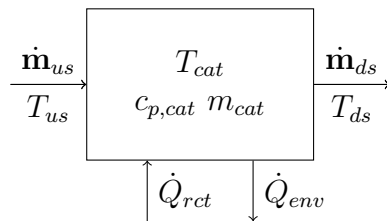
Figure 3.24: *Schematic of the catalytic converter.*

3.9.1 Derivation of the Reactions

In this section the reactions for all 14 gases are derived. Since the flow rate is handled in kg/s throughout the system, the equations are also transformed from mol to g. To determine the reactants (educts) and products of hydrocarbons, the equation for complete combustion is used:

$$C_xH_y + \left(x + \frac{y}{4}\right)O_2 \rightarrow xCO_2 + \frac{y}{2}H_2O + \Delta H_R \tag{3.63}$$
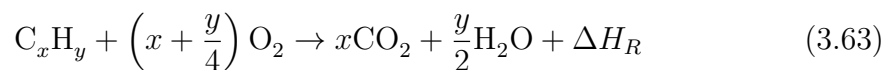
First the reaction equation is formed. Then the molar masses are inserted and both sides are divided by the molar mass of the hydro carbon, to calculate the masses of the gases. The reaction heat ΔH_R is calculated separately and is described in section 3.9.2 below.

CO **Reaction:**

$$2\,CO + O_2 \longrightarrow 2\,CO_2$$
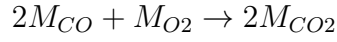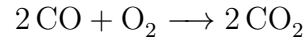
$$2M_{CO} + M_{O2} \rightarrow 2M_{CO2}$$

$$1\,g + \frac{M_{O2}}{2M_{CO}} \rightarrow \frac{2M_{CO2}}{2M_{CO}}$$

$$1\,g \cdot CO + 0.5712\,g \cdot O_2 \rightarrow 1.5712\,g \cdot CO_2 \tag{3.64}$$

H_2 **Reaction:**

$$2\,H_2 + O_2 \longrightarrow 2\,H_2O$$
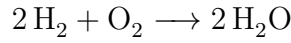
$$1\,g \cdot H_2 + 7.9363\,g \cdot O_2 \rightarrow 8.936\,g \cdot H_2O \tag{3.65}$$

CH_4 **Reaction:**

$$CH_4 + 2\,O_2 \longrightarrow CO_2 + 2\,H_2O$$
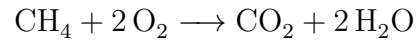
$$1\,g \cdot CH_4 + 3.989\,g \cdot O_2 \rightarrow 2.743\,g \cdot CO_2 + 2.2458\,g \cdot H_2O \tag{3.66}$$

C_3H_8 **Reaction:**

$$C_3H_8 + 5\,O_2 \longrightarrow 3\,CO_2 + 4\,H_2O$$
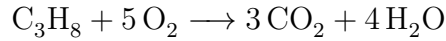
$$1\,g \cdot C_3H_8 + 3.628\,g \cdot O_2 \rightarrow 2.994\,g \cdot CO_2 + 0.408\,54\,g \cdot H_2O \tag{3.67}$$

C_4H_{10} **Reaction:**

$$2\,C_4H_{10} + 13\,O_2 \longrightarrow 8\,CO_2 + 10\,H_2O$$
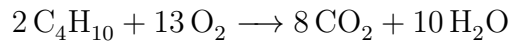
$$1\,g \cdot C_4H_{10} + 3.5784\,g \cdot O_2 \rightarrow 3.028\,68\,g \cdot CO_2 + 1.549\,74\,g \cdot H_2O \tag{3.68}$$

C_2H_6O **Reaction:**

$$2\,C_2H_6O + 6\,O_2 \longrightarrow 4\,CO_2 + 6\,H_2O$$

$$1\,g \cdot C_2H_6O + 2.083\,73\,g \cdot O_2 \rightarrow 1.9106\,g \cdot CO_2 + 1.173\,15\,g \cdot H_2O \tag{3.69}$$

CH_4O **Reaction:**

$$2\,CH_4O + 3\,O_2 \longrightarrow 2\,CO_2 + 4\,H_2O$$

$$1\,g \cdot CH_4O + 1.498\,g \cdot O_2 \rightarrow 1.3735\,g \cdot CO_2 + 1.124\,47\,g \cdot H_2O \tag{3.70}$$

$C_{12}H_{26}$ **Reaction:**

$$2\,C_{12}H_{26} + 37\,O_2 \longrightarrow 24\,CO_2 + 26\,H_2O$$

$$1\,g \cdot C_4H_{10} + 3.4753\,g \cdot O_2 \rightarrow 3.1004\,g \cdot CO_2 + 1.3749\,g \cdot H_2O \tag{3.71}$$

C_8H_{18} **Reaction:**

$$2\,C_8H_{18} + 25\,O_2 \longrightarrow 16\,CO_2 + 18\,H_2O$$

$$1\,g \cdot C_4H_{10} + 3.5015\,g \cdot O_2 \rightarrow 3.0821\,g \cdot CO_2 + 1.4194\,g \cdot H_2O \tag{3.72}$$
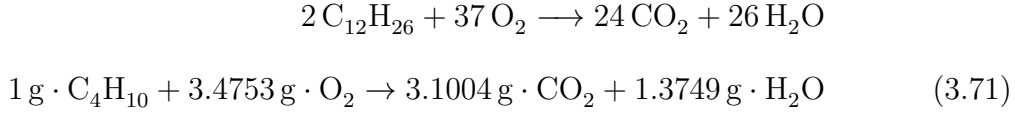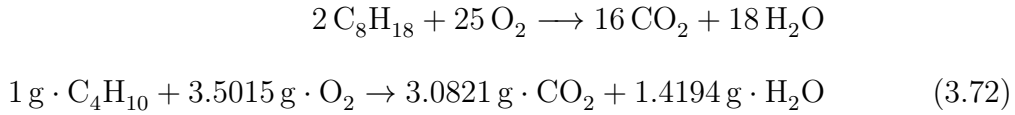
Knowing all the products for all reactions, a reduction vector for every gas can be generated. The mass flow of the downstream gas x can then be calculated by the equation below. Since a complete combustion is assumed, the only products are CO_2 and H_2O.

$$\dot{m}_{x,ds} = \dot{m}_{x,us} + (\boldsymbol{\eta} \circ \dot{\mathbf{m}}_{us}) \cdot \mathbf{v}_{red,x} \tag{3.73}$$

$$[1 \times 1] = [1 \times 1] + ([1 \times 14] \circ [1 \times 14]) \cdot [14 \times 1]$$

$$\mathbf{v}_{red,CO} = \begin{bmatrix} -1, 0, 0, 0, 0, 0, 0, 0, 0, 0, 0, 0, 0, 0 \end{bmatrix}^T$$

$$\mathbf{v}_{red,CO2} = \begin{bmatrix} 1.5712, 0, 0, 0, 2.7432, 0, 0, 0, 2.9952, 3.0289, 1.9106, 1.3736, 3.1096, 3.0825 \end{bmatrix}^T$$

$$\mathbf{v}_{red,H2O} = \begin{bmatrix} 0, 0, 0, 8.9365, 2.24583, 0, 0, 0, 1.6348, 1.5498, 1.1731, 1.1246, 1.3525, 1.4195 \end{bmatrix}^T$$

$$\mathbf{v}_{red,O2} = \begin{bmatrix} -0.571, 0, 0, -7.937, -3.989, 0, 0, 0, -3.63, -3.579, -2.084, -1.498, -3.462, -3.502 \end{bmatrix}^T$$

Where $\dot{m}_x$ is the mass flow of gas x in [kg/s]
$\quad\quad\boldsymbol{\eta}$ is the reaction efficiency vector in [-]
$\quad\quad\dot{\mathbf{m}}_{us}$ is the gas mass flow vector in [kg/s]
$\quad\quad\mathbf{v}_{red,x}$ is the gas reduction vector in [kg/kg].

Note that the ∘ symbol in Eq. 3.73 denotes the Hadamad product (element wise multiplication) while the · symbol denotes the scalar product.

$$A \circ B = (a_{ij} \cdot b_{ij}) = \begin{bmatrix} a_{11} \cdot b_{ii} & \dots & a_{1n} \cdot b_{1n} \\ \vdots & \ddots & \vdots \\ a_{m1} \cdot b_{m1} & \dots & a_{mn} \cdot b_{mn} \end{bmatrix} \quad \text{for A,B } \epsilon \; \mathbb{R}^{m \times n} \tag{3.74}$$

A complete list of all reduction vectors can be found in the appendix A.1.1.

3.9.2 Heat of Reaction Calculation

To determine the energy released by the reaction, the standard heat of formation $H_{f,0}$ is used. This is the energy needed to form a certain molecule. Stable molecules like O_2 have a forming enthalpy of 0. Otherwise it is negative, since energy is required to make the bonds. With the knowledge of the temperature dependent enthalpy and the composition of the gas before and after the reaction, the heat of reaction can be calculated. Tables for the heat of formation and many other properties can be found in [6].

3.10 Burner Model

The purpose of the burner is to heat up the system to its operating temperature. If the stack is high enough, the exothermic fuel cell reaction can begin and the burner is dialed down and turned off eventually. The system can then hold its temperature on its own. In the burner additional fuel (in this prototype Diesel is used) is injected to heat up the air and with it all subsequent components. There are ignition plugs mounted inside the unit which are required to ignite the air-fuel mixture.
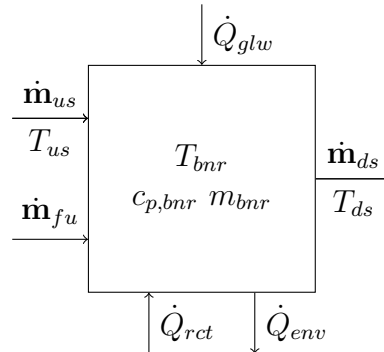
Figure 3.25: *Schematic of the start-up burner.*

The burner output temperature should be kept below a certain limit to prevent damage of the cathode heat exchanger which is downstream of the burner. The lower limit is dictated by the emission levels which may not be exceeded. An important value for combustion is the stoichiometric air to fuel ratio λ. At this ratio theoretically a complete combustion of the fuel can occur and all the available O_2 is consumed. The calculation of the air to fuel ratio is given by the equation below. [5, p. 90]

$$\lambda = \frac{\dot{m}_{air}}{f_{stoi} \cdot \dot{m}_{fu}}, \qquad (3.75)$$

where $\dot{m}_{air}$ and $\dot{m}_{fu}$ are the air and fuel mass flows in [kg/s] and
f_{stoi} is the stoichiometric constant for the given fuel [-].

Table 3.2: *Properties of ShellSol D100 [7]*

Property	Unit	Value	
Density @ 15 °C	kg/l	0.797	
Auto Ignition Temperature	°C	232	
Molecular Weight	g/mol	206	
Heat of Combustion	kJ/kg	45 000	
Heat of Combustion	kWh/kg	12.5	

The prototype is designed to accept a range of fuels but currently Diesel is used. For Diesel, λ needs to be between 1.3 and 12. At the upper limit the flame is blown of due to the excess air. It was determined experimentally.

To calculate the energy released during the reaction, a complete combustion is assumed and the heating value of Diesel is used:

$$\dot{Q}_{fuel} = \dot{m}_{fuel} \cdot H_{i,fu}, \tag{3.76}$$

where $H_{i,fu}$ is the lower heating value of the injected fuel in [kWh/kg]. The maximum thermal power of the burner is about $15\,\mathrm{kW_{th}}$ at $1200\,\mathrm{g/h}$. The thermal behavior of the unit is modeled by the thermal mass component, documented in section 3.7.

In Tab. 3.2 some relevant properties of the used Diesel are listed. More information can be found in [7].

3.10.1 Diesel Combustion

"Diesel is a complex mixture of paraffins, olefins, cycloalkanes and aromatics, containing up to 400 different hydrocarbon species, including organic sulfur compounds and additives." [20, p. 3]

Although the most important output of the burner model is the gas temperature, the composition of gases is also important since the emissions have to meet certain standards. As mentioned earlier, the temperature should be below 1000 °C since the NOx formation starts at this temperature. [5, p. 107]

The gross equation below is a simplification of the complex reactions during the combustion of hydrocarbons on molecular level. In Fig. 3.26 the intermediate products and the temperature progression is visualized. [5, p. 545]

$$\mathrm{C}_x\mathrm{H}_y + \left(x + \frac{y}{4}\right)\mathrm{O}_2 \rightarrow x\mathrm{CO}_2 + \frac{y}{2}\mathrm{H}_2\mathrm{O} + \Delta H_R \tag{3.77}$$
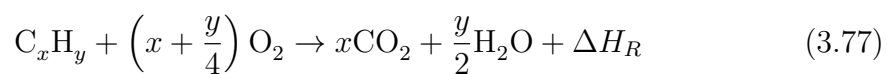
This is the equivalent one-step reaction which can be used to produce acceptable results. Since the interfaces between the components in Simulink are passing mass

Table 3.3: *Air composition [6]*

Gas	Symbol	Mass ratio μ	Volume ratio ν
Nitrogen	N_2	75.518 %	78.084 %
Oxygen	O_2	23.135 %	20.942 %
Argon	Ar	1.288 %	0.934 %
Carbon Dioxide	CO_2	0.058 %	0.038 %

flows for each gas and not molar flow, the equation is transformed to use masses in g instead of mol. The reaction heat is calculated separately and therefore left out during the calculation.

$$C_xH_y + \left(x + \frac{y}{4} \right) O_2 \rightarrow xCO_2 + \frac{y}{2}H_2O \tag{3.78}$$

$$(x \cdot M_C + y \cdot M_H) + \left(x + \frac{y}{4} \right) M_{O_2} \rightarrow x \cdot M_{CO_2} + \frac{y}{2} M_{H_2O} \tag{3.79}$$
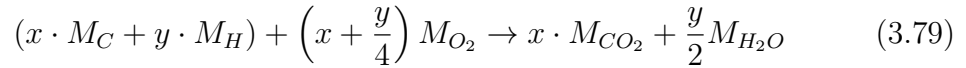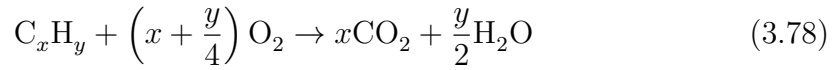
$$1 + \frac{\left(x + \frac{y}{4} \right) M_{O_2}}{(x \cdot M_C + y \cdot M_H)} \rightarrow \frac{x \cdot M_{CO_2}}{(x \cdot M_C + y \cdot M_H)} + \frac{y \cdot M_{H_2O}}{2(x \cdot M_C + y \cdot M_H)} \tag{3.80}$$

In Eq. 3.80 the reaction is divided by the molar mass of hydrocarbon. The result is the oxygen mass required to burn 1 g of fuel under stoichiometric conditions as well as the products created during the reaction. These equations are used to calculate the downstream gas composition by simply subtracting the oxygen used in the reaction from the oxygen content in the upstream gas and adding CO_2 and H_2O to the gas. The reaction heat is calculated by the heating value of the fuel.
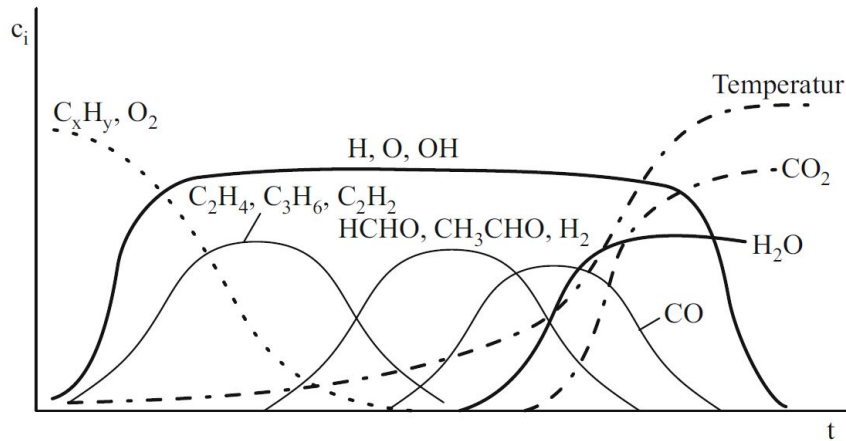
Figure 3.26: *Gas concentration and temperature over time during combustion of hydrocarbons. [5, p. 456]*

Since diesel is a very complex mixture of hydrocarbons, average values for x and y are used. Good examples can be found in [21, p. 5].

3.11 Full System Model

In the previous sections each component was viewed individually and models have been developed. These models were tested against measurement data from the prototype and pre-calibrated. In this section the full system model is built to see how the components work together.

Since the Simulink model is running in discrete time with a sample period of 10 ms and some signals need to be fed back (e.g. mass flow and temperature through the hot side of the CHEX), some algebraic loops needed to be broken. To do so, unit delays were inserted in the feedback loops.

The plant model features two input buses and one output bus. The `InputBus` holds the ambient temperature and pressure and the `DemBus` provides the demand values like air mass flow, fuel mass flow and throttle positions. The output bus named `SensorBus` is a collection of all relevant (virtual) sensors like fuel cell stack temperature, burner lambda and so on. It comprises 39 signals. Inside the plant all components are connected with the required feed-back loops. The Simulink *Signal Builder* block is used to generate input signals to the models. This block supports groups of signals to run and save different scenarios (also called test cases). The results are plotted using scopes, and can also be recorded for further investigation.
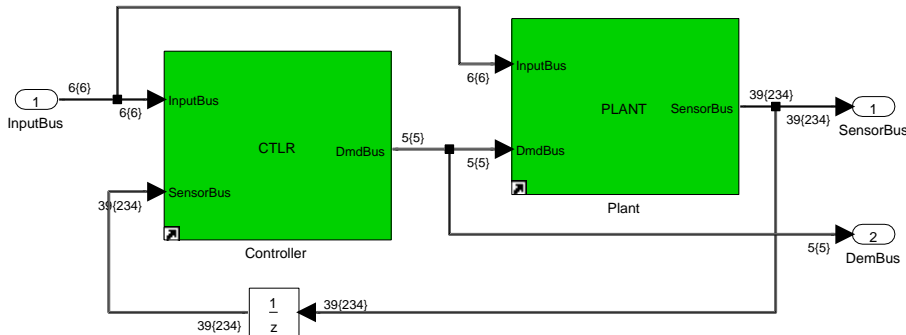
Figure 3.27: *Software system implemented in Simulink.*

3.12 Software Architecture

As mentioned before, the goal of this thesis is to model the cathode path of an SOFC system and its thermal behavior to find a suitable heat-up strategy. Two other theses will focus on different parts of the fuel cell with the objective to merge them to a complete system. To do so, it is important to define a clear software

architecture with common interfaces. It should also be possible to modify the structure for different kinds of fuel cells. Ideally the software consists of building blocks which can be altered as needed. As described in Section 3.6, a pipe network needs some form of feedback from one node to another. So the building block approach is slightly restricted.

There are two main kinds of blocks: pressure nodes and flow elements. A pressure node can be seen as a manifold volume connecting two components. A flow element can be a pipe, throttle or any flow restriction. These blocks need to be placed in an alternating manner to form a physical network. It is possible to create branches and junctions to model any pipe network. The inputs of a pressure node are incoming and outgoing mass flow. The latter is fed back from the consecutive flow element. Like in an electrical network where the voltage difference determines the current through a resistor, in fluid dynamics the pressure difference causes a mass flow through a pipe, throttle, etc. So upstream and downstream pressure are the inputs for a flow element block. The latter coming again from the consecutive pressure node. The boundary conditions of the system are atmospheric pressure at the inlet and outlet.

3.12.1 Folder Structure and Test Environment

Since there are many components and the system will grow in the future, a clear and expandable folder structure is necessary The software can be divided into three levels. A component (e.g. fuel cell stack) is on the lowest level 3. This is the smallest piece of software which is tested. The interconnection of components happens at level 2. For example the plant model which contains all physical parts (for now CCMP, CHEX, BTHR, CAT, BNR and FCS) is a level 2 composition. Another level 2 component is the controller. Finally level 1 is the entire system with plant and controller, which can run on its own. The complete system is called SwSys (Software System). this structure is commonly used in automotive projects. [22]
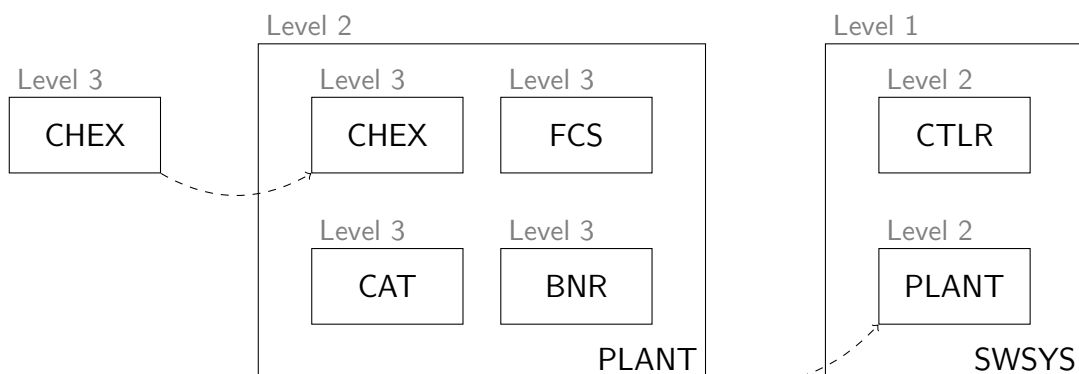
Figure 3.28: *System hierarchy.*

Each component is situated in its own directory while the structure resembles the system hierarchy shown in Fig. 3.28. Based on the cathode heat exchanger, the file structure will now be explained. Each component has a prefix, a short and a long name:

Prefix: CHEX
Short Name: CathdHex
Long Name: Cathode Heatexchanger

The prefix is used in the signal- and parameter labels, for example a calibration parameter of the cathode heat exchanger could be: `CHEX_TMax_P` (more details on the naming convention are in 3.12.2). The short name is used for the directory and all files within it. For each component there are at least four files:

`CathdHex.mdl` → Library containing the model,
`CathdHex_SigPar.m` → Parameter declaration m-Script,
`CathdHex_test.mdl` → Test environment,
`CathdHex_docu.pdf` → Function documentation.

```
SwSys
├── _SwSys
├── Plant
│   ├── _Plant
│   ├── CathdCmpr
│   ├── CathdHex
│   │   ├── CathdHex.mdl
│   │   ├── CathdHex_SigPar.m
│   │   ├── CathdHex_test.mdl
│   │   └── CathdHex_docu.pdf
│   ├── FuCellStack
│   ├── BypThr
│   ├── Cat
│   └── Brnr
├── Ctlr
│   └── ...
├── ProjectLib.mdl
└── InterfaceList.xslx
```
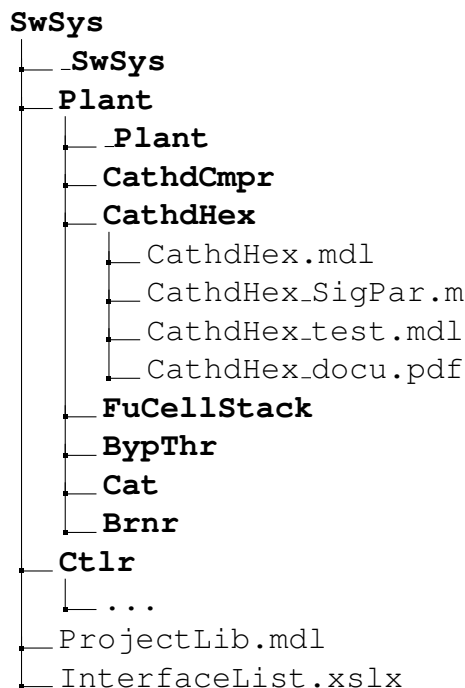
Figure 3.29: *Directory tree of the software system.*

The test environment links the component from the library and is used to stimulate the model, to test its behavior. The script `_SigPar.m` is called before simulation to load the calibration values into the MATLAB workspace. The library is also used in the upper levels. This way every change in the model can be tested on the lowest level, before running the full system. The `_docu.pdf` features the theory behind the implementation as well as the Simulink diagrams on every level with short descriptions. The latter is generated by a MATLAB script which scans

through the model and extracts the information. The output of the script is a LaTeX file and a folder containing images of every subsystem, which is later compiled to a PDF document.

In addition to the components, there is also a project library which contains commonly used blocks (e.g. unit conversion, filters, turn-on/turn-off delay,...). These blocks can be found in `ProjectLib.mdl`. The `InterfaceList.xlsx` contains every label in the system and will be discussed in the following section.

3.12.2 Naming Convention

An important topic in software development is the used naming convention. Each Simulink model comprises many internal signals, parameters and calibration maps, as well as input and output signals. The names should be clear to read and self explanatory. At AVL a modeling guideline with naming convention was developed, both were used to develop clean, readable Simulink models.

Every component has a distinct prefix, e.g. CHEX for the cathode heat exchanger. This prefix is leading every name inside one component. The grammar of the names is defined in [22]. Signals (internal and external) do not have a postfix whereas parameters use _P, axes _A, maps and curves _M and global constants use _C. To keep track of every label, its limits and units, a global interface list is used. This big table has one entry for each label and features the following columns: type (input, output, parameter,...), prefix (e.g. CHEX), name, description, physical unit, typical value (for parameters), minimum, maximum, dimension and full name. The complete table can be found in the appendix A.4.

3.12.3 Fast Implementation

Big advantages of computer simulation against real world testing is for one the possibility to try maneuvers which might damage the hardware and second a simulation speed faster than real-time. Heating up the fuel cell takes several hours while simulation should be finished in seconds. In some cases however, Simulink block diagrams can get very big and not easy to read. Sometimes it is easier to write a short MATLAB script and include it in the models.

There are different methods to use MATLAB code within a Simulink model. The *Embedded MATLAB Code* block is interpreting the code during runtime and can drastically slow down the simulation. Therefore it should be avoided as far as possible. The *MATLAB Function* block should be used instead.

The usage of MATLAB code improves readability in some cases, especially when for-loops are used. However it should be kept in mind that the function gets compiled to a mexw32 file which does not support the variable step solver. The com-

Table 3.4: *Model simulation performance*

TestCase	Sim. mode	Sim. Time	Real Time	Factor
1	normal	1000 s	25.78 s	38.8
2	normal	2000 s	33.00 s	30.1
3	accelerator	1000 s	9.03 s	110.7

plete software therefore should be written without continuous states. A discrete solver with a fixed sample time of 10 ms should be set in the Model Configuration Parameters. This also ensures a smooth transition to embedded code later in the development process. Also note that there is a list of supported MATLAB commands on the Mathworks website, since not every command is allowed in this block.

It can occur for certain inputs (e.g. transients at the cathode compressor) that the system becomes instable and values become `Inf` during simulation. Because of the great amount of signals it is not always easy to keep track of all the signals. A good indicator for instability is the calculation time. If any signal is `Inf`, the simulation slows down significantly and can be stopped for investigation.

After connecting all level 3 components to the full system, some tests have been performed to measure the required simulation time. In Tab. 3.4 the speed is shown for different test cases. With the simulation engine in *Accelerator* mode a simulation speed of well above 100 times real time can be achieved.

4

Control Design and Simulation Results

In this chapter, the control design based on the simulation model is described. As discussed in chapter 2, there are already strategies which were refined over the years. The main goal of the control design is to remove human interaction from the control loop and make sure that all limits – predominantly component temperatures – are satisfied. The heat-up process is done using a state machine which switches between different controllers according to the current state. The controller parameters were found using established methods and the simulation results are presented at the end of this chapter.

4.1   Control Structure

To control complex systems, a widely used concept is the finite state machine. The states represent all possible situations in which the system can be in. There is only a finite number of states and the transition can only occur in a predefined scheme – defined in a transition matrix. [23] The states are changed on transition conditions. A possible condition could be a timeout or the reach of a desired temperature in the system. It is important to note, that not every state can reach every other one. For example it is not possible to switch the system directly into operation mode.

The operation of the prototype can be split into five states. In each state different algorithms are implemented to provide the demand values for the system actuators. Below the states are named and their task is briefly described.

State 0: Idle

In the first state, the system is cold and waiting for the start bit to go high ("turning the key"). All actuators are set to zero.

State 1: Flush&Ignite

If the start bit is set, a state transition occurs. Now the cathode compressor is started and all valves are opened. The whole system is flushed for a certain time. After that, both valves are closed to increase the counter-pressure of the cathode compressor. Then the air mass flow can be reduced to the starting quantity. The start-up burner is turned on and then the fuel injection can be ramped up. If the temperature rises and fuel combustion is detected, the state is switched to *Heat-Up*.

State 2: Heat-Up

After detecting a flame inside the burner, the state is switched to *Heat-Up*. Now a number of control loops provide the demand values for all actuators. The goal is to reach operating temperature in all components.

State 3: Operation

In this state, the system is self-preserving, producing heat and electricity. Since (electro) chemical models for the reformer and the fuel cell stack are developed in a future thesis, the control algorithm for the active operation will also be done in the future.

State 4: Cool-Down

This state can be entered from all the others and is needed to cool down the system. Additional safety features need to be added in the future to protect sensitive components. This state can then be accessed to shut down the system as fast as possible.

In Fig. 4.1 the top level state transition diagram is pictured. In each of the five states, the tasks can be split up again.

4.2   Control Algorithm

The main focus lies on the two states *Flush&Ignite* and *Heat-Up* since *Operation* is not considered – due to the lack of chemical models of some components. The states *Idle* and *Cool-Down* do not include control loops, but only provide constant demand values to the actuators.

The manipulated variables in the system are:

- Cathode compressor mass flow

- Burner fuel mass flow

- Burner glow plugs
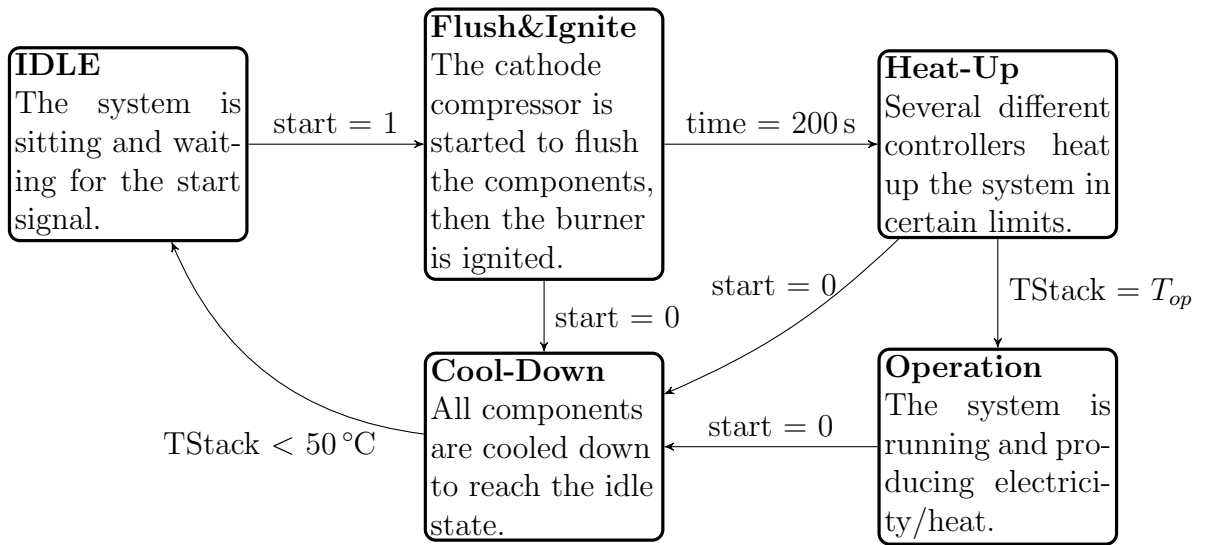
Figure 4.1: *State transition diagram.*

- Bypass throttle angle

- Reformer throttle angle

4.2.1 Flush & Ignite

This state is flushing the system so every component is filled with fresh air. After that, the ignition of the burner is performed. If the temperature at the burner outlet is high enough and ignition is detected, the state machine can switch into *Heat-Up*. The required steps are listed below.

1. Open both throttle valves fully

2. Ramp up the cathode compressor mass flow

3. Flush the system for a few seconds

4. Turn on the burner glow plugs

5. Ramp up the burner fuel mass flow to reach the ignition air/fuel ratio (λ)

6. Switch to state *Heat-Up* if the burner downstream temperature is high enough (ignition detected)

Each step is triggered by a delay line with calibratable delay times. The system is flushed for 30 s, then the glow plugs are turned on and after another 30 s the fuel injection is ramped up. The required air/fuel ratio to ignite Diesel dictates the air and fuel mass flows in this state.

4.2.2 Heat-Up

After the burner is ignited, all valves are closed and the *Heat-Up* state is entered. The task to bring the system to operating temperature is split up into two phases:

Phase 1
The air mass flow is held constant to achieve stable conditions in the system. The fuel quantity is controlled to hold the burner downstream temperature at 850 °C. However, the stack upstream temperature cannot heat up this far with the bypass valve closed. If a stable temperature is reached, the bypass valve controller is activated. The targeted temperature is the highest allowed difference between inlet and outlet of the stack. Opening the bypass valve decreases the cold mass flow through the heat exchanger, and therefore increases the outlet temperature. The burner controller needs to compensate the additional cold air mixed into the upstreaming gas. Now a stack temperature of 750 °C can be achieved. This completes the first phase of the heat-up procedure.

Phase 2
In the second phase, the anode path is activated and current is drawn from the stack. Since the anode path is still to be modeled, the only effects considered are the drawn current from the stack and the exothermic reactions inside the catalyst, during conversion of the anode exhaust gas. The internal resistance of the stack is very high at these comparatively low temperatures, but drawing current is required to reach operating temperature. The resistance rises very slowly, so this phase takes several hours. The fuel cell reaction is also exothermic, so the cathode exhaust gas will heat up inside the stack as well. Until the fuel cell reaction emits enough heat, the burner controller needs to reduce the fuel quantity to compensate for the higher inlet temperature. This can only be done in a certain range, because once the injection mass flow reaches its lower limit (upper lambda limit), the burner flame is blown out. This is a critical point in the heat-up procedure, since the temperature drops very rapidly. The goal is to increase the catalyst temperature as fast as possible by ramping up the H_2 content in the anode gas.

To achieve the desired heat-up behavior explained above, a number of different PI-controllers is used. Since the same controller structure is reused, the Simulink implementation is addressed at this point.

The PI-controller is one of the standard control structures. It is discussed in many text books. The relation between manipulated variable u, controlled variable y and target value r is given by: [24, p. 258]

$$e(t) = r(t) - y(t) \tag{4.1}$$

$$u(t) = K_p \cdot e(t) + \frac{K_P}{T_I} \int_0^t e(\tau) \, d\tau \tag{4.2}$$

$$R(s) = K_p \left(1 + \frac{1}{sT_I} \right) \tag{4.3}$$
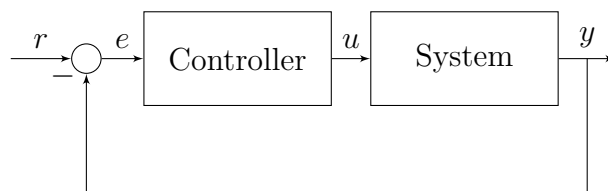
Figure 4.2: *Standard control loop.*

Where r is the target value,
$\quad$ u is the manipulated variable,
$\quad$ y is the controlled variable,
$\quad$ e is the control error,
$\quad$ K_P is the proportional gain,
$\quad$ K_I is the integral gain and
$\quad$ T_I is the settling time.

Since the implemented software is running in discrete time steps ($T_s = 10\,\text{ms}$), the transfer function needs to be translated into a difference equation. In [25, p. 4] the derivation of one possible implementation is explained:

$$e_k = r_k - y_k \tag{4.4}$$

$$u_k = u_{k-1} + K_P \cdot e_k + \left(\frac{K_P}{T_I} T_s - K_P \right) e_{k-1} \tag{4.5}$$

Every controller has an additional input for the selected and limited u_{true} value. This is important since the controller needs to know if it is selected/limited or not. If the output is limited, the integrator of the controller needs to be reset, to eliminate windup.

The windup effect is an undesirable phenomenon in control loops which are using integrating elements. In practice, the manipulated variable can only be operated inside boundaries. For example, the throttle valve angle is limited between $0\,°$ to $90\,°$. The controller does not know that and may try to open the valve further. To avoid this, the manipulated variables are limited to their maximum values. In the period where the manipulated variable is limited, the integrating

element in the controller winds up and drastically worsens the performance. [24, p. 199]

If one controller is not selected and the deviation between u and u_{true} is bigger than a calibratable threshold, the controller is reset to u_{true}. Although the final implementation does not feature parallel controllers acting on the same variable, there have been tests with such a structure. To operate controllers in parallel and select them afterwards (e.g. based on the minimum), it is important that the anti-windup algorithm does not reset the controller right away but only at a certain deviation. The selector then can decide which controller is best.

An established PI-controller block was used in Simulink, where the anti-windup logic was added. In Fig. 4.3 the implementation is pictured. The selection of the control parameters is described in section 4.2.3
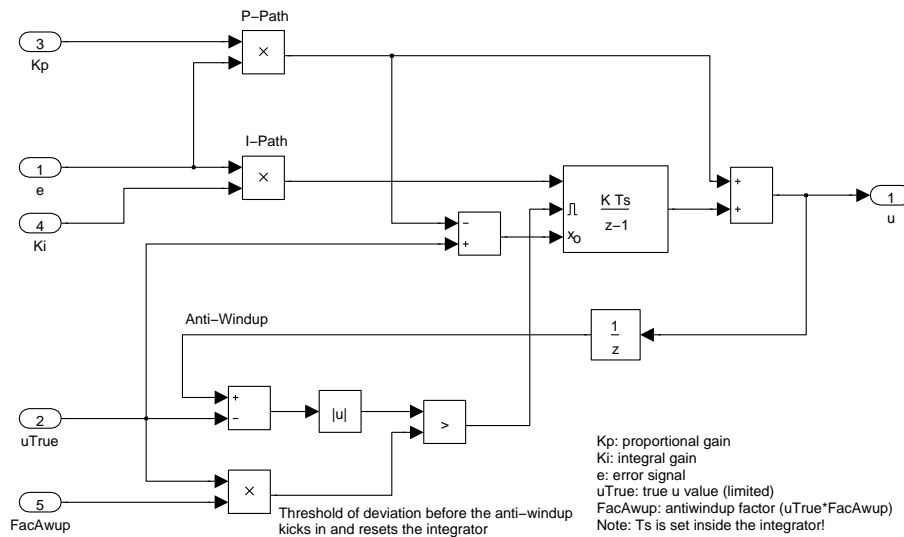
Figure 4.3: *Discrete PI-controller with anti-windup logic (Simulink).*

In Fig. 4.4 the anti-windup function is visualized. The given controller is trying to inject more fuel (blue) than the selected one (red). Every time it reaches a 5 % threshold, the controller is set to the selected output u_{true}. If the observed controller was selected, u would be equal to u_{true} and the anti-windup were disabled.

There have been different tests with different control strategies to find the best one. All control loops, their purpose and findings during the tests are described below.

Controller 1
Controlled variable: y = Burner downstream temperature,
Target value: $r = 850\,°C$ at burner outlet,
Manipulated variable: u = Burner fuel mass flow.

This controller has the higherst priority since the heat exchanger upstream temper-
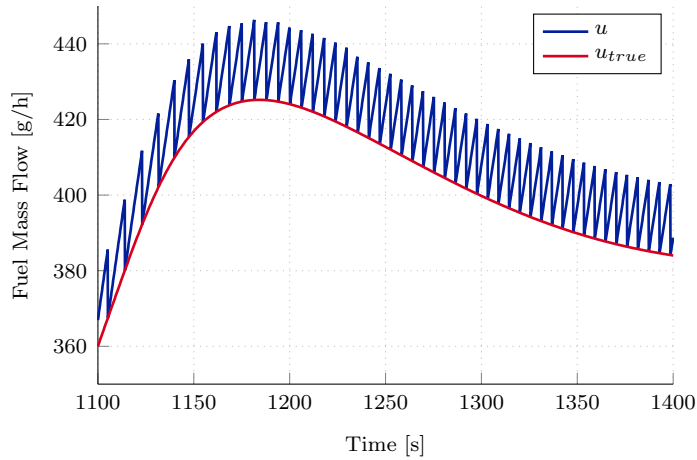
Figure 4.4: *Anti-Windup for selected controller.*

ature must not exceed a certain limit, otherwise it could be damaged. In addition to this temperature limit, NO_x emissions become dominant from $1000\,°C$ and up, which must be avoided as well. The flame is blown out at an air/fuel ratio $\lambda > 12$. At this point the fuel injection is turned off. If the stack downstream temperature is high enough, the system can hold the temperature and the burner is turned off.

Controller 2
$y =$ Fuel cell stack upstream/downstream temperature difference,
$r =$ constant upstream/downstream temperature difference,
$u =$ Burner fuel mass flow.

This control loop tries to hold the temperature difference between fuel cell stack inlet and outlet constant by manipulating the amount of injected fuel. Too high temperature differences lead to damage of the component.

Simulations showed that this temperature difference cannot be reached, unless the burner temperature rises well above $1000\,°C$. It is desirable to have a constant temperature at the burner, which is achieved with *Controller 1*.

Controller 3
$y =$ Fuel cell stack downstream temperature gradient,
$r =$ maximum temperature gradient at cathode outlet,
$u =$ Cathode air mass flow.

The transmitted energy depends primarily on the air mass flow, since air is the transport medium. Since *Controller 1* holds the temperature at heat exchanger inlet constant, the energy depends on the moved air mass. The air mass flow is pre-controlled and the controller increases it if the temperature gradient gets smaller – towards the end of the heat-up process.

Controller 4
y = Fuel cell stack upstream temperature,
r = Constant fuel cell stack upstream temperature,
u = Bypass throttle angle.

The maximum achievable fuel cell stack upstream temperature is below the stack operating temperature if the bypass valve is closed. Since this is not enough for operating the fuel cell, the bypass valve can be closed to reduce the cold mass flow through the heat exchanger. This controller is only active if this limit is reached and stable to transmit the maximum amount of energy initially. If the self-holding temperature is reached, the valve angle is frozen.

Controller 5
y = Fuel cell stack upstream temperature,
r = Fuel cell stack downstream temperature + ΔT limit,
u = Bypass throttle angle.

This is an improvement of *Controller 4*. The only difference is that the target temperature now depends on the current stack outlet. There is an effect in the real system where a too small mass flow through the cold side of the heat exchanger results in lower stack upstream temperatures because of losses in the pipes. At the moment, losses are only considered in the components, not in the pipes. If these losses are implemented in the future, a maximum valve angle could be determined to limit the controller.

The different controllers explained above are all implemented in the software and can be activated individually or in combination. For the current calibration the optimal heat-up behavior is achieved with *Controller 1* and *Controller 5*. In section 4.3 the simulation results of this control strategy are discussed.

4.2.3 Control Parameters

To determine the controller parameters the Ziegler/Nichols[1] open-loop method was used. These parameters are often used as starting points and work well for delaying processes. Characteristic for such processes is the turning point in the step response. It is well suited for systems where disturbances need to be rejected. For a PI-controller the parameters K_P and T_I are calculated using the equations below. [24, p. 261]

---

[1] John G. ZIEGLER (1909 - 1997) and Nathaniel B. NICHOLS (1914 - 1997), American control engineers.

Table 4.1: *Burner fuel controller parameters*

Fuel	a_1	a	T_V	K_P	T_I	K_I
⌐ 200 g/h	20.7	124.4	1.3	0.0072	3.9	0.0019
⌐ 400 g/h	39.4	118.2	1.3	0.0076	3.9	0.0020
⌐ 800 g/h	87.4	131.1	1.4	0.0069	4.2	0.0016
⌐ 1200 g/h	119.4	119.4	1.4	0.0075	4.2	0.0018

$$R(s) = K_P \left(1 + \frac{1}{sT_I} \right) = K_P + \frac{K_I}{s} \tag{4.6}$$

$$K_P = 0.9a^{-1} \tag{4.7}$$

$$T_I = 3T_V \tag{4.8}$$

To determine the values a and T_V, four fuel steps have been performed. A tangent was fitted at the turning point in each step response. In Tab. 4.1 the tangent and controller parameters are listed. Note that column a_1 is the value from the diagram but needs to be scaled to the maximum fuel step (1200 g/h). The corrected value is in column a. In Fig. 4.5 one step is shown. Note that the temperature will increase since there is a positive feedback in the system.
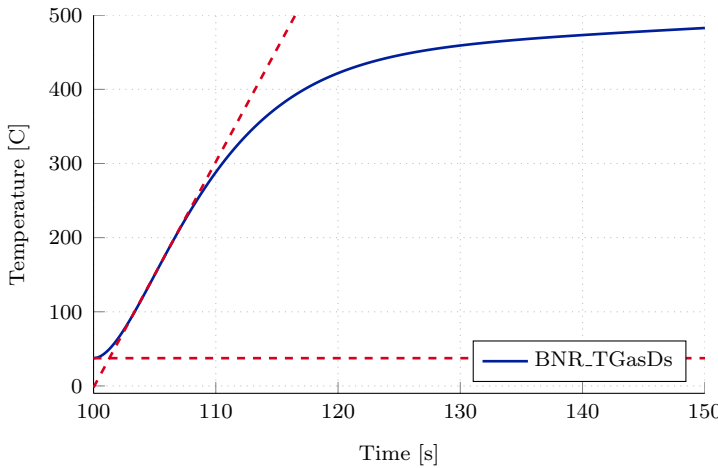
Figure 4.5: *Burner downstream temperature step response* 400 g/h.

The Ziegler/Nichols method did deliver a good starting point where the system is stable, holds the desired temperature very well and has a good disturbance rejection. However, the parameters have been updated to increase the performance a bit further. The throttle controller was calibrated slower than the burner controller, since it depends on the burner downstream temperature – and also affects it. The slower response time of the throttle controller allows the burner downstream temperature to settle and no oscillation appears. In Tab. 4.2 the

Table 4.2: *Bypass throttle controller parameters*

Throttle Angle	a_1	a	T_V	K_P	T_I	K_I
$\llcorner$ 45°	12.5	25	30	0.036	90	0.000 40
$\llcorner$ 90°	18	18	30	0.05	90	0.000 56

parameters for the throttle controller are listed. The steps were measured in the stable region, where the stack upstream temperature has settled. This is the only operating point where the throttle controller is active.

4.3   Simulation Results

In this section the final simulation results are presented, and the performance of the control algorithm is shown. These tests have been performed on the full system. Note that the heat-up speed of some components is faster than in the prototype.

4.3.1   Test-Case 1: Heat-Up (Phase 1)

This test case starts the system and the state machine takes care of the heat up until a stable temperature is reached at the outlet of the fuel cell stack. In Fig. 4.6 all relevant temperatures are plotted, normalized to the burner outlet target temperature. At the beginning of the test the system is at room temperature.

Beginning at 130 s the state machine starts *state 1* (Flush&Ignite). The burner is ignited and the temperature at its outlet (solid blue line) initially rises to 1500 °C due to a very low lambda. After a few seconds the fuel mass flow controller holds the burner downstream temperature at its target value. Note that the bypass valve is fully closed, so the gas temperature at the outlet of the heat exchanger can only reach a maximum of about 70 % of the target temperature. Once this point is reached and stable, the bypass throttle controller starts to act and tries to increase the stack upstream temperature to the maximum stack upstrem/downstream difference. Note that the fuel mass flow controller has to compensate for the drop in the air temperature, due to the shift in mass flows. The light blue line in 4.6 represents the air temperature entering the burner. Except for a short dip in the burner downstream temperature (at 3500 s), the controller can compensate for this disturbance.

In Fig. 4.7 all actuators are plotted. The first diagram shows the air and fuel mass flows. The initial peak in the fuel mass flow is during the burner ignition. After that *Controller 1* is active. The injected fuel decreases steadily because there is a positive feedback in the system. As the fuel cell stack temperature increases, the air entering the burner also gets hotter and the controller needs to reduce
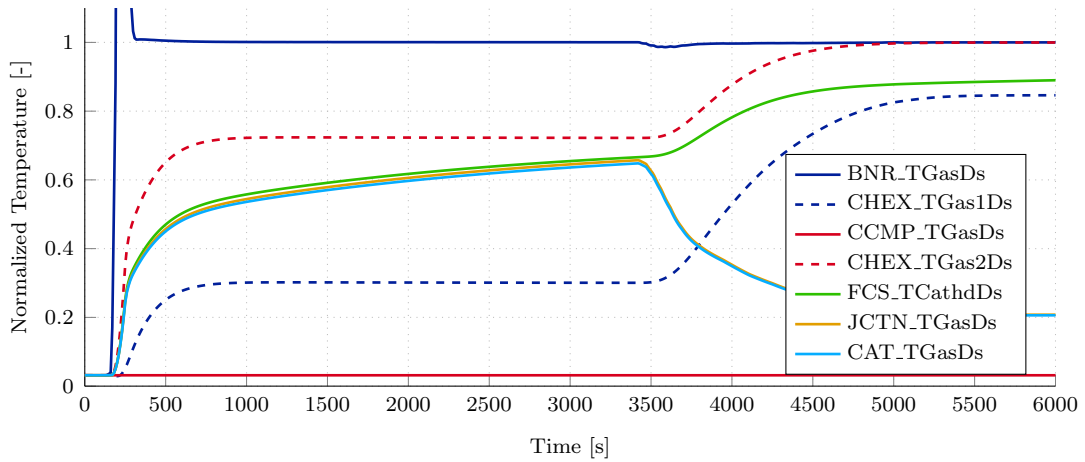
Figure 4.6: *System Simulation: Gas Temperatures.*

the fuel quantity. After the bypass throttle controller becomes active (*Controller 5* at 3400 s) the fuel mass flow increases to compensate for the burner upstream temperature (see Fig. 4.6, light blue line).

In the second diagram the bypass throttle angle is plotted. To achieve the maximum allowed temperature difference between inlet and outlet of the stack, the bypass throttle is gradually opened to reduce the mass flow through the cathode heat exchanger.
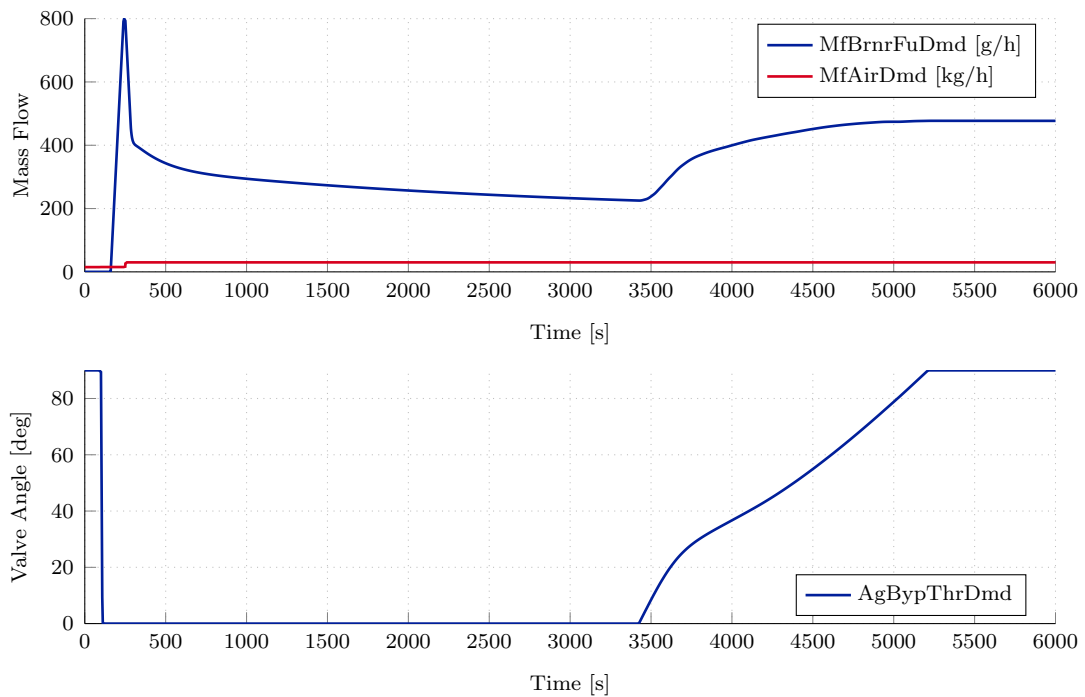
Figure 4.7: *System Simulation: Demand values.*

4.3.2 Test-Case 2: Heat-Up (Phase 1+2)

This test case is the continuation of the first one, including phase 2 in which anode exhaust gas is added and current is drawn from the stack. The anode exhaust gas is converted inside the catalyst where heat is released. The drawn current also results in a heat up of the stack.

In Fig 4.8 the system temperatures are plotted with respect to the burner target temperature. At 6000 s the anode exhaust gas is ramped up. This results in an increase of the catalyst downstream temperature (light blue line). The fuel mass flow is reduced to keep the temperature at the burner outlet constant. At 7000 s current is ramped up which heats up the stack. The stack downstream temperature (green line) rises and the burner is turned off. This completes the heat-up and the system can hold its temperature without the need of the start-up burner.
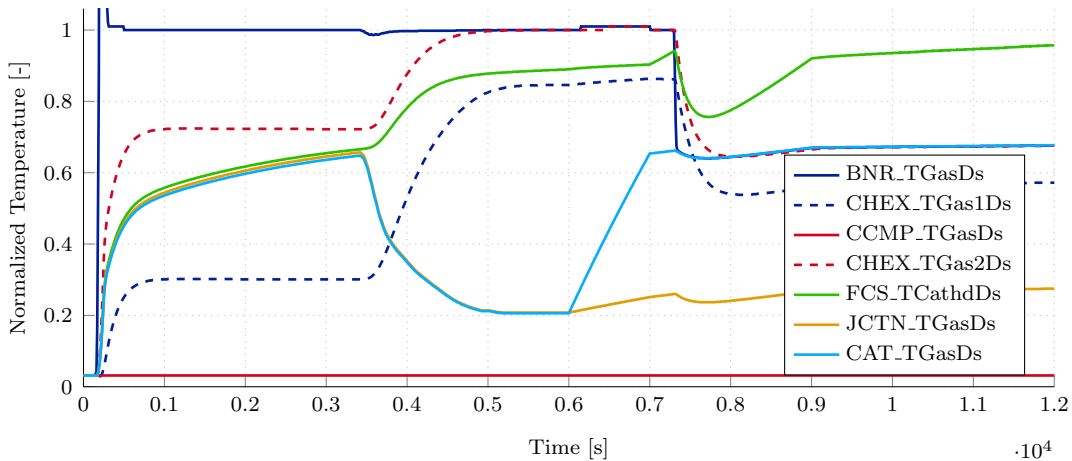
Figure 4.8: *System Simulation: Gas Temperatures.*

In Fig. 4.10 the mass flows throughout the system are shown. The effect of the bypass throttle is higher than in cold conditions, since the counter pressure in the heat exchanger increases with the temperature. We can also see the additional anode exhaust gas at 6000 s.
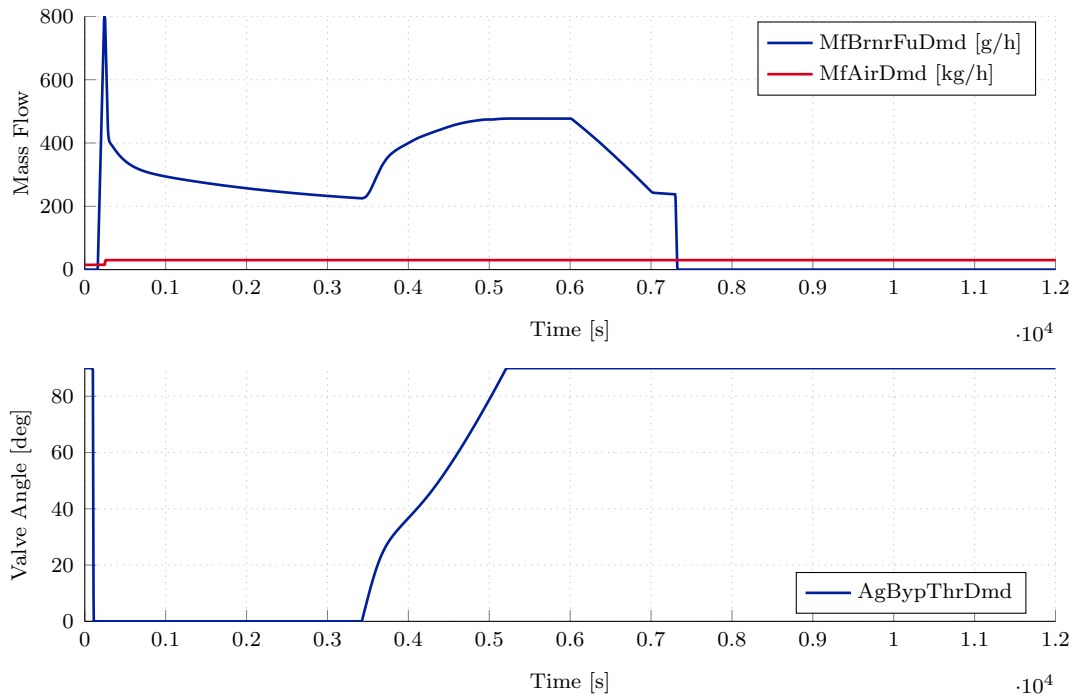
Figure 4.9: *System Simulation: Demand values.*
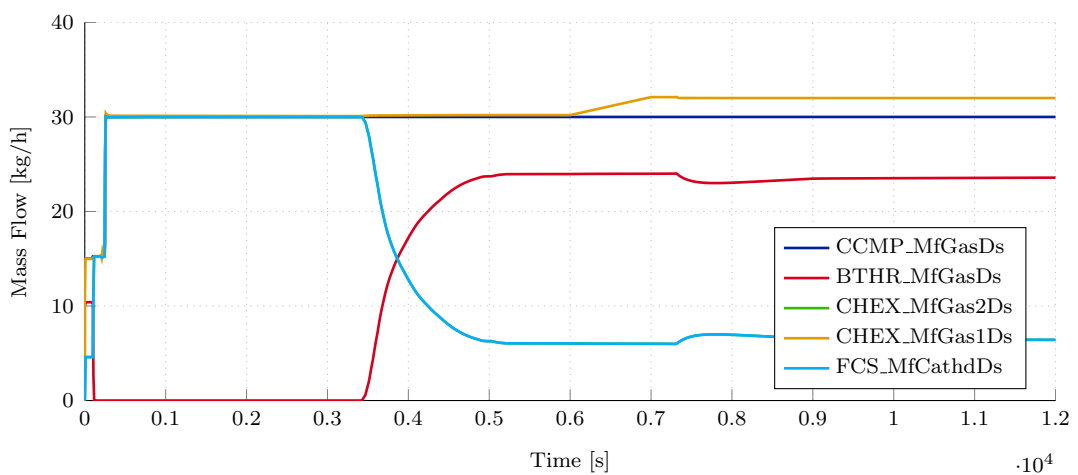
Figure 4.10: *System Simulation: Mass flow.*

5

Conclusion and Outlook

5.1 Conclusion

Modeling physical systems is a challenge, since much time can be spent refining the models and including more and more effects. For control design, the model does not need to cover every physical detail. It is more important for the model to show the same behavior in the regions of interest. For this work, the most important effects are heat-up of physical components and the influence of different mass flow rates on the heat transfer. These effects were modeled sufficiently to find a suitable control strategy.

During this thesis a set of building blocks was developed to build an arbitrary system architecture. The components can be calibrated to fit the needs of the setup. The full system then offers a testing environment to design control strategies and try out maneuvers, which would be to risky (and time consuming) to conduct on the real system. A set of controllers has been developed which can be used individually or in combination to learn more about the behavior of the system. For the current development status of the prototype, the proposed control strategy delivers reasonable results.

The biggest challenge was to match the measurement data, knowing very little about the physical components. The proposed heat-up strategy shows some significant improvements to the previously used, mainly manually performed steps. The simulation showed for instance, that the lambda controller is not ideal, instead a constant air flow and a controlled fuel quantity supplies constant power to the system and the response is more predictable.

5.2 Outlook

The modeled components form about one third of the full fuel cell system. The other parts like the chemical models of the stack and reformer, will be developed in two other theses. This work is the basis for these extensions. Also different fuel cell applications (e.g. mobile) will use the building blocks.

The models are kept as simple as possible, with room for improvement. New measurements, especially when the new controller is used on the prototype can lead to new insights, which should be used to refine the models. This work offers an expandable and easy to use environment, on which future research can build on.

5.2.1 Linking Software and Hardware

The software is implemented in Simulink to be as flexible as possible. Independent of the final hardware, the software can be compiled for different platforms. The current prototype is operated by a CompactRIO (cRIO) System from National Instruments. This is a processing platform with many inputs and outputs. Not only the control software (programmed in LabVIEW) is currently running on it, also the sensor and actuator interfaces (PWM, DAC/ADC,..) are driven by this device.

In the future, the LabVIEW software should be replaced by the Simulink implementation, since the models can be tested with approved tools and methods. As shown in Fig. 5.1, the Simulink implementation is divided into two main parts. The plant which models the behavior of the real system and the controller which reads sensor values and sends appropriate demand values to all actuators. In this environment the control strategies can be tested and refined. Afterwards only the controller is used to generate C Code which can then be compiled for a rapid prototyping system like the ETAS ES1000. This device allows to monitor signals and update parameters during runtime via the calibration tool INCA. The ES1000 communicates with the cRIO via a CAN bus connection. Like in the Simulink architecture, the demand values for all actuators and all sensor values are communicated through this channel. The cRIO then no longer runs all the algorithms but only functions as an interface between software and the real world. It converts the demand values into electrical signals for each actuator (e.g. PWM for throttle valves) and reads back all sensor values (e.g. ADC). This closes the loop between software and real world hardware. During operation all signals can be monitored and logged by INCA. This data can then be used to refine the Simulink models.
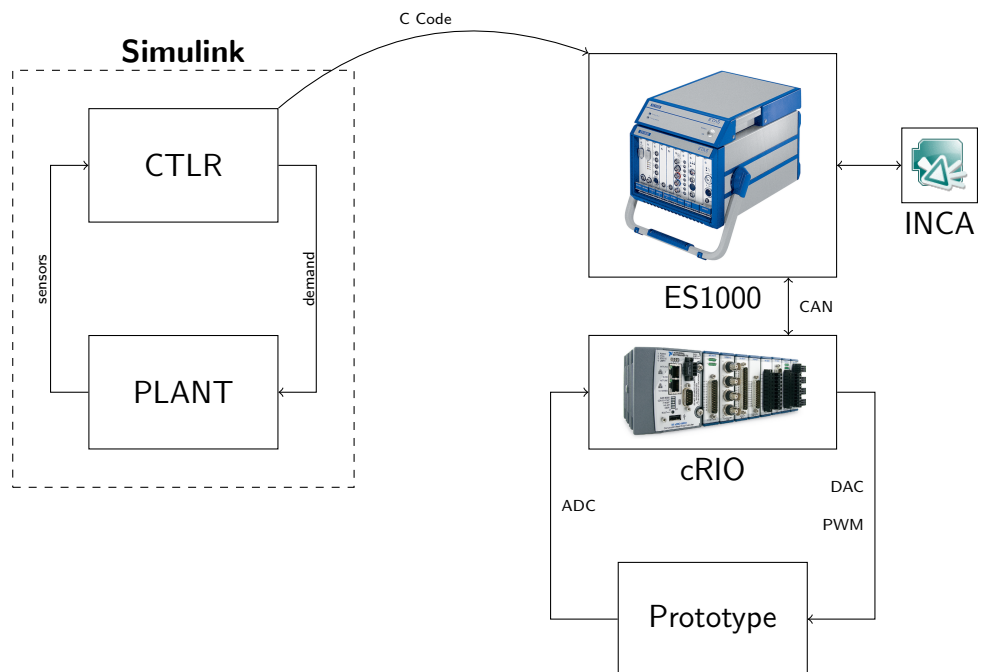
Figure 5.1: *Testing and operation environment.*

Bibliography

[1] J. Hirschenhofer, D. Stauffer, R. Engleman, and M. Klett, *Fuel Cell Handbook*. Parsons Corporation, 1998.

[2] C. Wächter, *Modellierung, Regelung und Simulation des Betriebsverhaltens eines SOFC/GT-Hybridkraftwerks*. PhD thesis, Helmut-Schmidt-Universität, Hamburg, 2008.

[3] P. Carlsson, "Flow through a throttle body," Master's thesis, Linköping University.

[4] H. Sigloch, *Technische Fluidmechanik*. Springer Berlin Heidelberg New York, 2008. ISBN 978-3-540-44633-0.

[5] G. P. Merker, C. Schwarz, and R. Teichmann, *Grundlagen Verbrennungsmotoren*. 5. Auflage, Vieweg+Teubner Verlag, 2011. ISBN 978-3-8348-1393-0.

[6] I. Barin, *Thermochemical Data of Pure Substances*. VCH Verlagsgesellschaft, third edition ed., 1995. ISBN 3-527-28745-0.

[7] S. Chemicals, "Shellsol d100," 2009. Data Sheet.

[8] A. Heinzel, M. Cappadonia, U. Stimming, K. V. Kordesch, and J. C. Oliveira, *Fuel Cells. Ullmann's Encyclopedia of Industrial Chemistry*. VCH Verlagsgesellschaft, 2000.

[9] F. Barbir, *PEM Fuel Cells: Theory and Practice*. Elsevier Academic Press, 2005. ISBN 0-12-078142-5.

[10] J. T. S. Irvine and P. Connor, *Solid Oxide Fuel Cells: Facts and Figures*. Springer London Heidelberg New York Dordrecht, 2013. ISBN 978-1-4471-4455-7.

[11] K. A. Adamson, *Stationary Fuel Cells - An Overview*. Elsevier, 2007. ISBN 978-0-08-045118-3.

[12] B. Sorensen, *Hydrogen and Fuel Cells. Emerging Technologies and Applications*. Elsevier Academic Press, 2005. ISBN 978-0-12-655281-2.

[13] J. T. Pukrushpan, *Modeling and Control of Fuel Cell Systems and Fuel Processors*. PhD thesis, University of Michigan, 2003.

[14] H. D. Baehr and K. Stephan, *Wärme- und Stoffübertragung.* 7. Auflage, 2010. ISBN 978-3-642-05500-3.

[15] T. W. Peter Böckh, *Wärmeübertragung. Grundlagen und Praxis.* Springer Vieweg, 2014. ISBN 978-3-642-37730-3.

[16] S. V. Automotive, "Specification smart acv actuator," 2003. Data Sheet.

[17] O. Bratland, *Pipe Flow 1.* Dr. Ove Bratland, 2013. ISBN 978-616-335-925-4.

[18] Dubbel, *Taschenbuch fuer den Maschinenbauer.* 22. Auflage, Springer Berlin Heidelberg New York, 2007. ISBN 978-3-540-49714-1.

[19] A. Batalov, "Pressure flow network modeling," 2011. Project Report.

[20] S. Martin, G. Kraaij, T. Ascher, P. Baltzopoulou, G. Karagiannakis, D. Wails, and A. Wörner, "Direct steam reforming of diesel and diesel-biodiesel blends for distributed hydrogen generation," 2014.

[21] R. C. Flagan, *Fundamentals of Air Pollution Engineering.* Prentice Hall, 1988. ISBN 0-13-332537-7.

[22] AVL, "Modeling for embedded systems with simulink based toolchains," 2013. Internal document.

[23] F. Wagner, R. Schmuki, T. Wagner, and P. Wolstenholme, *Modeling Software with Finite State Machines. A Practical Approach.* Auerbach Publications, 2006. ISBN 978-0-8493-8086-0.

[24] N. Dourdoumas and M. Horn, *Regelungstechnik.* Pearson, 2004. ISBN 3-8273-7059-0.

[25] F. Gausch, A. Hofer, and K. Schlacher, *Digitale Regelkreise.* Technische Universität Graz, 1991.

<div align="right">

A

</div>

Appendix

A.1 Project Library

To manage reoccurring blocks like unit conversion, filters, heat capacity calculation, etc., a project library was set up. These blocks are linked into the system, to be able to update them in only one place. Another benefit of moving even simple conversion routines into a library, is to provide readability in bigger models.

In Fig. A.1 a first order low-pass filter is shown. This implementation was used several times in the model. The derivation of the difference equation is described in section 3.1.

$$H(z) = \frac{\frac{T_s}{\tau}}{1 - (\frac{\tau - T_s}{\tau})z^{-1}} \tag{A.1}$$

$$y[n] = \frac{T_s}{\tau}(x[n] - y[n-1]) + y[n-1] \tag{A.2}$$

A.1.1 Catalyst Reduction Vectors

In the catalyst model, reduction vectors are used to calculate the gas concentrations at the outlet. Here is a complete list of these vectors. These vectors represent
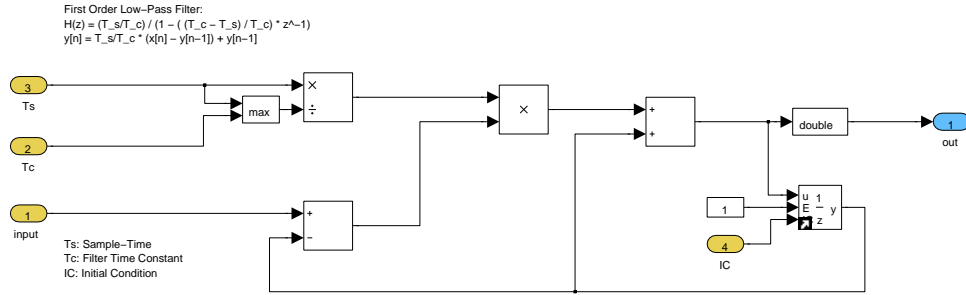
Figure A.1: *Library block: first order low-pass filter*

the change in mass of each gas, after complete combustion/catalytic conversion. The derivation of these values is described in section 3.9.

$$\mathbf{v}_{red,CO} = \begin{bmatrix} -1, 0, 0, 0, 0, 0, 0, 0, 0, 0, 0, 0, 0, 0 \end{bmatrix}^T$$

$$\mathbf{v}_{red,CO2} = \begin{bmatrix} 1.571, 0, 0, 0, 2.743, 0, 0, 0, 2.995, 3.029, 1.911, 1.374, 3.110, 3.083 \end{bmatrix}^T$$

$$\mathbf{v}_{red,H2O} = \begin{bmatrix} 0, 0, 0, 8.937, 2.246, 0, 0, 0, 1.635, 1.550, 1.173, 1.125, 1.353, 1.420 \end{bmatrix}^T$$

$$\mathbf{v}_{red,H2} = \begin{bmatrix} 0, 0, 0, -1, 0, 0, 0, 0, 0, 0, 0, 0, 0, 0 \end{bmatrix}^T$$

$$\mathbf{v}_{red,CH4} = \begin{bmatrix} 0, 0, 0, 0, -1, 0, 0, 0, 0, 0, 0, 0, 0, 0 \end{bmatrix}^T$$

$$\mathbf{v}_{red,O2} = [-0.571, 0, 0, -7.937, -3.989, 0, 0, 0, -3.630, -3.579, -2.084, -1.498,$$
$$- 3.462, -3.502]^T$$

$$\mathbf{v}_{red,N2} = \begin{bmatrix} 0, 0, 0, 0, 0, 0, 0, 0, 0, 0, 0, 0, 0, 0 \end{bmatrix}^T$$

$$\mathbf{v}_{red,Ar} = \begin{bmatrix} 0, 0, 0, 0, 0, 0, 0, 0, 0, 0, 0, 0, 0, 0 \end{bmatrix}^T$$

$$\mathbf{v}_{red,C3H8} = \begin{bmatrix} 0, 0, 0, 0, 0, 0, 0, 0, -1, 0, 0, 0, 0, 0 \end{bmatrix}^T$$

$$\mathbf{v}_{red,C4H10} = \begin{bmatrix} 0, 0, 0, 0, 0, 0, 0, 0, 0, -1, 0, 0, 0, 0 \end{bmatrix}^T$$

$$\mathbf{v}_{red,C2H6O} = \begin{bmatrix} 0, 0, 0, 0, 0, 0, 0, 0, 0, 0, -1, 0, 0, 0 \end{bmatrix}^T$$

$$\mathbf{v}_{red,CH4O} = \begin{bmatrix} 0, 0, 0, 0, 0, 0, 0, 0, 0, 0, 0, -1, 0, 0 \end{bmatrix}^T$$

$$\mathbf{v}_{red,C12H26} = \begin{bmatrix} 0, 0, 0, 0, 0, 0, 0, 0, 0, 0, 0, 0, -1, 0 \end{bmatrix}^T$$

$$\mathbf{v}_{red,C8H18} = \begin{bmatrix} 0, 0, 0, 0, 0, 0, 0, 0, 0, 0, 0, 0, 0, -1 \end{bmatrix}^T$$

A.2   Helper Function Documentation

During the course of this thesis, some MATLAB functions where written to pre-process measurement data and generate documentation for example. In this section these helper scripts are listed with a short description.

```
convertData;
```

The testbed data is stored in a CSV format which consists of labels in the first row and with tabulator separated data in the columns. The format looks something like this:

```
time   sensor1   sensor2   ..
0   23.4   452.4   ..
1   24.2   450.9   ..
```

Since this format is not very well to handle because of the big file sizes, a script was written to convert the data to a MATLAB mat file. In the mat file every sensor is stored as a vector with two columns, the first is the time and the second the data. This format is needed to import measurement data into Simulink using *From Workspace* blocks.

```
cutData;
```

This script asks for a mat file (generated by `convertData`) and allows the user to cut different parts from the measurements. This is useful if a specific procedure should be tested and the whole measurement is too long to simulate. The time vector is modified to start at zero, so Simulink does not produce an error.

```
Tester;
```

The tester script provides a simple GUI to run Simulink simulations and most importantly save the logged signals into a mat-file. This file has a convenient structure to use the simulation results in other scripts (e.g. for plotting) or even import it into Simulink again.
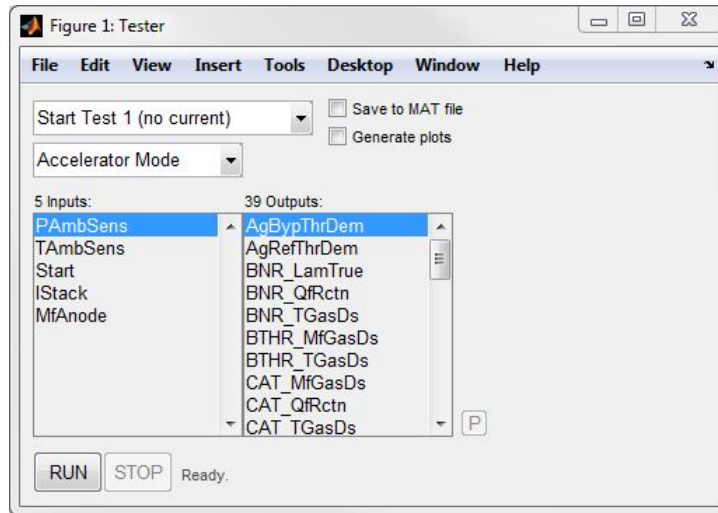
Figure A.2: *Tester GUI.*

In Fig. A.2 the user interface is shown. The script is looking for Signal Builder blocks in the currently active Simulink model. It extracts data like simulation time and test cases from this block and lets the user make some setting. The simulation mode, as well as the simulation time of the selected test case are set and via the RUN/STOP buttons, the simulation can be controlled. If the checkbox *Save to MAT file* is selected, the logged signals (blue antennas at block output) are formatted correctly and saved into a mat-file. If the *Generate plots* checkbox is set, PDF plots of all output signals are generated and saved.

```
genCompDocu;
```

This script generates a documentation LATEX file which can be imported into an existing document. Some variables need to be set in the script (like component name). The model is captured and all subsystem levels are stored as images. Information about calibration data and the models is obtained by the block properties and the global interface list (xlsx).

```
texStr = xls2ltx(FileName,range,align)
```

It can be very time consuming to import Excel sheets into a Latex document. Therefore a short script was written to do exactly that. Given a filename, the

range inside the table (e.g. 'A2:J39') and the alignment (e.g. 'l' for left or 'c' for centered, respectively), the function returns a string with latex code which can directly be copied into a Latex document. Some special characters like '_' or 'ˆ' are replaced by '_' and '\\ˆ{}'. A caption and a label is also added based on the filename.

A.3 Controller State Machine

The following lines of code represent the state machine of the controller. It is responsible to switch states (e.g. from *Flush&Ignite* to *Heat-Up*). The inputs are the start bit, the current system time in seconds and the upstream and downstream temperatures of the stack. Note that the cyan variables are persistent, which means that they stay in memory after the first call of the function. This way the state and start time of the system are available at every time step without the need of a feedback loop.

Code A.1: *Controller State Machine.*

```matlab
function state = StateManager(start, time, TCatdhUs, TCathdDs)
%#codegen

persistent state_int start_time;

deltaTStack = TCatdhUs - TCathdDs;
KELVIN = 273;

if isempty(state_int)
  state_int = 0;
  start_time = 0;
  fprintf('==== State-Manager ====\n');
end

switch(state_int)
  case 0  % IDLE
    if (start == 1)
      state_int = 1;
      start_time = time;
      fprintf('State: 0 -> 1 (%.1f s)\n',time);
    end

  case 1  % FLUSH & IGNITE
    if (time-start_time >= 200)
      state_int = 2;
      fprintf('State: 1 -> 2 (%.1f s)\n',time);
    elseif (start == 0)
      state_int = 4;
      fprintf('State: 1 -> 4 (%.1f s)\n',time);
    end

  case 2  % HEAT-UP
    if (start == 0)
      state_int = 4;
      fprintf('State: 2 -> 4 (%.1f s)\n',time);
    end
```

```
37
38    case 3   % ACTIVE OPERATION
39
40    case 4   % COOL-DOWN
41      if(TCathdDs <= -1) % state inactive!!
42        state_int = 0;
43        fprintf('State: 4 -> 0 (%.1f s)\n',time);
44      end
45  end
46
47  state = state_int;
```

A.3.1   Simulation Findings

This sections should give the people who will build on this software a few hints for working with the system.

Valve position: The valves can cause instability if the initial position (on start up) is not correct. The bypass valve needs to be opened while the reformer valve needs to be closed.

Air mass flow: The initial air mass flow must not be zero ($15\,\text{kg/h}$ is recommended). Also bigger down-steps cause oscillation and instability.

Burner/Catalyst: These components share a pipe, since they are also combined in the prototype. However the big temperature difference between inlet and outlet leads to pressure differences which are higher than in reality. Therefore the outlet temperature is set to the same as the inlet temperature for a stable simulation. The pipe model needs to be revisited in the future, since the temperature dependent pressure rise is too high.

Map-Settings: A problem which caused the pressure drop over a pipe to decrease after a certain temperature (which is physically wrong), was due to the lambda (friction coefficient) and viscosity maps. These maps were calibrated to fit the measurement data, however in the full system the range of the input was exceeded and the interpolation algorithm of the look-up table block returned no plausible values. For the first system tests these maps have been set constant over the entire range. The pipe block contains the square root of both upstream and downstream pressures squared, which can lead to undefined outputs. This equation is only valid for $p_2 \geq p_1$. During the first tests, the downstream pressure dropped below the upstream pressure, causing the output to be complex. This happened because of an incorrect bypass throttle calibration. Later, this effect was not encountered again.

Also the manifold blocks can undefined outputs, if they are too small. For now the system is stable if all three volumes are set to $0.1\,\text{m}^3$.

System pressures: The pressures are too high at the moment. The reason for this calibration is, that the system becomes instable very quickly if the friction of

the flow elements is lower and/or the manifold volume is smaller. For the thermal simulation the mass flow (and temperature) is the most important property, which is not affected by the pressure. The flow ratio is still correct. However in the future the pressure needs to be more accurate, since the fuel cell model will need it.

Algebraic loops: They can be a problem, since the demand values are calculated based on the current states (mostly temperatures in the system). In the real system, this is no problem, since the states are coming from sensors. To solve it, a unit delay was placed in the return path of the sensor bus. Since the system is inert, we can do this without instability problems.

A.4   Interface List

The tables below feature a complete list of every label (signal, parameter, map,. . .) in the system. The first column denotes the type of label: I = input signal, O = output signal, P = parameter, A = axis for look-up tables, M = table data for look-up tables, L = local parameter.

In the second column the prefix, of the component in which the label is used, is stated. This can be for example BNR for burner, CAT for catalyst and so on.

Then the label name (according to the AVL naming convention) and a description is given in columns 3 and 4.

The unit, the calibration value (only for parameters) and the dimension of the label is given in columns 5 through 6.

In the last column the full name is stated. Note that parameters, axes and maps end with _P, _A and _M respectively. Signals (inputs or outputs) do not have a postfix. This naming allows for easily relatable signals in such a big system.

Table A.1: *Interface list, (part 1/3)*

Type	Component	Name	Description	Unit	Value	Dimension	Full Name
I	CCMP	MfAirDmd	Cathode mass-flow demand value	kg/s		1	CCMP_MfAirDmd
I	CCMP	TGasUs	Gas temperature at cathode compressor inlet	K		1	CCMP_TGasUs
I	CCMP	PGasUs	Gas pressure upstream	Pa		1	CCMP_PGasUs
I	CCMP	PGasDs	Gas pressure downstream	Pa		1	CCMP_PGasDs
I	CCMP	MuGasUs	Mass concentration vector	kg/kg		14	CCMP_MuGasUs
P	CCMP	CswGasTDsClcn	Controlswitch, downstream temperature calculation	-	0	1	CCMP_CswGasTDsClcn_P
P	CCMP	CswGasMfFilt	Controlswitch, mass flow filtering	-	1	1	CCMP_CswGasMfFilt_P
P	CCMP	TcFilt	Filter time constant	s	2	1	CCMP_TcFilt_P
A	CCMP	SpdCmpr	Compressor speed axis	rpm		8	CCMP_SpdCmpr_A
A	CCMP	MfCmpr	Compressor mass flow axis	kg/s		8	CCMP_MfCmpr_A
M	CCMP	EffCmpr	Compressor efficiency map	-		8x8	CCMP_EffCmpr_M
O	CCMP	MfGasDs	True cathode mass-flow after compressor	kg/s		14	CCMP_MfGasDs
O	CCMP	TGasDs	Gas temperature at the cathode compressor outlet	K		1	CCMP_TGasDs
I	MFLD	MfGasIn	Mass flow into the pipe network	kg/s		14	MFLD_MfGasIn
I	MFLD	TGasIn	Temperature of gas entering the manifold	K		1	MFLD_TGasIn
I	MFLD	MfGasOut	Mass flow out of the pipe network	kg/s		14	MFLD_MfGasOut
L	MFLD	PMnfldIni	Initial manifold pressure	Pa	100000	1	MFLD_PMnfldIni_L
L	MFLD	VMnfld	Volume of manifold	m^3	0.1	1	MFLD_VMnfld_L
O	MFLD	MconcMnfld	Mass concentration of gases leaving the manifold	kg/kg		14	MFLD_MconcMnfld
O	MFLD	PGasDs	Press inside the manifold	Pa		1	MFLD_PGasDs
O	MFLD	TGasDs	Temperature of gas after the manifold	K		1	MFLD_TGasDs
I	CHEX	MfGas1	Mass-flow vector hot gas	kg/s		14	CHEX_MfGas1
I	CHEX	TGas1Us	Temperature of hot gas upstream	K		1	CHEX_TGas1Us
I	CHEX	TGas2Us	Temperature of hot gas upstream	K		1	CHEX_TGas2Us
I	CHEX	MfGas2	Mass-flow vector cold gas	kg/s		14	CHEX_MfGas2
P	CHEX	TcFilHex	Filter time constant for outlet temperatures	s	130	1	CHEX_TcFilHex_P
P	CHEX	TGasHotIni	Initial outlet temperature of at the hot side, cathode heat exchanger	K	300	1	CHEX_TGasHotIni_P
P	CHEX	TGasColdIni	Initial outlet temperature of at the cold side, cathode heat exchanger	K	300	1	CHEX_TGasColdIni_P
P	CHEX	NrHexCells	Number of hex cells	-	3	1	CHEX_NrHexCells_P
P	CHEX	HtcHexCell	Heat transfer coefficient of a heat exchanger cell	J/(m^2*K)	1000	1	CHEX_HtcHexCell_P
P	CHEX	ArSurfHex	Heat transfer area of entire heat exchanger	m^2	2	1	CHEX_ArSurfHex_P
P	CHEX	EffHex	Efficiency factor of the heat exchanger	-	1.12	1	CHEX_EffHex_P
A	CHEX	TIsln	Mean temperature of isolation material, axis	K		9	CHEX_TIsln_A
M	CHEX	CdtythrmIsln	Thermal conductivity of isolation material over temperature	W/(m*K)		9	CHEX_CdtythrmIsln_M
P	CHEX	RhoIsln	Density of isolation material	kg/m^3	230	1	CHEX_RhoIsln_P
P	CHEX	RdHexPipe	Radius of HEX pipe	m	0.04	1	CHEX_RdHexPipe_P
P	CHEX	LenHexPipe	Length of HEX pipe	m	0.5	1	CHEX_LenHexPipe_P
P	CHEX	LamHexPipeCorrn	Friction coefficient correction factor	-	40	1	CHEX_LamHexPipeCorrn_P
O	CHEX	MfGas1Ds	Mass-flow vector with entries for each gas species at the hot outlet	kg/s		14	CHEX_MfGas1Ds
O	CHEX	TGas1Ds	Downstream gas temperature at the hot outlet	K		1	CHEX_TGas1Ds
O	CHEX	MfGas2Ds	Mass-flow vector heat exchanger downstream	kg/s		14	CHEX_MfGas2Ds
O	CHEX	TGas2Ds	Downstream gas temperature at the cold outlet	K		1	CHEX_TGas2Ds
I	FCS	MfGasCathdUs	Mass-flow vector cathode upstream	kg/s		14	FCS_MfGasCathdUs
I	FCS	TGasCathdUs	Temperature of cathode gas upstream	K		1	FCS_TGasCathdUs
I	FCS	PGasCathdUs	Gas pressure at cathode upstream	Pa		1	FCS_PGasCathdUs
I	FCS	PGasCathdDs	Gas pressure at cathode downstream	Pa		1	FCS_PGasCathdDs
I	FCS	MfGasAnodeUs	Mass-flow vector anode upstream	kg/s		14	FCS_MfGasAnodeUs
I	FCS	TGasAnodeUs	Temperature of anode gas upstream	K		1	FCS_TGasAnodeUs
I	FCS	PGasAnodeUs	Gas pressure at anode upstream	Pa		1	FCS_PGasAnodeUs
I	FCS	PGasAnodeDs	Gas pressure at anode downstream	Pa		1	FCS_PGasAnodeDs
I	FCS	IStack	Current drawn from the stack	A		1	FCS_IStack
I	FCS	TAmbSens	Ambient temperature	K		1	FCS_TAmbSens
P	FCS	Mstack	Mass of the fuel cell stack	kg	15	1	FCS_Mstack_P
P	FCS	ChtStack	Heat capacity of the fuel cell stack	J/(kg*K)	450	1	FCS_ChtStack_P
P	FCS	HtcStack	Heat transfer coefficient of the fuel cell stack	J/K	100	1	FCS_HtcStack_P
P	FCS	TFcsIni	Initial stack temperature	K	300	1	FCS_TFcsIni_P
P	FCS	ArSurfFcs	Stack surface area	m^2	0.1	1	FCS_ArSurfFcs_P
A	FCS	IStack	Stack current	A		8	FCS_IStack_A
M	FCS	PwrStack	Stack power	W		8	FCS_PwrStack_M
O	FCS	MfGasCathdDs	Mass-flow vector downstream	kg/s		14	FCS_MfGasCathdDs
O	FCS	TGasCathdDs	Temperature of gas downstream	K		1	FCS_TGasCathdDs
O	FCS	MfGasAnodeDs	Mass-flow vector downstream	kg/s		1	FCS_MfGasAnodeDs
O	FCS	TGasAnodeDs	Temperature of gas downstream	K		14	FCS_TGasAnodeDs
O	FCS	TStackMean	Mean stack temperature	K		1	FCS_TStackMean
O	FCS	UStack	Stack voltage	V		1	FCS_UStack
I	PPE	MconcGasUs	Mass concentration of upstream gas (mass-flow of one gas / total mass-flow)	kg/kg		14	PPE_MconcGasUs
I	PPE	PGasUs	Gas pressure at pipe inlet (absolute)	Pa		1	PPE_PGasUs
I	PPE	TGasUs	Temperature of gas upstream	K		1	PPE_TGasUs
I	PPE	PGasDs	Gas pressure at pipe outlet (absolute)	Pa		1	PPE_PGasDs
I	PPE	TGasDs	Gas temperature of gas downstream	K		1	PPE_TGasDs
L	PPE	RdPipe	Radius of the pipe	m	0.04	1	PPE_RdPipe_L
L	PPE	LenPipe	Length of the pipe	m	1	1	PPE_LenPipe_L
L	PPE	ArPipe	Cross section area of the pipe	m^2		1	PPE_ArPipe_L
L	PPE	LamPipeCorrn	Correction factor for pipe friction coefficient (lambda)	-	30	1	PPE_LamPipeCorrn_L
P	PPE	TcFiltPipeMf	Filter time constant for pipe mass-flow output	s	0	1	PPE_TcFiltPipeMf_P
A	PPE	PDropPipe	Pressure drop over pipe	Pa		8	PPE_PDropPipe_A
M	PPE	LamPipe	Friction coefficient lambda over pressure drop	-		8	PPE_LamPipe_M
M	PPE	LamCorrnVisc	Friction coefficient correction for fluid viscosity	-		8	PPE_LamCorrnVisc_M
A	PPE	TMeanGas	Mean gas temperature along pipe length	K		8	PPE_TMeanGas_A
O	PPE	MfGasDs	Mass-flow vector downstream	kg/s		14	PPE_MfGasDs
O	PPE	TGasDs	Temperature of gas downstream	K		1	PPE_TGasDs

Table A.2: *Interface list, (part 2/3)*

Type	Component	Name	Description	Unit	Value	Dimension	Full Name
I	CAT	MfGasUs	Mass-flow vector catalyst upstream	kg/s		14	CAT_MfGasUs
I	CAT	TGasUs	Temperature gas catalyst upstream	K		1	CAT_TGasUs
I	CAT	TAmbSens	Ambient temperature	K		1	CAT_TAmbSens
P	CAT	MCat	Mass of catalyst	kg	10	1	CAT_MCat_P
P	CAT	ChtCat	Heat capacity of catalyst	J/(kg*K)	450	1	CAT_ChtCat_P
P	CAT	HtcCat	Heat transfer coefficient	J/(m^2*K)	10	1	CAT_HtcCat_P
P	CAT	ArSurfCat	Surface area of catalyst for heat transfer	m^2	0.05	1	CAT_ArSurfCat_P
P	CAT	TCatRctnMin	Minimum reaction temperature of catalyst	K	300	1	CAT_TCatRctnMin_P
P	CAT	TcFiltRctnEna	Filter time constant for reaction enable condition	s	50	1	CAT_TcFiltRctnEna_P
P	CAT	TCatIni	Initial catalyst temperature	K	300	1	CAT_TCatIni_P
P	CAT	RednCO	Reaction vector CO	-		14	CAT_RednCO_P
P	CAT	RednCO2	Reaction vector CO2	-		14	CAT_RednCO2_P
P	CAT	RednH2O	Reaction vector H2O	-		14	CAT_RednH2O_P
P	CAT	RednH2	Reaction vector H2	-		14	CAT_RednH2_P
P	CAT	RednCH4	Reaction vector CH4	-		14	CAT_RednCH4_P
P	CAT	RednO2	Reaction vector O2	-		14	CAT_RednO2_P
P	CAT	RednN2	Reaction vector N2	-		14	CAT_RednN2_P
P	CAT	RednAr	Reaction vector Ar	-		14	CAT_RednAr_P
P	CAT	RednC3H8	Reaction vector C3H8	-		14	CAT_RednC3H8_P
P	CAT	RednC4H10	Reaction vector C4H10	-		14	CAT_RednC4H10_P
P	CAT	RednC2H6O	Reaction vector C2H6O	-		14	CAT_RednC2H6O_P
P	CAT	RednCH4O	Reaction vector CH4O	-		14	CAT_RednCH4O_P
P	CAT	RednC12H26	Reaction vector C12H16	-		14	CAT_RednC12H26_P
P	CAT	RednC8H18	Reaction vector C8H18	-		14	CAT_RednC8H18_P
O	CAT	MfGasDs	Mass-flow vector catalyst downstream	kg/s		14	CAT_MfGasDs
O	CAT	TGasDs	Temperature gas catalyst downstream	K		1	CAT_TGasDs
O	CAT	QfRctn	Heat flow from reaction	W		1	CAT_QfRctn
I	BNR	MfGasUs	Mass-flow vector upstream	kg/s		14	BNR_MfGasUs
I	BNR	TGasUs	Temperature of gas upstream	K		1	BNR_TGasUs
I	BNR	TAmbSens	Ambient temperature	K		1	BNR_TAmbSens
I	BNR	GlwPlgDem	Glow plug for fuel ignition demand	-		1	BNR_GlwPlgDem
I	BNR	MfFu	Fuel (Diesel) mass flow	g/h		1	BNR_MfFu
P	BNR	MBrnr	Mass of burner	kg	6	1	BNR_MBrnr_P
P	BNR	HtcBrnr	Heat transfer coefficient of the burner	J/(m^2*K)	4	1	BNR_HtcBrnr_P
P	BNR	ArBrnr	Burner area	m^2	0.1	1	BNR_ArBrnr_P
P	BNR	ChtBrnr	Heat capacity of the burner	J/(kg*K)	4	1	BNR_ChtBrnr_P
P	BNR	TBrnrIni	Initial burner temperature	K	300	1	BNR_TBrnrIni_P
P	BNR	TBrnrRctnMin	Minimum temperature for burner reaction	K	400	1	BNR_TBrnrRctnMin_P
P	BNR	LamRctnMax	Maximum air to fuel ratio for burner reaction	-	50	1	BNR_LamRctnMax_P
P	BNR	TcRctnEna	Filter time constant for burner reaction enable condition	s	5	1	BNR_TcRctnEna_P
P	BNR	PwrGlwPlg	Thermal power of glow plugs	W	500	1	BNR_PwrGlwPlg_P
P	BNR	TcAirMf	Filter time constant for burner mass flow	s	20	1	BNR_TcAirMf_P
O	BNR	MfGasDs	Mass-flow vector downstream	kg/s		14	BNR_MfGasDs
O	BNR	TGasDs	Temperature of gas downstream	K		1	BNR_TGasDs
O	BNR	QfRctn	Heat flow from fuel combustion	W		1	BNR_QfRctn
O	BNR	LamTrue	Calculated lambda value	-		1	BNR_LamTrue
I	BTHR	PGasUs	Pressure throttle upstream	Pa			BTHR_PGasUs
I	BTHR	PGasDs	Pressure throttle downstream	Pa			BTHR_PGasDs
I	BTHR	TGasUs	Temperature of gas entering the bypass throttle	K		1	BTHR_TGasUs
I	BTHR	AgThrDem	Throttle angle (90deg = fully open, 0deg = fully closed)	deg		1	BTHR_AgThrDem
I	BTHR	MconcGasUs	Mass concentration of gas entering the throttle valve	kg/kg		14	BTHR_MconcGasUs
M	BTHR	FacThrAgToAr	Factor to convert throttle angle to effective opening area	-		19	BTHR_FacThrAgToAr_M
A	BTHR	AgThr	Throttle angle axis	deg		19	BTHR_AgThr_A
A	BTHR	AgThr1	Throttle angle axis	deg		10	BTHR_AgThr1_A
L	BTHR	ArThr	Cross section area of throttle pipe (without plate thickness correction)	m^2	0.05	1	BTHR_ArThr_L
P	BTHR	FacCoeffDchaCorrn	Correction factor for angle dependent discharge coefficient	-	0.001	1	BTHR_FacCoeffDchaCorrn_P
M	BTHR	CoeffDcha	Discharge coefficient of throttle valve over throttle plate angle	-		10	BTHR_CoeffDcha_M
O	BTHR	MfGasDs	Mass flow vector bypass throttle downstream	kg/s		14	BTHR_MfGasDs
O	BTHR	TGasDs	Temperature of gas downstream	K		1	BTHR_TGasDs
I	JCTN	MfGas1	First mass-flow into the junction	kg/s		14	JCTN_MfGas1
I	JCTN	TGas1	First gas temperature into the junction	K		1	JCTN_TGas1
I	JCTN	MfGas2	Second mass-flow into the junction	kg/s		14	JCTN_MfGas2
I	JCTN	TGas2	Second gas temperature	K		1	JCTN_TGas2
I	JCTN	TAmbSens	Ambient temperature	K		1	JCTN_TAmbSens
P		TJctnIni	Initial junction temperature	K	300	1	TJctnIni_P
P		ChtJctn	Heat capacity of junction body	J/(kg*K)	450	1	ChtJctn_P
P		MJctn	Mass of junction body	kg	1	1	MJctn_P
P		HtcJctn	Heat transfer coefficient of junction walls	J/(m^2*K)	10	1	HtcJctn_P
P		ArJctn	Area of junction	m^2	0.05	1	ArJctn_P
O	JCTN	MfGasDs	Combined mass-flow downstream	kg/s		14	JCTN_MfGasDs
O	JCTN	TGasDs	Resulting gas temperature downstream	K		1	JCTN_TGasDs

Table A.3: *Interface list, (part 3/3)*

Type	Component	Name	Description	Unit	Value	Dimension	Full Name
I	HUC	State	Current controller state (idle = 0, ignite = 1, heat-up = 3, active = 4, cool-down = 5)	-		1	HUC_State
I	HUC	SensorBus	Bus containing all plant sensors			39	HUC_SensorBus
I	HUC	DmdBusSeld	Selected and limited demand bus			5	HUC_DmdBusSeld
P	HUC	EnaBypThrCtlr	Enable bypass throttle controller (controlled value: stack upstream temperature)	-	1	1	HUC_EnaBypThrCtlr_P
P	HUC	EnaMfAirCtlr	Enable air mass flow controller (closed loop)	-	0	1	HUC_EnaMfAirCtlr_P
P	HUC	CswHeatUpStgy	Select heat-up strategy	-	1	1	HUC_CswHeatUpStgy_P
P	HUC	TCathdUsTgt	Cathode upstream target temperature	degC		1	HUC_TCathdUsTgt_P
P	HUC	TBrnrDsTgt	Burner downstream target temperature for controller	degC		1	HUC_TBrnrDsTgt_P
P	HUC	TCathdUsDsTgt	Cathode upstream-downstream temperature difference target	degC		1	HUC_TCathdUsDsTgt_P
P	HUC	MfCathdCmprOlTgt	Cathode compressor open-loop target mass flow	kg/h	30	1	HUC_MfCathdCmprOlTgt_P
P	HUC	CswTCathdDsGrdtTgt	0 = constant value, 1 = map based	-	0	1	HUC_CswTCathdDsGrdtTgt_P
A	HUC	TCatDs	Catalyst downstream temperature, axis	K		8	HUC_TCatDs_A
M	HUC	MfBrnrFuDmdOl	Fuel mass flow open loop demand	g/h		8	HUC_MfBrnrFuDmdOl_M
M	HUC	TGrdtCathdDsDmd	Temperature gradient cathode downstream demand	K/h		8	HUC_TGrdtCathdDsDmd_M
A	HUC	TCathdDs	Cathode downstream temperature, axis	K		8	HUC_TCathdDs_A
O	HUC	DmdBus	Demand bus	-		5	HUC_DmdBus
I	DLN	DmdBusIn	Input for demand bus	-		5	DLN_DmdBusIn
I	DLN	State	Current controller state	-		1	DLN_State
P	DLN	MfAirMax	Maximum air mass flow of cathode compressor	kg/h		1	DLN_MfAirMax_P
P	DLN	MfAirMin	Minimum air mass flow of cathode compressor	kg/h		1	DLN_MfAirMin_P
P	DLN	MffFuMax	Maximum fuel mass flow for burner	g/h		1	DLN_MffFuMax_P
P	DLN	MffFuMin	Minimum fuel mass flow for burner	g/h		1	DLN_MffFuMin_P
O	DLN	DmdBus	Output of limited demand bus	-		5	DLN_DmdBus
C		KELVIN	Celsius zero point in Kelvin	K	273.15	1	KELVIN_C
A		TGas	Gas temperature axis	K		8	TGas_A
M		ChtCO	Heat capacity over temperature map: CO	J/(kg*K)		8	ChtCO_M
M		ChtCO2	Heat capacity over temperature map: CO2	J/(kg*K)		8	ChtCO2_M
M		ChtH2O	Heat capacity over temperature map: H2O	J/(kg*K)		8	ChtH2O_M
M		ChtH	Heat capacity over temperature map: H	J/(kg*K)		8	ChtH_M
M		ChtCH4	Heat capacity over temperature map: CH4	J/(kg*K)		8	ChtCH4_M
M		ChtO2	Heat capacity over temperature map: O2	J/(kg*K)		8	ChtO2_M
M		ChtN2	Heat capacity over temperature map: N2	J/(kg*K)		8	ChtN2_M
M		ChtAr	Heat capacity over temperature map: Ar	J/(kg*K)		8	ChtAr_M
M		ChtC3H8	Heat capacity over temperature map: C3H8	J/(kg*K)		8	ChtC3H8_M
M		ChtC4H10	Heat capacity over temperature map: C4H10	J/(kg*K)		8	ChtC4H10_M
M		ChtC2H6O	Heat capacity over temperature map: C2H6O	J/(kg*K)		8	ChtC2H6O_M
M		ChtCH4O	Heat capacity over temperature map: CH4O	J/(kg*K)		8	ChtCH4O_M
M		ChtC12H26	Heat capacity over temperature map: C12H26	J/(kg*K)		8	ChtC12H26_M
M		ChtC8H18	Heat capacity over temperature map: C8H18	J/(kg*K)		8	ChtC8H18_M
C		Ts	Sample Time	s	0.01	1	Ts_C
C		RgasUniv	Universal gas constant	J/(mol*K)	8.3145	1	RgasUniv_C
C		RgasAir	Gas constant	J/(kg*K)	287.058	1	RgasAir_C
C		MmolC8H18	Molar mass	g/Mol	114.231	1	MmolC8H18_C
C		MmolC12H26	Molar mass	g/Mol	170.34	1	MmolC12H26_C
C		MmolC12H23	Molar mass	g/Mol	167.311	1	MmolC12H23_C
C		MmolCH4O	Molar mass	g/Mol	32.042	1	MmolCH4O_C
C		MmolC2H6O	Molar mass	g/Mol	46.069	1	MmolC2H6O_C
C		MmolC4H10	Molar mass	g/Mol	58.123	1	MmolC4H10_C
C		MmolC3H8	Molar mass	g/Mol	44.097	1	MmolC3H8_C
C		MmolAr	Molar mass	g/Mol	39.948	1	MmolAr_C
C		MmolN2	Molar mass	g/Mol	28.013	1	MmolN2_C
C		MmolCH4	Molar mass	g/Mol	16.043	1	MmolCH4_C
C		MmolH2	Molar mass	g/Mol	2.016	1	MmolH2_C
C		MmolH	Molar mass	g/Mol	1.008	1	MmolH_C
C		MmolCO	Molar mass	g/Mol	28.01	1	MmolCO_C
C		MmolO2	Molar mass	g/Mol	31.9988	1	MmolO2_C
C		MmolC12H23	Molar mass	g/Mol	167.311	1	MmolC12H23_C
C		MmolCO2	Molar mass	g/Mol	44.0095	1	MmolCO2_C
C		MmolH2O	Molar mass	g/Mol	18.0153	1	MmolH2O_C
C		MmolC	Molar mass	g/Mol	12.011	1	MmolC_C
C		MmolAir	Molar mass of Air	g/Mol	28.97	1	MmolAir_C
C		FacStoiDsl	Stoichiometric constant for Diesel (Oxygen/Diesel)	-	3.3947	1	FacStoiDsl_C
C		HeatValLoDsl	Lower heating value of Diesel	kJ/kg	11.83	1	HeatValLoDsl_C
C		RatCpCvAir	Ratio of specific heats (Cp/Cv) often denated as gamma or kappa	-	1.4	1	RatCpCvAir_C
P	CTLR	CswIgDmdValOvrr	Switch to override ignition demand values for air and fuel mass flow	-		1	CTLR_CswIgDmdValOvrr_P
P	CTLR	MffFuIg	Ignition fuel mass flow	g/h		1	CTLR_MffFuIg_P
P	CTLR	LamBrnrIg	Ignition lambda	-		1	CTLR_LamBrnrIg_P